AFCRL-70-0168(I)

STUDY OF METEOR WIND MEASUREMENT TECHNIQUES

by

Norman F. Deegan
Robert J. Fitzpatrick
Giuseppe Forti
Mario D. Grossi
Mario R. Schaffner
Richard B. Southworth

Smithsonian Astrophysical Observatory
60 Garden Street
Cambridge, Massachusetts 02138

Contract AF 19(628)-3248

Project No. 6682

Task No. 668207

Final Report (Volume I)

Period covered: 1 June 1963 to 31 May 1966

February 1970

Contract Monitor: Wilbur H. Paulsen

Aerospace Instrumentation Laboratory

Prepared

for

AIR FORCE CAMBRIDGE RESEARCH LABORATORIES
OFFICE OF AEROSPACE RESEARCH
UNITED STATES AIR FORCE
BEDFORD, MASSACHUSETTS 01730

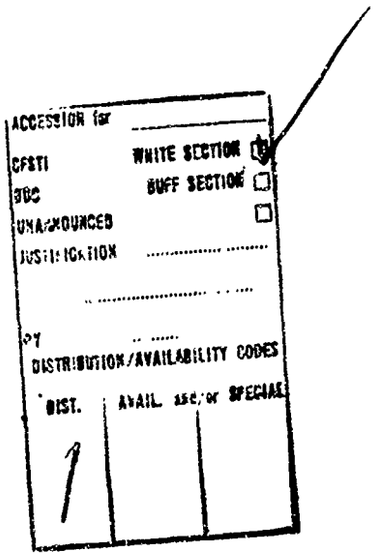

Qualified requestors may obtain additional copies from the Defense Documentation Center. All others should apply to the Clearinghouse for Federal Scientific and Technical Information.

AFCRL-70-0168(I)

STUDY OF METEOR WIND MEASUREMENT TECHNIQUES

by

Norman F. Deegan
Robert J. Fitzpatrick
Giuseppe Forti
Mario D. Grossi
Mario R. Schaffner
Richard B. Southworth

Smithsonian Astrophysical Observatory
60 Garden Street
Cambridge, Massachusetts 02138

Contract AF 19(628)-3248

Project No. 6682

Task No. 668207

Final Report (Volume I)

Period covered: 1 June 1963 to 31 May 1966

February 1970

Contract Monitor: Wilbur H. Paulsen
Aerospace Instrumentation Laboratory

Prepared
for

AIR FORCE CAMBRIDGE RESEARCH LABORATORIES
OFFICE OF AEROSPACE RESEARCH
UNITED STATES AIR FORCE
BEDFORD, MASSACHUSETTS 01730

TABLE OF CONTENTS

Volume I

TABLE OF CONTENTS (Cont.)

ACKNOWLEDGMENTS

The principal contributors to the Meteor Wind Program sponsored by the Air Force under Contract AF 19(628)-3248, also authors of this final report, are (in alphabetical order):

- Mr. Norman F. Deegan, EE and Project Engineer (main author of Section 3, Vol. I)
- Mr. Robert J. Fitzpatrick, Mathematician (author of Section 1, Vol. II)
- Dr. Giuseppe Forti, Astronomer and Data Analyst (main author of Section 4, Vol. I)
- Dr. Mario D. Grossi, EE (author of Sections 1.1, 1.2, 5 and contributor to Section 3, Vol. I)
- Dr. Mario Schaffner, EE (designer of the meteor radar processor and author of Section 3.9, Vol. I)
- Dr. Richard B. Southworth, Astronomer and Chief of Analysis (author of Sections 1.3, 1.4, 2 and contributor to Section 4, Vol. I).

This program has been conducted under the supervision of Dr. Fred L. Whipple, Director, Smithsonian Astrophysical Observatory, and of Dr. Richard B. Southworth.

Dr. Mario D. Grossi served as Principal Investigator.

Mr. Wilbur H. Paulsen, AFCRL-Aerospace Instrumentation Laboratory, was the Contract Monitor for the U.S. Air Force.

* * *

The authors wish to acknowledge the contributions of Dr. Winfield W. Salisbury to the development and calibration of the radar instrumentation.

ABSTRACT

Wind data in the height range 80 to 100 km can be obtained with a multistatic VHF phase-coherent pulse-doppler meteor radar capable of monitoring a volume in space measuring approximately 50 km × 50 km horizontally, and 20 km vertically.

An eight-station phase-coherent system has been established for this purpose near Havana, Illinois, by reworking an existing six-station, incoherent, pulse meteor radar operating at 40.92 MHz.

A 4-Mw transmitter and eight receiving sites dispersed up to 50 km away from the transmitter site have been locked together in phase within a few parts in 10^{10} by distributing a 2.5 kHz reference tone via commercial telephone lines.

The system operates satisfactorily and is capable of collecting enough range-doppler samples from meteor trails for an adequate description of the wind pattern at meteor heights.

Wind profiles have been obtained by processing in Cambridge with a CDC-6400 computer the multichannel digital tapes recorded in Havana.

The method can, potentially, be used for real-time wind measurements. It competes favorably with alternative approaches when wind measurements at meteor height must be performed with continuity and without resorting to horizon-to-horizon spatial averaging.

STUDY OF METEOR WIND MEASUREMENT TECHNIQUES

Contract AF 19(628)-3248

Volume I

I. METEOR WIND MEASUREMENTS BY PULSE-DOPPLER RADAR

1.1 Introduction and Summary of Section 1

An eight-station multistatic phase-coherent pulse-doppler radar system for meteor research has been completed in the countryside between Peoria and Springfield, Illinois, under the terms of the Contract AF 19(628)-3248. The system is composed of: (a) a main site where the transmitter and a dual-channel receiver are located; (b) five outlying sites arranged in a cluster around the main site, each equipped with a single-channel receiver; and (c) two remote sites at about 33 and 50 km, respectively, from the main sites, and each again equipped with a single-channel receiver.

The network is a rework of the six-station noncoherent pulse radar system operated in Illinois since 1961 by the Harvard Radio Meteor Project (Hawkins, 1963).

The new system is able to collect phase-coherent meteor echoes from a volume in the upper atmosphere that is not sharply bounded but that measures roughly 50 × 50 km horizontally and 20 km vertically, with the vertical dimension extending from about 80 to 100 km above the ground. The volume under radar patrol is approximately above Decatur, Illinois.

For analysis of the spatial structure of the wind field, we divide the observable volume into "cells." We take 1 km as the vertical extent of a cell, approximately our accuracy of height measurement. Subject to later revision, we take 15 km as the extent of a cell in both horizontal directions;

this is the order of distance in which we expect to be able to resolve differences in horizontal-wind components. Accordingly, we observe on the order of 220 wind cells.

When a cell is crossed by a meteor trail, echoes are received at the main site if the trail in the cell is tangent to a sphere that is centered at the main site and has a radius equal to the distance of the cell from this site (the backscattering case). An outlying or a remote site then receives an echo when the trail is tangent to the ellipsoid having as foci the receiving station under consideration and the transmitter location (main site).

At the main site (where a 4-Mw peak power VHF transmitter is located), a dual-channel receiver provides range, angle of arrival, Fresnel pattern, and doppler information (radial velocity) on the echoes backscattered by a trail.

At each one of the outlying and remote sites, a single-channel receiver provides, for the echoes scattered to the site by the trail, information concerning range, Fresnel pattern, and doppler shift. The doppler information provides the wind velocity component perpendicular to the ellipsoid determined by the echo circulation time from the main site to the meteor to the outlying (or remote) site.

A three-dimensional wind determination in a certain cell (measurement of the wind vector in its horizontal and vertical components) requires that echoes from the cell be received simultaneously at the main site (or, which is equivalent, at one of the outlying sites) and at both remote sites (or, for a less accurate measurement, at one remote site and two outlying sites distant from each other). Because, in general, a single trail does not scatter echoes in all the needed directions, we have to wait until the cell is crossed by more than one trail nearly at the same time in order to obtain the basic echoes required for three-dimensional wind measurements.

Assuming (conservatively) that 15 samples per hour for each cell are necessary to describe adequately the temporal variation of the wind, 3333 independent samples per hour are required in the overall volume surveyed.

The expectations at the beginning of the project were that this hourly amount of information could be routinely collected by the eight-station radar network. The frequency of reducible meteors was expected in fact to be 500/hr with 2000 one-dimensional wind-velocity determinations per hour (every meteor track provides an average of four segments, each capable of providing an independent determination) and 4000 independent samples per hour (each one-dimensional wind-velocity determination gives two pieces of information because both the wind velocity and its derivative with respect to position along the trail are found).

Reconstruction of wind pattern was judged possible from the one-dimensional wind-velocity determinations (2000/hr), from the small amount of two- and three-dimensional data (80/hr and 2/hr, respectively), and from a consideration of continuity. Operation of the Havana system since its completion has shown that the average hourly rate of reducible meteors, from after midnight to midafternoon, is somewhat smaller than expected (approximately 250/hr instead of the predicted 500/hr). This means that we are actually able to collect 2000 independent samples per hour and to make about 1000 one-dimensional velocity measurements per hour, 40 two-dimensional measurements per hour, and 1 three-dimensional wind-velocity measurement per hour.

From midafternoon to shortly after midnight, the average rate of reducible meteors is of the order of 50/hr. In this period, we take the horizontal extent of a wind cell to be the same as the observable volume.

Considering the uncertainties that unavoidably afflict a research program like the one reported, the performance of the Havana meteor radar as a wind measuring instrument came reasonably close to the predicted values. The system is actually capable of measuring time-variable wind patterns characterized by time constants only a factor of 2 larger than those contemplated at the beginning of the program.

The basic wind-measurement recording and analysis procedure is outlined in the following sections.

The measurements are mechanized by conveying to the main site (for processing in a digitizer and recording in a multichannel digital tape recorder) all the data collected by the eight stations and by playing back the tape in a CDC-6400 computer appropriately programed to print out the wind profiles.

The computer program reads the tape, where 34 channels of information are recorded, processes the data to obtain positional information of the meteor trail and of its motion due to the wind, smoothes these data, and prints out the results.

1.2 Data-Acquisition System

1.2.1 Meteor wind-measurement philosophy

1.2.1.1 Monostatic vs. multistatic systems. In general, the determination of the instantaneous velocity vector and of the position in three-dimensional space of a target by radars having low-directivity antennas requires the use of at least three monostatic pulse-doppler radar stations (each equipped with transmitter and receiver) located at the vertices of a triangle with sides preferably comparable in length with the distance of the target from each one of the vertices. In other words, a point target in this configuration is at the apex of a pyramid that has a triangular base, the other vertices (of the base) being the three radar stations. A line target, such as a meteor trail, lies tangent to three spheres centered at the stations. If the scattering properties of the target are such that sufficient energy is scattered toward the ground in forwardscatter as well as in direct backscatter, the system can be simplified to a multistatic configuration with a single radar station (transmitter and receiver) at one of the vertices (main site) and only receivers at the other two vertices (remote sites). The main site radiates the RF pulses and receives backscattered echoes; the remote sites receive forwardscattering.

As far as target motion determination is concerned, there is this minor difference between the two solutions: with the three monostatic radars, each station measures the velocity component along the line of sight from the radar to the target. In the "multistatic" scheme, this applies only to the main site, while for the two remote sites, the velocity component is measured in the propagation plane along the bisector of the angle that separates the main site and remote site as seen from the target.

As far as ranging is concerned, the determination of the location in three-dimensional space of the target is obtained (when three monostatic radars are used) from the intersection of three spheres, each centered at one of the stations and each with a radius equal to the delay between target and station.

In the multistatic case, two of three spheres become ellipsoids, each with a focus at the main site and the other at each one of the remote sites. An ellipsoid is identified by the measured circulation time delay of the echo in the propagation path from the main site to the target to the remote site. The target (meteor trail) location is found as a line tangent to the two ellipsoids and the sphere. There may be an ambiguity of solution; more important, the available accuracy in range measures may not yield a good position determination. To find the target position better, extra information can then be obtained by using interferometric arrangements at one or more of the sites and measuring echo angles of arrival. For each interferometer, a cone is identified at every echo reception, which provides additional intersecting surfaces for target positioning.

1.2.1.2 Scattering properties of a meteor trail. A simplified picture of the scattering phenomenon can be obtained by considering that a radiowave at VHF (as in our case) incident on the column is scattered by individual free electrons, each of which oscillates as if no other were present (underdense trail condition). The "specular reflection point" (for a station or pair of stations) is the point on the trail at minimum distance from the station, or minimum sum of distances from the pair of stations. Echoes from electrons near the specular reflection point arrive in phase and are observed; echoes from points distant from the specular reflection point arrive out of phase and cancel each other.

Of the whole trail, the effective length that contributes to the scattering is the first Fresnel zone around the specular reflection point, half of which equals $\sqrt{\frac{R_0\lambda}{2}} \cong 1$ km, in the normal incidence case, for monostatic radar (R_0 is the distance of the trail from the radar station, and λ the wavelength). In bistatic radar cases, this zone has a more complicated expression for oblique incidence. Different pairs of stations receive scattered signals from different parts of the trail.

Upper atmospheric winds displace the effective specular reflection points and physical processes alter the amplitude of received echoes, but both effects are almost always of second order in determining the position of a trail. They are discussed below.

The scattering properties of a meteor trail dictate the use of a multistatic system rather than widely spaced monostatic radars. If the monostatic radars are separated adequately for good position determination (more than 50 km on the ground), the specular reflection points are much farther separated than the usual length of a meteor trail, so that no meteor is observed at all three radars. On the other hand, the separation of the specular reflection points is directly useful in position determination with a multistatic system.

1.2.1.3 Position of the meteor trail. The locations of the original six Havana stations, which are the main transmitter and receiver site (site 3) and the "outlying" receiver sites, were specially chosen for the determination of meteor-trail positions, in addition to other parameters. The locations of the two newer "remote" receiving sites were chosen primarily for wind measures, but these sites also assist in position determinations for meteor trails that they observe.

We use the motion of the meteoroid that forms the meteor trail (the "target") to find the position of the trail. As the trail is extended past a specular reflection point, the addition of electrons that are alternately in phase and out of phase with the main echo from the principal Fresnel zone generates a characteristic "Fresnel" pattern in the received signal. From the spacing in time of the oscillations in this pattern and the length of the principal Fresnel zone, we find the velocity of the meteoroid (McKinley, 1961; Southworth, 1962). From that velocity and the spacing in time between the Fresnel patterns observed at different stations, we find the distances between specular reflection points. Two such distances, corresponding to noncolinear pairs of stations, determine the direction of motion of the meteoroid; additional distances may strengthen the determination.

At this stage in the reduction, we know that the specular reflection point from the main site lies in a plane normal to the direction of motion of the meteoroid, at an observed range from the main site. (We also used the observed range in computing the velocity.) The meteor trail lies on a cylinder normal to that plane. Measures of differential range from our closely spaced sites are, in general, not sufficiently accurate to fix the location of the meteor trail on the cylinder; but this location is determined by an interferometric measure at the main site. Finally, a general iterative procedure uses all the observations in least-squares fits to find the best position.

1.2.1.4 Wind measurements. The echo received at each station conveys information concerning a part of the meteor trail (the principal Fresnel zone) roughly 1 km long. In general, each station observes a different part of the trail, with some overlapping. The spacing between centers of adjacent parts observed on the trail by different stations is 0 to 3.5 km along the trail, and 0 to 2.7 km in height.

Phase measurements at a station furnish the "radial" component of the mean wind velocity, averaged over the corresponding part of the trail. This component is directed along the bisector of the angle between the directions to the transmitter and the receiver. We normally convert this to a "horizontal radial" component, on the assumption that there is no vertical component; but the actual vertical component is sometimes computed, as described below. The phase measurements also normally furnish the first derivative of the radial component with respect to position along the trail. Both the wind and its derivative are also used to correct the determination of the meteoroid's position and direction of motion.

To determine two components of the wind velocity at a point, it is necessary to receive an echo and measure its phase at one of the remote sites and also to measure the radial wind component (by phase measurements at one or more of the stations of the cluster of six original stations) in the same part of the trail. With phase measured at all the stations of the cluster, the radial wind component can be found, by interpolation, at every point of the

observed portion of a trail. Then every meteor observed at two or more stations of the cluster, and also observed in the same portion of the trail at a remote site, yields one two-dimensional wind determination.

For three-dimensional wind-velocity determinations, we must note that virtually no trail can ever scatter an echo toward the cluster and also toward both remote sites. Therefore, we have to use, for three-dimensional velocity determinations at a given point in space, two different trails that cross the same point within a short interval of time, each of which satisfies all the requirements for positional determination. Together, the two meteors must yield components from one or both remote sites and two widely separated outlying sites.

The detail possible in describing the wind field depends upon the meteor influx rate, which is comparatively high from shortly after midnight to mid-afternoon. During this part of the day, the average rate of reducible meteors has been found to be of the order of 250/hr; about 40 of these will also be observed at one or the other of the remote sites. With all stations equipped to measure phase, there are about 1000 one-dimensional wind determinations and 40 two-dimensional determinations per hour. The number of three-dimensional determinations also depends on how close together the two meteors must be in time and space. If 4 min, 15 km horizontally, and 1 km vertically are allowed, then there is roughly one three-dimensional determination per hour.

The system can furnish vastly more information about the wind than has been available heretofore. The amount of information necessary to specify the wind field if the pattern is not known can be roughly estimated as follows. We take these estimates for the volume of space surveyed and the scales of the dominant variations in the wind:

Volume		Variation (wavelength)	
height	20 km	vertical	5 km
width	50 km	horizontal	75 km
length	50 km	time	20 min

We may assume (conservatively) that five points per wavelength are required to describe a variation. Then the number of independent pieces of information needed per hour is

$$\sim 5\left(\frac{20}{5}\right) \times 5\left(\frac{50}{75}\right) \times 5\left(\frac{50}{75}\right) \times 5\left(\frac{60}{20}\right) = 3333 \quad .$$

In Havana, we routinely obtain one-half of this hourly information. However, if we assume that four samples for wavelength are sufficient for the descriptions of the variations, the information collected by the Havana system becomes more than adequate.

From midafternoon to after midnight, the average rate of reducible meteors is of the order of 50/hr. In this period, we would subdivide the observing volume only into layers 1 km thick, but would look for linear horizontal variations of the wind within each layer. If the dominant wavelength for horizontal variation is 200 km or more, as seems very possible, the lower rate of meteors still yields a sufficient description of the wind field.

1.2.2 Phase-coherent system

The basic scheme of the meteor radar redeveloped in this program and installed near Havana, Illinois, is provided in Figure 1-1, while Figure 1-2 gives the simplified block diagram of the main site, where a 4-Mw transmitter operating at 40.92 MHz is located.

In any phase-coherent network with stations miles apart from one another, the heart of the problem is represented by the phase locking of the various sites among themselves.

The requirement in our case is to have a relative phase jitter between the transmitter and the local oscillators of the various superheterodyne receivers of the multistatic network not larger than 10% of the minimum detectable doppler. For a signal-to-noise ratio of 20 db and a meteor-trail duration of approximately 0.05 sec, the minimum detectable doppler corresponding to the radiated waveform is 0.25 Hz (Grossi, 1963). Consequently, the

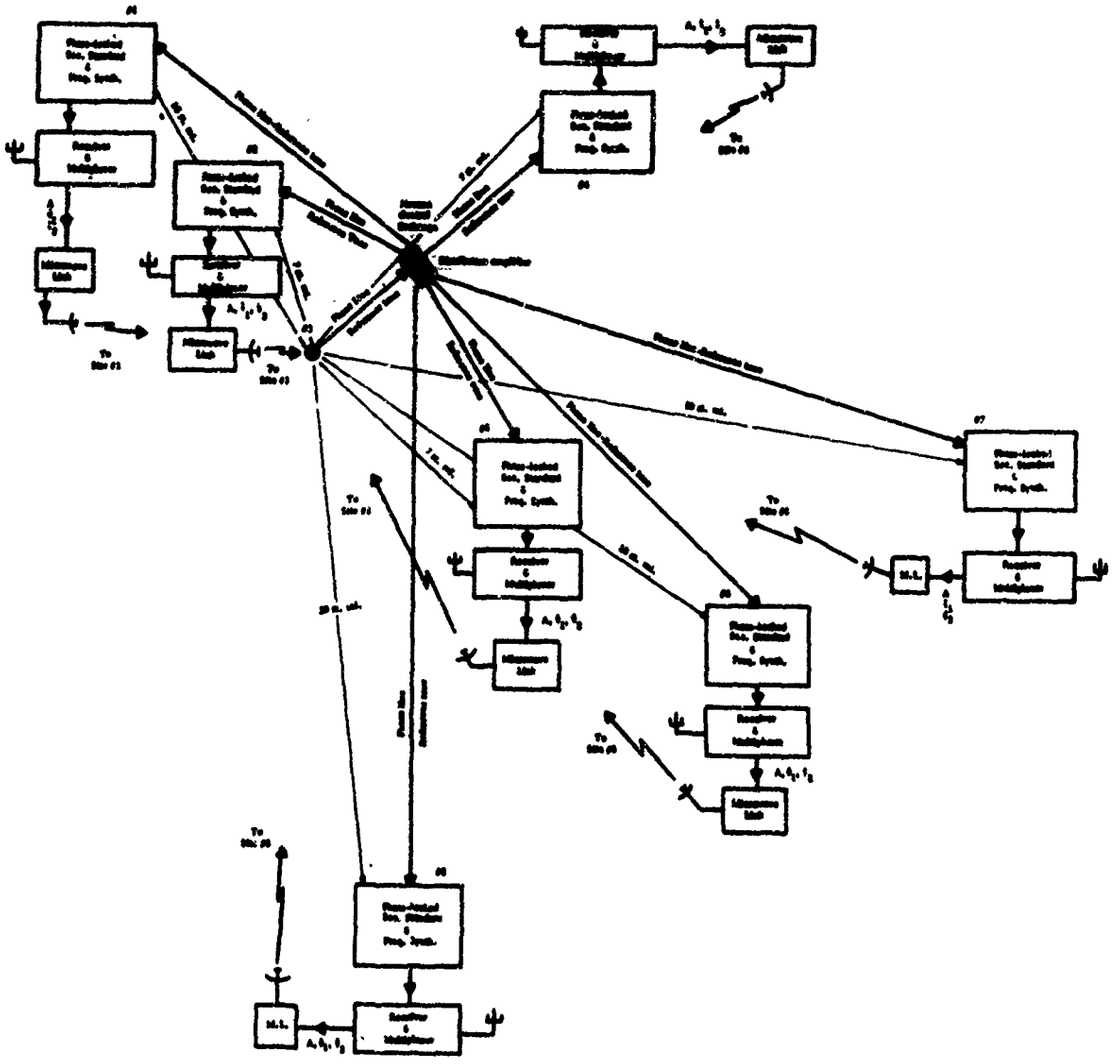

Figure 1-1. General system layout.

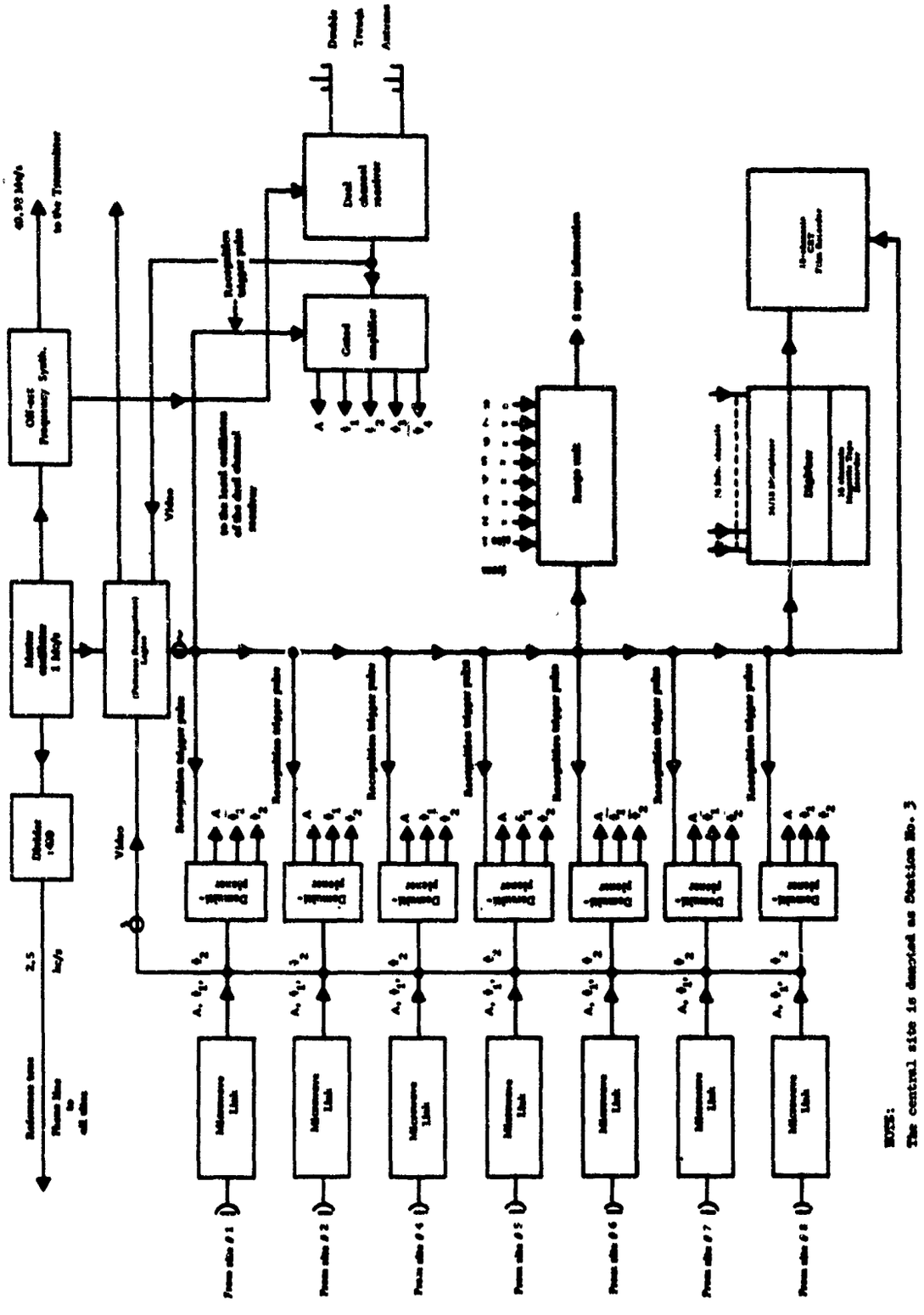

Figure 1-2. Main site simplified block diagram.

relative phase stability must be on the order of 5 parts in 10^{10}. The Havana radar meets this requirement routinely by using a single master oscillator at 1 MHz at the main site, from which, by frequency synthesis, the frequency required for the transmitter, and the local-oscillator frequencies required by the local dual-channel receivers have been obtained. Then, by dividing down the 1 MHz to 2.5 KHz (400:1 ratio) a reference signal is obtained that is distributed by telephone line to the other seven sites of the network. This tone, however, cannot be used directly at the remote end by multiplication and frequency synthesis because the telephone lines are not phase-jitter free. By averaging phase observations for a minimum interval of 10 min, we can obtain reliable phase reference. At each outlying and remote site, the phase of the reference tone that arrives via telephone line is compared to the phase of a secondary standard (VCO) locally available. The output of the phase comparator, followed by an integrator with 10-min time constant, locks the phase of the local secondary standards to the 10-min average of the phase of the incoming reference tone.

Requirements in range measurement are less stringent when one considers that the ideal capability of the radiated waveform with signal-to-noise ratio of 20 db, pulse width of 6 μsec, prf period of 1355 μsec, time on target of 0.05 sec is characterized by errors of $\sigma \approx 10$ m, and this is better than the tolerable range error by about an order of magnitude (Grossi, 1963). It was therefore found easily feasible to implement a range unit capable of providing the necessary accuracy both for backscatter echo delay and for forwardscattering circulation time measurements.

1.2.3 Format of the raw data and example of digital recording

The digital tape recorder has 18 channels, which record the following information for each pulse (i.e., each prf period) of the echo train, in one 8-bit word per channel.

Channel 1 – This records phase information (ϕ_1/ϕ_2) for station 1. The channel is time-shared between A sin ϕ_1, called $(\phi_1)_1$, and A cos ϕ_1, called $(\phi_2)_1$. Every pulse of the returned train is given a serial number. Pulses with odd numbers carry sin ϕ_1 information, pulses with even numbers carry cos ϕ_1 information. These are the two outputs of the phase detector. (A, the amplitude of the echo, is recorded on channel 2.) Amplitude calibration signals (11 levels) are injected into the system once per hour.

Channel 2 – This contains echo amplitude A_1 for station 1. Amplitudes are usually recorded on a logarithmic scale, unlike the linear scale used in the phase channels.

Channel 3 – Time-shared between $(\phi_1)_2$ and $(\phi_2)_2$, station 2, as in channel 1.

Channel 4 – Echo amplitude A_2, station 2.

Channel 5 – Time-shared between $(\phi_1)_4$ and $(\phi_2)_4$, station 4, as in channel 1.

Channel 6 – Echo amplitude A_4, station 4.

Channel 7 – Time-shared between $(\phi_1)_5$ and $(\phi_2)_5$, as in channel 1.

Channel 8 – Echo amplitude A_5, station 5.

Channel 9 – Time-shared between $(\phi_1)_6$ and $(\phi_2)_6$, as in channel 1.

Channel 10 – Echo amplitude A_6, station 6.

Channel 11 – Time-shared between $(\phi_1)_7$ and $(\phi_2)_7$, as in channel 1.

Channel 12 – Echo amplitude A_7, station 7.

Channel 13 – Time-shared between $(\phi_1)_8$ and $(\phi_2)_8$, as in channel 1.

Channel 14 – Echo amplitude A_8, station 8.

Channel 15 – Time-shared between $(\phi_1)_3$ and $(\phi_2)_3$, as in channel 1.

Channel 16 – Echo amplitude A_3, station 3.

Channel 17— Time-shared between $(\phi_3)_3$ and $(\phi_4)_3$, phase information from the second receiver of station 3, time-shared as in channel 1.

Channel 18— Range information from that one of the eight stations of the network where the meteor was most recently recognized by the pattern-recognition logics. For every measure, 5 prf periods are used to provide adjacent time segments that are occupied by the range information. The first two carry the octal word 000 and are used as synchronizing information. The third prf period is used to identify the station according to the following correspondence table:

	Station
200	1
100	2
040	3
020	4
010	5
004	6
002	7
001	8

The fourth prf period is used by an 8-bit word that gives the high-order digits of the range information (800 km maximum range). The fifth prf period is used by an 8-bit word that gives the least-significant digits of the range information. The range information is the number of quarter microseconds between transmission and reception of a pulse via the meteor and the station named.

An example of digital recording is given in Figure 1-3.

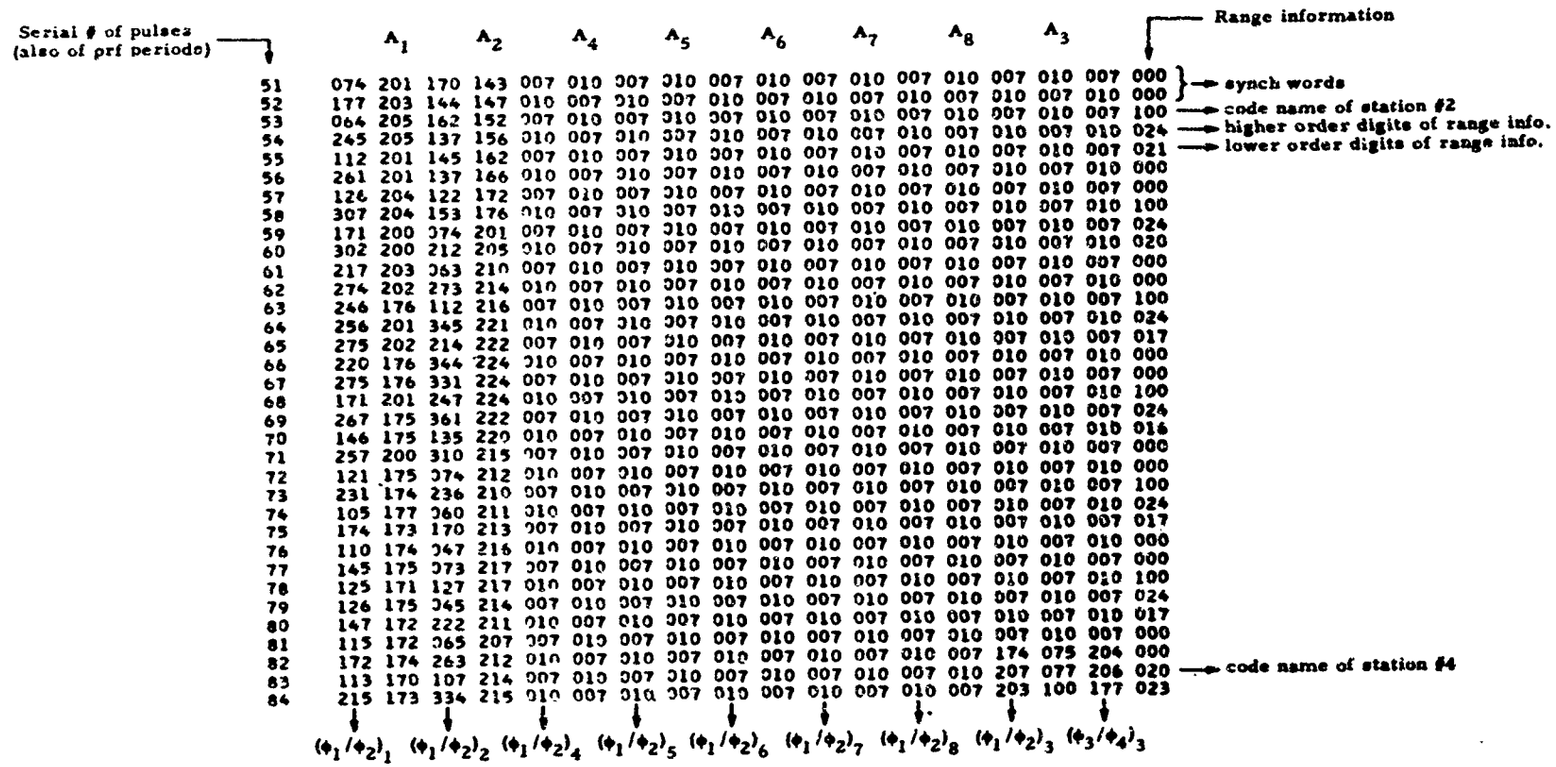

Figure 1-3. Example of digital recording (from a meteor simulation run).

1.3 Mathematical Formulations and Outline of Reductions

1.3.1 Theoretical model of wind phase information

The radar echo received from the ionized column left behind a moving meteoroid is, for practical purposes, entirely scattered back to the observer by free electrons in the column, since scattering by free ions or the solid surface is negligible. Kaiser (1955), among others, has discussed the echo from a meteor; some additional features are described by Southworth (1962). The amplitude and phase of the observable echo are the integrated vector sum of the echoes from individual elements of the column. In an "underdense" column, such as are mostly observed by the Radio Meteor Project, one can consider separate electrons as these elements. In a denser column, it is necessary to consider secondary scattering by nearby electrons of radar waves already once scattered by other electrons or else to use some approximation involving continuous media. We will not attempt to measure winds by using columns as dense as those usually called "overdense," which act as opaque reflectors of the radar waves. Furthermore, if we attempt to measure winds by using the brighter underdense meteors that may be affected by a resonant scattering effect dependent on the polarization of the incident wave and the orientation of the column (Kaiser, 1955), we will not use the early parts of the phase data that are affected by the resonance.

For underdense meteors, it is correct and convenient to divide the column into independent elements distributed along the column and to consider each element as located exactly on the column axis. The effective number of electrons in each element will then be variable; in an underdense column, the effective number decreases exponentially with time because the electrons diffuse away from the axis, so that echoes from electrons on different sides of the column become out of phase with each other and interfere. In a resonant column, the effective number may first increase and then decrease, and some phase shifts may be superposed, both depending on the polarization. Fortunately, whenever this phase shift is large, it takes a form that cannot arise from winds of the type considered below; so that we will know if it is significant in our results.

The phase of the radar echo from each element of the column, with respect to the phase of the transmitted wave, is determined by the distance from the radar station to the element (neglecting effects of resonance or of overdense trails). Consider first the case where the radar transmitter and receiver are at the same point; separate transmitter and receivers will be treated later.

Let the trajectory of the meteor be the x axis; and let the radar station lie on the negative y axis at a distance R, so that R is the minimum distance from the station to the meteor trajectory. The distance D from any point (x, y) to the radar station is

$$D = \left[(R+y)^2 + x^2\right]^{1/2} = R + y + \frac{x^2}{2R} - \frac{x^2 y}{2R^2} - \frac{x^4}{8R^3} + \ldots \quad . \qquad (1\text{-}1)$$

For the small values of y and moderate values of x to be used here, it will always be sufficient to limit equation (1-1) to three terms. The phase (now taken with respect to an element at the origin of coordinates and differing only by a constant from the phase with respect to the transmitted wave) is

$$\phi = \frac{4\pi}{\lambda}(D-R) = \frac{2\pi x^2}{\lambda R} + \frac{4\pi y}{\lambda} \quad . \qquad (1\text{-}2)$$

Atmospheric winds will have negligible effect on the meteoroid but will carry the ionized column away from the meteor trajectory. Only the component of the wind along the y axis (i.e., along the radar beam) need be considered. We will assume that the radial component of the wind depends linearly on x within the part of the ionized column that reflects radar waves to any one receiving station. This assumption is necessary because it will not usually be possible to derive sufficient information from the received echo to specify any more complicated wind field. In particular, we do not resolve wind variations within the principal Fresnel zone, roughly 1 km long. It is also a convenient assumption because it makes the analysis comparatively simple and because the resultant description of the radial wind is very well suited for further processing. Ultimate justification for the assumption

must come from our results, but the observed absence of turbulence at the heights where we measure (Layzer and Bedinger, 1969) supports our use of the assumption. Accordingly, let the radial wind speed be of the form

$$\dot{y} = a(x - x_w) \text{ m sec}^{-1} \tag{1-3}$$

so that a represents the wind shear (m sec^{-1} m^{-1}, or radian sec^{-1}) and x_w represents a point (perhaps extrapolated) on the trajectory where there is no radial wind. Let time t be measured from the moment when the meteoroid passes the origin; then the coordinates of the meteoroid are (Vt, 0) where V is its velocity.

The y coordinate of any element of the column can then be found from its radial speed and the interval τ since it was generated by the meteoroid:

$$\begin{aligned} y &= \dot{y}\tau \\ &= a(x - x_w)(t - x/V) \\ &= -\frac{a}{V}\left[x^2 - (x_w + Vt)x + x_w Vt\right] \quad . \end{aligned} \tag{1-4}$$

Equation (1-4) shows that the ionized column takes a time-dependent parabolic form.

The phase of the echo from an element at x is found by substituting (1-4) into (1-2) as

$$\phi = \frac{2\pi}{\lambda R}(1 - 2\,aR/V)\left[x + \left(\frac{aR(t + x_w/V)}{-1 - 2aR/V}\right)\right]^2 \quad .$$

$$- \frac{2\pi a^2 R}{\lambda}\left[\frac{(t + x_w/V)^2}{1 - 2aR/V} + \frac{2x_w t}{aR}\right] \tag{1-5}$$

(which corrects equation (17) of Southworth, 1962). It is convenient to define a parameter α that represents the importance of the wind shear (discussed further below) as

$$\alpha \equiv \frac{aR}{V} \tag{1-6}$$

and to rewrite (1-5) as

$$\phi = \frac{2\pi}{\lambda R}(1 - 2\alpha)\left[x + \left(\frac{\alpha}{1 - 2\alpha}\right)(x_w + Vt)\right]^2$$

$$- \frac{2\pi}{\lambda R}\alpha\left[\left(\frac{\alpha}{1 - 2\alpha}\right)(x_w + Vt)^2 + 2x_w Vt\right] \quad . \tag{1-7}$$

The second line of (1-7) is independent of x and therefore applies directly to the phase of the integrated radar echo (from all the elements at all values of x). Remarkably, the first line of (1-7) is the phase that would be observed if the station were in fact at a different distance from the meteor and moving, with coordinates

$$\left[-\frac{R}{1 - 2\alpha}, -\left(\frac{\alpha}{1 - 2\alpha}\right)(x_w + Vt)\right] \quad . \tag{1-8}$$

Thus, the amplitudes (which are determined by the first line of (1-7)) have the form of the Fresnel pattern of a meteor of velocity V′ that crosses the specular reflection point at a time δt after the real meteor does, where

$$V' = V(1 - \alpha)(1 - 2\alpha)^{-1/2} \tag{1-9}$$

$$\delta t = \frac{-\alpha x_w}{(1 - \alpha)V} \quad . \tag{1-10}$$

Measuring time t′ from the apparent crossing of the specular reflection point, we have

$$t' = t - \delta t = t + \frac{\alpha x_w}{(1 - \alpha)V} \quad . \tag{1-11}$$

The second line of (1-7) represents a variation in phase superposed on the normal Fresnel variation and is the observable phase variation due to wind. Denoting this observable wind phase by Φ, we have, in terms of V' and t',

$$\Phi = \frac{-2\pi}{\lambda R}\left(\frac{a}{1-a}\right)^2 (V't')^2 - \frac{4\pi}{\lambda R}\left[1 - \left(\frac{a}{1-a}\right)^2\right]\frac{a x_w}{\sqrt{1-2a}}\, V't'$$

$$+ \text{constant} \quad . \tag{1-12}$$

Observation of the Fresnel pattern in amplitude yields V' and t' (i. e., the origin of t' in the system used for observing time). The quantities R and λ are already known; thus, observation of the phase yields the coefficients

$$\left(\frac{a}{1+a}\right)^2 \quad \text{and} \quad \frac{a x_w}{\sqrt{1-2a}} \quad . \tag{1-13}$$

These furnish the necessary factors for correcting the apparent velocity and time of passing the specular reflection point, since

$$\frac{V}{V'} = \left[1 - \left(\frac{a}{1-a}\right)^2\right]^{1/2} \tag{1-14}$$

and

$$\delta t = -\left(\frac{1}{V'}\right)\frac{a x_w}{\sqrt{1-2a}} \quad . \tag{1-15}$$

The actual geometry of the ionized column is quite different from the geometry that would be deduced directly from the apparent Fresnel pattern or from the geometry when there is no wind shear. The curvature of the ionized column is 2a times the curvature of the radar wavefront. To have only a single point of tangency (specular reflection point) between the wavefront and the column, we must have

$$2a < 1 \quad . \tag{1-16}$$

Other cases will give very anomalous Fresnel patterns, which can easily be rejected. Previous observations of winds at meteor heights show that the most probable value of a is of the order of ± 0.1 but that occasional meteors may not satisfy inequality (1-16).

The actual point of tangency between the radar wavefront and the ionized column (produced if necessary) is at

$$x_0 = -\left(\frac{a}{1 - 2a}\right)(x_w + Vt)$$

$$y_0 = (a - 1)\, x_0^2/R - a x_w Vt/R \quad , \tag{1-17}$$

which describes a parabola concave toward the station. The negative coefficient of t^2 in the first term of equation (1-12) is the result of this parabola.

When the Fresnel oscillations are empirically smoothed out, the remaining phase Φ and amplitude A variations refer to the principal Fresnel zone centered on the moving point $(x_0\ y_0)$. Irregularities in the ion column within the length of the principal Fresnel zone are averaged out; its length is

$$F = \sqrt{\frac{R\lambda}{1 - 2a}} \quad , \tag{1-18}$$

which is the order of 1 km.

Observations of the wind phase at a station yield the value of the wind at one point, and also two possibilities for the derivative of the wind, as follows. The observed coefficients of t and t^2 in (1-12) give the values of

$$G = \left|\frac{a}{1 - a}\right|$$

$$H = \frac{V}{V'}\,\frac{a x_w}{\sqrt{1 - 2a}} = \frac{a x_w}{1 - a} \quad , \tag{1-19}$$

whence either

$$a = VG/R(1 + G) \quad x_w = H/G \quad , \tag{1-20a}$$

or

$$a = -VG/R(1 - G) \quad x_w = -H/G \quad . \tag{1-20b}$$

The value of the wind at one point

$$x = -H \quad \dot{y} = -HV/R \tag{1-21}$$

is common to both (1-20a) and (1-20b); this is the point where the moving meteor crosses the point of tangency between the radar wavefront and the ionized column; i. e., it is the actual specular reflection point.

The derivative a of the wind is primarily useful for interpolation between the points observed by different stations. It will generally be necessary to interpolate in order to measure two components of the wind (with use of observations from one of the distant stations), and it is helpful to be able to interpolate when the general wind field is being delineated. When the ambiguity between (1-20a) and (1-20b) is significant — that is, when $|a|$ is appreciable — there are two methods for resolving it: by neighboring wind measures, or by the diffusion constant. On any meteor trail, reflection points from adjoining stations in our network differ by less than 3 km in height, and frequently by much less. It appears from other observations (e. g., Bedinger et al., 1968; Greenhow and Neufeld, 1959) that the derivative of the wind with height reverses sign in more than 3 km in height, on the average. Consequently, we can usually resolve the ambiguity by selecting the derivative that makes a better fit to neighboring measures.

Diffusion offers a second way to resolve the ambiguity. We regularly use the exponential decay of the amplitude A of the echo from the principal Fresnel zone to measure the rate D of diffusion of the electrons away from the axis of the ion column. Taking into account the shift of the principal

Fresnel zone to a part of the ion column with a different age and electron density, we have

$$D = \left(\frac{\lambda}{4\pi}\right)^2 \left[(\alpha - 1)\frac{1}{A}\frac{dA}{dt} + 0.921034\left(\frac{\alpha}{1 - 2\alpha}\right)\frac{dM}{dt}\right] \quad . \qquad (1\text{-}22)$$

Here dM/dt is the slope of the "ionization curve" representing the electron line density generated by the meteoroid as a function of time in terms of the meteor's "radar magnitude" M,

$$M = 40 - 2.5 \log_{10} q \quad , \qquad (1\text{-}23)$$

where q is the electron line density per meter. The slope dM/dt is determined by combining magnitude data observed at different stations. Since D is known as a function of height in the atmosphere, the value of α can be selected as the one that makes (1-22) give a better fit. However, it is preferable to select the values of α at different stations on one meteor to give the best fit to the logarithmic derivative of D with respect to height, since both this derivative and the differences of height between stations are better known than individual values of D or height. As Section 2 of this report will show, it is also necessary to be sure that recombination has not distorted the observed value of D. Since we have only recently learned the importance of recombination, we have not yet formulated exact methods for being sure that it is not present in practical cases. Consequently, we do not now use diffusion to resolve wind ambiguities, but it appears from particular examples that diffusion will be very useful for this purpose in the future.

The case where the transmitter and the receiver are at different sites is very similar to the case where they are at the same site, particularly for the meteors observed on this project. The essential difference is that the wind component observed is the component along the direction bisecting the angle between the directions from the two stations to the specular reflection point. Stations 1 to 6 and their antenna beams are so arranged that the distance along an observable meteor track between the feet of perpendiculars

dropped from station 3 (the transmitter) and any other station cannot generally exceed 15 km. The specular reflection point is roughly halfway between these perpendiculars. Since echoes at stations 7 or 8 will be analyzed only when they are reflected from parts of the meteor track observed at other stations, perpendiculars from stations 7 or 8 will also be within 15 km of the perpendicular from station 3. In these circumstances, equation (1-2) and all subsequent developments remain valid with three substitutions: (a) the origin of x and ϕ is shifted to the new specular reflection point; (b) the perpendicular distance R from the station to the track is replaced by the harmonic mean of either the perpendicular distances from the two stations or the distances of the stations from the specular reflection point; and (c) the wind displacement y is replaced by $y \cos(\psi/2)$, where ψ is the angle between the directions from the stations to the specular reflection point.

1.3.2 Geometrical reduction

This section outlines the principles and procedure for finding a meteor's position and vector velocity from observed data.

The amplitude and phase of the Fresnel pattern generated by a meteor of constant magnitude, without diffusion, can be expressed in terms of the Fresnel integrals of classical analysis (e.g., McKinley, 1961); but numerical integrations are necessary to predict the effects of diffusion or varying magnitude (Loewenthal, 1956; Southworth, 1962). When, as with our stations, the "range" (distance to the meteor trail) is much larger than the distance between the transmitting and the receiving stations, it is convenient and entirely adequate to use the concept of an "effective station." This is the position that would receive the same signal by direct backscatter as the actual receiving station receives by forwardscatter at a small angle; it is located on the bisector of the angle between lines joining the specular reflection point with the transmitting and the receiving stations, and its range R from the meteor is the harmonic mean of the transmitting and receiving ranges. The position and speed of the meteor are deduced primarily from the times of the maxima and minima (collectively, "extrema") of the Fresnel

pattern; diffusion, radar magnitude, and other physical quantities are deduced primarily from the amplitudes of the extrema. The times of the extrema are the times when the meteoroid is at known multiples of the length F (equation (1-18)) of the "principal Fresnel zone" from the specular reflection point. From the numerical integrations cited above, we find that the "known multiples" depend on apparent diffusion, but not much on other likely events. Diffusion shifts maxima earlier and minima later than in a pattern without diffusion. However, the time of the first maximum also depends on the slope of the ionization curve (Southworth, 1962, Table 3). From the integrations, an empirical expression for the distance x_1, from the specular reflection point to the point corresponding to the first maximum of the Fresnel pattern is

$$F(0.861 - 1.535C + 2.75C^2 - 3.0C^3 + CS/\sqrt{2})/\sqrt{2} \quad , \qquad (1\text{-}24)$$

where S is the slope of the ionization curve in magnitudes per length F, and C is Loewenthal's "decay constant":

$$C = \frac{8\pi D}{\lambda^2 V}\sqrt{\frac{\lambda R}{2}} = T_F/2\sqrt{2}\,\pi\,T_D \quad . \qquad (1\text{-}25)$$

Here, D is the diffusion constant, V is the meteor's velocity, T_F is the time for the meteor to cross the principal Fresnel zone, and T_D is the time for the voltage amplitude of the signal to decay by a factor e under diffusion. Equation (1-24) replaces the approximation given in Southworth (1962), which was vulnerable to distortion of amplitudes by fragmentation of the meteoroid.

Unpublished analytical developments by Southworth (1962) show that the amplitudes of the Fresnal patterns may be quite accurately analyzed by smoothing out the oscillations and then regarding the smoothed curve as denoting the decaying amplitude from the principal Fresnel zone, and the oscillations from the smoothed curve as denoting the amplitudes of the later Fresnel zones as each is formed. Such an analysis yields C, S, and the radar magnitude at the specular reflection points and at the extrema. It also yields the phase corrections necessary for wind measurements in the Fresnel pattern. Further uses are described in Section 2.

The "radiant" (named for the point in the sky from which visual shower meteors appear to radiate) is the direction opposite to the direction of motion of a meteor and is the common way to denote the direction of motion. Evidence for the radiant is found in the time intervals between crossings of different specular reflection points, seen as time intervals between beginnings of Fresnel patterns. The distance traveled by the meteoroid in a given time interval is known from the velocity (found from the spacing of Fresnel oscillations). This distance is the projection of the distance between the corresponding effective stations onto the meteor trajectory. Given at least two such projections from noncolinear interstation distances, the radiant is determined.

The position in space of the specular reflection point from station 3 (the transmitting station) is determined from the radiant, the range (directly measured), and difference in phase between the signals received at the two halves of the antenna at station 3. The difference in phase determines the angle between the direction from one-half of the antenna to the other, and the direction to the meteor. There is an ambiguity between two or three possible values of the angle, which can nearly always be resolved by requiring the meteor to be in the antenna beam and at a plausible height; any doubtful cases are discarded.

The reduction procedure begins by treating the range observations, i. e., the observed time intervals between the transmission of a pulse and its return to station 3 via the meteor, or via the meteor and another station. Discrepant values are discarded, and one average loop range formed for each station with range measures.

The observed (amplitude) Fresnel patterns are measured by a specially devised semiempirical pattern-recognition program. This finds the time and amplitude of each extremum, thus giving the same data as we previously read from analog film records. The program uses the spacing of extrema found at one station to predict the spacing at others. If it fails in an attempt

to measure the pattern at any station, it will try again when it gets a better prediction from some other station. The oscillations from a smoothed curve are found for each pattern.

The wind phase Φ is next measured at each station for which an amplitude pattern was measured. The recorded phase data are an analog representation of s = amplitude $\times$ sin (phase) at odd pulses, and c = amplitude $\times$ cos (phase) at even pulses. (These are the outputs of the phase detectors.) Initially, the missing alternate values are interpolated. For a first approximation to the phase variation, the phases are found at the Fresnel maxima, multiples of 2π being added where necessary for continuity. These are then fitted with an expression of the form

$$\Phi = E_0 + E_1 p + E_2 p^2 \quad , \tag{1-26}$$

where p is the pulse number (measuring time). Next, the phase at each observed pulse after the first maximum is corrected for the oscillating part of the Fresnel pattern by subtracting a rotating vector

$$\left.\begin{aligned} s_{corr} &= s - C_F \sin(\phi_F + E_0 + E_1 p + E_2 p^2) \\ c_{corr} &= c - C_F \cos(\phi_F + E_0 + E_1 p + E_2 p^2) \\ \tan\phi_{corr} &= s_{corr}/c_{corr} \quad . \end{aligned}\right\} \tag{1-27}$$

Here, C_F is the amplitude of the oscillating part, interpolated between extrema; and ϕ_F is the phase of the oscillating part, defined to be 0 at the first extremum, π at the second, 2π at the third, etc., also interpolated. The corrected phases are fitted with (1-26), and the process then iterated once more. If E_2 is inadequately determined or significantly positive, it is rejected, and

$$\Phi = E_0 + E_1 p \tag{1-28}$$

is fitted instead.

The amplitude Fresnel pattern is next analyzed at each station by using a provisional value of the range. This yields velocities and times at specular reflection points, for the geometric reduction proper, as well as various physical data such as diffusion.

The geometric reduction proper (determining the position and velocity) follows next; it proceeds by iteration. First, the effective station positions are estimated. Next, the velocities and times at specular reflection points are corrected by using (1-14) and (1-15). Then, the velocities V and times t are fitted to an expression of the form

$$V = B + C\overline{K} \exp(\overline{K}t) \quad . \tag{1-29}$$

Whipple and Jacchia (1957) have shown that this form is suitable for the analysis of photographic (Super-Schmidt) meteors. Since it does not yet appear practical to attempt to evaluate $\overline{K}$ from individual radar meteors, we use a value characteristic of faint photographic meteors — namely, 5/4 of the value expected for unfragmenting meteoroids in an exponential atmosphere. Accordingly,

$$\overline{K} = 1.25\, \overline{V} \cos Z_R / 5.3 \quad , \tag{1-30}$$

where $\overline{V}$ is the mean observed velocity, Z_R is the zenith distance of the radiant, and the atmospheric scale height is taken to be 5.3 km. We do not impute great accuracy to (1-29), but consider that it is a more reasonable bridging formula than most others, especially polynomials. The distances between specular reflection points are now found by integrating (1-29), and the radiant fitted to these and the effective stations. Finally, the specular reflection point from station 3 is found by fitting the position of the whole trail (not varying the radiant) to the difference of phase at station 3 and to all observed ranges.

Successive iterations begin by computing the effective stations using the newly computed position of the trail and continue by correcting velocities for the difference between the original provisional ranges and the latest values. The iteration is carried to convergence (or failure).

Throughout the reduction, it is general practice to "fit" by least squares and to carry an estimate of the uncertainty of nearly every quantity deduced. This estimate is kept as realistic as possible and usually depends on both the internal scatter in a least-squares fit and the previously estimated uncertainties of the data fitted. In case of doubt, we try not to underestimate the errors.

1.3.3 Wind profiles from individual meteors

This section describes the computation of profiles of the horizontal radial component along individual meteor trajectories and of wind values normal to the radial direction.

Winds are computed in a rectangular coordinate system whose origin is at sea level, 100 km horizontally from station 3 in the direction of the antenna beam – namely, 113° east of true north. The Z coordinate is measured vertically from that point; the X coordinate horizontally in the prolongation of the antenna beam; and the Y coordinate horizontally at right angles to X and Z, in a generally north-northeast direction. The great majority of our wind data are collected within, say, 30 km horizontally from the origin of these coordinates. "Horizontal" winds are defined as winds parallel to the X–Y plane; thus, they may be up to about 1/3 degree from the true local horizontal. "Radial" winds are defined as winds in a vertical plane containing station 3, positive to the east and southeast. "Cross" winds are defined as winds in a vertical plane normal to a vertical plane containing station 3, positive to the north and northeast. However, when there are insufficient data to determine both radial and cross wind components at a given point, any wind component measured at stations 1 to 6 will be regarded as a radial component. This coordinate system has been chosen to be suitable

for the data in an intermediate stage of processing, not for examination of results. When there are sufficient data, the final results can be expressed in any convenient scheme.

In computing a wind profile from an individual meteor, we invariably assume that there is no vertical component to the wind and transform all observed wind components to horizontal wind components on that assumption. However, we retain information for studying vertical components by combining more than one meteor; this is described further on.

The quantities used in computing a wind profile are the meteor trajectory (one point and the radiant), the corrected positions of the specular reflection points and the corrected velocities at those points (both corrected for wind), the phase coefficients E_0, E_1, E_2 (equation (1-26)) at each station, and expected errors of all these. The phase coefficients are reduced to wind components by (1-19) and (1-20) (x_w is measured from the specular reflection point) and by projection onto a horizontal plane. When there is an ambiguity at a station (when E_2 was accepted), it is resolved by comparing the errors of fit of both alternatives to the unambiguous wind values found from (1-21). Here we compute both the sum of the squared errors and the sum of squared errors expected from the prior estimates of the wind uncertainties. Furthermore, we give high weight to errors within the portion of the trajectory occupied by the principal Fresnel zone during the wind-phase measurement (equations (1-17) and (1-18)) and rapidly decreasing weight outside that portion; the two alternatives correspond to different portions of the trajectory. Comparing the observed errors with the expected errors, we estimate the separate probabilities of the alternatives. The more likely alternative is then chosen, but its estimated squared error is increased by the squared difference between the alternatives multiplied by the relative probability of the rejected alternative.

A profile of horizontal radial wind is now constructed by using all observations from stations 1 to 6. Each linear "profile" (a, x_w) observed at a particular station is replaced by four points lying on the linear profile

and spread over the part of the trajectory occupied by the specular reflection point during wind-phase measurement. Then, at each integral kilometer in height within the part of the trajectory where winds were measured, a cubic polynomial in distance along the trajectory is fitted to whatever wind points are near that height. The weights assigned these points depend on their estimated uncertainties and decrease rapidly for points away from the height in question. The tabular wind at each height is then taken from the cubic centered at that height.

For each tabular value of horizontal radial wind, we also compute the interpolated effective station position. This defines the actual direction of the measured radial wind component, as averaged in the process of combining data from different stations to make one profile. This "interpolated station" is computed by finding the effective position of each station (as defined in Section 3.2) and then fitting these positions with a linear expression in distance along the trajectory at the same time and with the same weights, as a cubic is fitted to the winds (described above).

One or more values of horizontal cross wind are computed when there is a reliable wind measure (E_2 accepted) from station 7 or 8 at a height within the profile of horizontal radial wind and within the portion of the trajectory occupied by the principal Fresnel zone from that station during wind-phase measurement. At each such height, we have two horizontal wind measures, one from the effective position of station 7 or 8, and one from the interpolated effective station position for that point on the profile. These are combined vectorially to yield the radial and cross components, and the newly found radial component replaces the less exact value in the profile.

To determine vertical wind components, we will try to take advantage of the baseline represented by the separation of our stations 1 and 2 from stations 5 and 6, as well as the two baselines between stations 7 or 8 and our remaining stations. When the baseline 1-2-5-6 is used, we still need to have two meteors nearly at the same point at nearly the same time, but we need have measures from station 7 or 8 on only one of the meteors. For

this purpose, we compute interpolated station numbers, corresponding to interpolated effective station positions, for effective positions between stations 1 and 2, or 5 and 6. We use these numbers to mark suitable wind values and to convey the effective station positions to the computation that combines data from different meteors.

1.3.4 Wind field computed from many meteors

The bulk of our wind observations occur in a volume defined horizontally by the antenna-gain pattern and vertically by the occurrence of meteor trails. The horizontal extent is, roughly, 50 km in the X direction and 30 km in the Y direction; the vertical extent is roughly 20 km (see Figure 2-1 in Section 2). At peak rates, several hundred meteors per hour are observed in this volume. The computer can readily average and smooth all these data, but we must first decide upon the resolution in space and time.

A vertical resolution of 1 km has been chosen because: 1) it seems appropriate to the scale of wind irregularities observed by rocket wind measures, 2) it is approximately the accuracy of the radar height measures (so that a finer resolution would fail), and 3) it is approximately the height resolution in the individual radar wind profiles. Here we estimate the resolution in individual profiles from the vertical separation of adjacent specular reflection points, which is always less than 3 km and has a mode near 1 km, and from the loss of any resolution within the principal Fresnel zone, which has a vertical extent approximately from 0.1 to 0.5 km. The vertical resolution is also now fixed by our data formats.

Unlike the vertical resolution, the horizontal and temporal resolutions are not yet fixed, and the computer program will use whatever resolution we ask. With one or two thousand radial wind values per hour (at 1-km vertical resolution), we can resolve a few hundred cells in space-time. The natural scale for horizontal variation seems to be a hundred or more kilometers, and for temporal variation to be an hour or perhaps less. If we try for fine spatial resolution, we can select, say, a 10-km horizontal

interval and a 20-min time interval; if we look for fine time resolution, we might choose a 30-km horizontal interval and a 1-min time interval. At less than peak measurement rates, we should not choose resolutions this fine, and it will always be necessary to use lower resolution for cross winds.

The computation of the wind fields begins with the radial and cross wind values computed from many meteors in a defined interval of time. Each 1-km interval in height is treated independently. The tabular intervals in horizontal position and in time are specified in advance for each computation. At each point in the X – Y time grid, a value of horizontal radial wind is computed if there are six or more measures within the eight neighboring cells in X – Y – time space. The value is found by fitting a linear expression in X, Y, and time to the measures and taking its value at the tabular point. Similarly, a value of cross wind is computed if there are six or more cross wind measures. For convenience in later use, missing tabular values are then interpolated if there were at least six adjacent tabular values determined. The interpolation uses the same fitting procedure, starting with the tabular values rather than measures; interpolated values are marked as such.

1.3.5 Three-dimensional wind measures

Whenever in the course of tabulating the wind field we find that any one space-time cell contains either cross wind measures from both stations 7 and 8 or a cross wind measure effectively from stations 1 to 2 or 5 to 6 and a radial wind measure from 5 to 6 or 1 to 2, respectively, a vertical wind component will be computed. First, the error in relative height between the two meteors will be eliminated as accurately as possible by matching their horizontal radial profiles. Then, all the relevant observed components will be transformed back to the original radial observations from different effective stations and combined vectorially (by least squares where possible) to find three components of the wind. More advantageous solutions will be possible when more than two meteors are available.

1.3.6 Expected wind-measurement accuracies

It is certain that the accuracy of measurement will vary widely from one measure to another, and the computer programs have been carefully planned to give as realistic an estimate of the errors as possible in each case. We will here only attempt to predict some typical accuracies.

The basic phase accuracy per pulse will be of the order of 0.05 to 0.1 rad, limited mostly by noise and digitizer resolution for weak pulses and by saturation and Fresnel corrections for strong pulses. In a typical observation lasting 0.1 sec (74 pulses) with only partly random errors, the phase-rate accuracy is of the order of 0.3 rad/sec, corresponding to 1.0 m/sec radial wind at our wavelength and to 1.2 m/sec horizontal radial wind.

Interpolation of the wind between specular reflection points (construction of a wind profile) adds considerable error, depending on the second and higher derivatives of the wind with height, but perhaps typically 3 m/sec.

Cross wind measures always use interpolated wind values and must be computed by combining two vectors at an angle of about 0.15 rad. Consequently, their typical error will be 20 m/sec.

Combination of the data from different meteors to evaluate the wind field will tend to increase the apparent errors of the horizontal radial wind because the errors in height (1 km) combined with typical wind shears (0.01 sec^{-1}) will appear as errors in the wind (10 m/sec). However, the errors in tabular mean values will be smaller, perhaps 5 m/sec. Combination of cross winds, when there are sufficient data, will tend to decrease the errors to 10 or 15 m/sec.

The typical error in a vertical wind component when only two meteors are used will be similar to the error in a single cross wind. Interpolating errors in two matched profiles should partly cancel to give a relative error of 2 m/sec, but this must be divided by an angle of about 0.1 rad. Combining four meteors, the typical error would perhaps be 10 m/sec.

1.4 Examples of Results

Figure 1-4 shows a few recently computed profiles of horizontal radial wind.

The downward progression of the profiles with time is highly suggestive of the presence of a gravity wave.

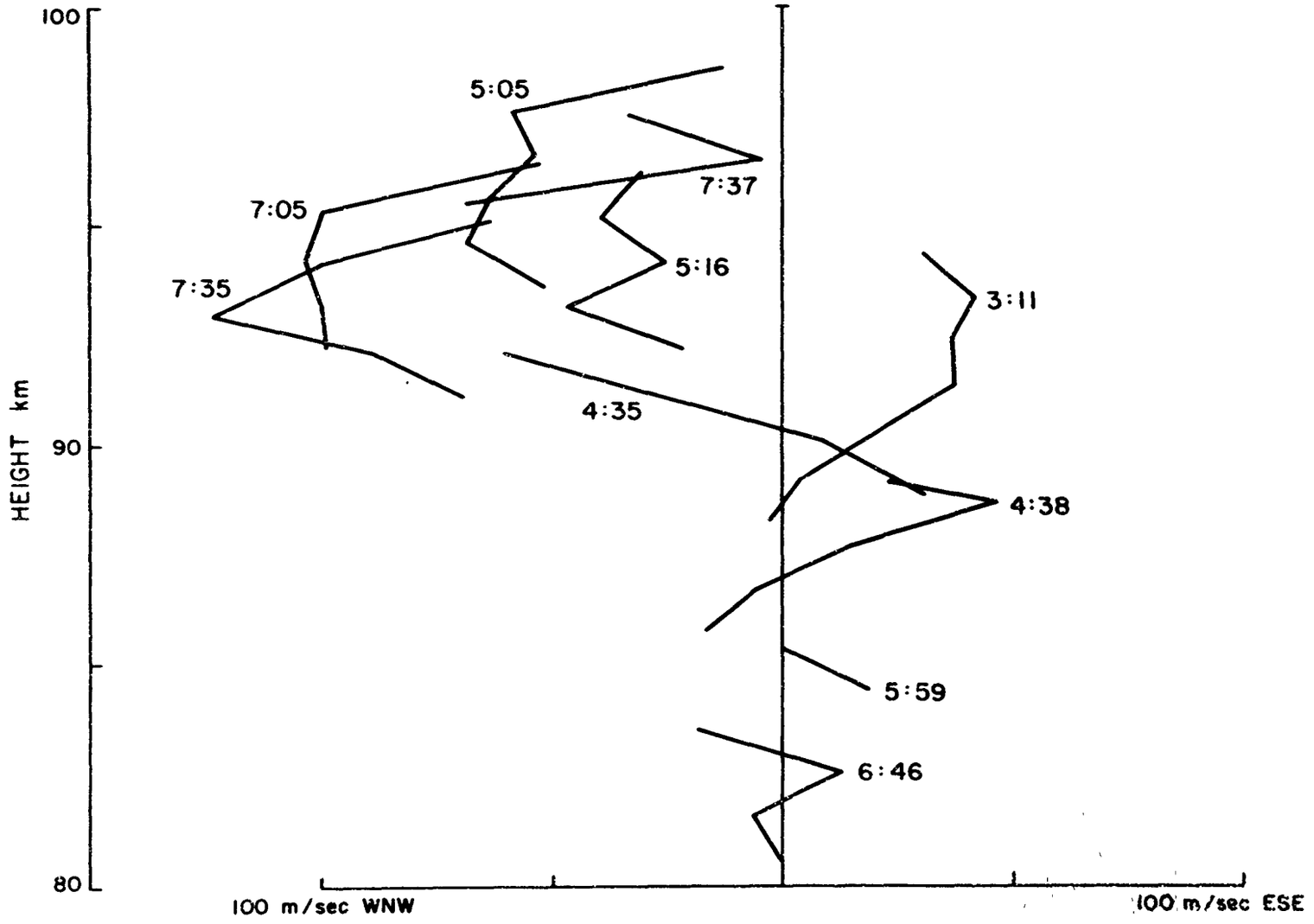

Figure 1-4. Wind profiles, over Decatur, Illinois on the morning of 25 August 1969. (Labeled in Central Standard Time)

2. DENSITY, PRESSURE, TEMPERATURE, AND SCALE-HEIGHT MEASUREMENTS

2.1 Introduction

Radar echoes from underdense meteor trails characteristically exhibit a nearly exponential decay in echo strength caused by ambipolar diffusion of the ions and electrons.

Other effects are superimposed on the decay, such as Fresnel oscillations at the beginning of the echo and sometimes beats between multiple reflection points toward the end of an echo; but it is usually possible to measure the rate of decay approximately and often possible to measure it to within a few percent. If the meteor's distance and velocity are known, one can then deduce the diffusion rate and hence (very nearly) the atmospheric density. If, furthermore, the meteor's height is known, this constitutes at least a potentially useful measure of the atmosphere. Conversely, if one assumes atmospheric density as a function of height, an observation of diffusion yields the height of the meteor. Both approaches have often been taken.

The Radio Meteor Project observes apparent diffusion rates at several points on the trails of meteors. This section describes our studies on the feasibility of measuring atmospheric density by observing diffusion in radar meteors.

2.2 Organization of this Section

We have learned that there are significant difficulties in the interpretation of apparent diffusion rates. The next two subsections describe two techniques for analysis of our data: quantitative analysis of Fresnel patterns from individual meteors and statistical analysis of diffusion heights from

many meteors. The next several subsections describe results on several aspects of meteor physics and end with an example showing that recombination in the ionized column is a very important source of systematic error in atmospheric-density measures from meteors. Subsection 2.11 then discusses the random errors in density measurements that are caused by wind shears. Finally, subsection 2.12 contains our conclusions on the feasibility of density measurements from meteors.

2.3 Fresnel-Pattern Analysis

Since the installation of equipment to calibrate all amplitudes of received meteor echoes, we can rely upon physical properties that we deduce from the amplitudes. Earlier, we could consider these properties only very cautiously and only in statistics from large numbers of meteors.

Theoretical Fresnel patterns computed by Southworth (1962) depend on diffusion rates and ionization curves. "Diffusion" is ambipolar diffusion of the ions and electrons away from the axis of the ionized column left by the meteoroid. Diffusion causes an exponential decay of echo strength with time in underdense meteor trails, i. e., when multiple scattering of the radar wave by the electrons can be neglected. The "ionization curve" is the distribution of the electrons along the meteoroid's trajectory. Our analysis fits a smooth curve between the maxima and minima (collectively called "extrema") of observed Fresnel patterns and then treats the deviations of the extrema from this curve and fits an exponential to the curve. Further studies of the theoretical Fresnel pattern have shown that this method yields accurate values of diffusion and ionization when no other processes affect the observed amplitudes. The smooth curve measures the signal received from the principal Fresnel zone at the foot of the perpendicular from the observing station to the ionized column. The effective length of the principal zone is (neglecting wind shears)

$$F_0 = \sqrt{\lambda R/2} \quad , \tag{2-1}$$

where $\lambda = 733.1$ cm is the radar wavelength, and $R \sim 150$ to 300 km is the distance to the ionized column; F_0 is usually a little under 1 km. We measure this signal from the first minimum of the Fresnel curve at the time

$$t_{01} \approx 1.3\, F_0/V \tag{2-2}$$

after the passage of the meteoroid through the foot of the perpendicular (where V is the meteor velocity) to the last observed extremum but one, at the time

$$t_{02} \approx (F_0/V)\sqrt{n - 5/4} \tag{2-3}$$

(where n extrema were observed). The deviations from the smooth curve measure the amount of ionization in later Fresnel zones. Their effective lengths are

$$F_i \approx F_0/(\pi\sqrt{i - 3/4}) \tag{2-4}$$

(for the ith extremum, $i > 1$), and they are measured

$$t_i \approx F_0/(4V\sqrt{i - 3/4}) \tag{2-5}$$

after the meteoroid passes the center of the zone. Thus, we observe the ionized column at various intervals after its formation, from ~0.001 sec (t_i for a late zone of a fast meteor) to ~0.3 sec (t_{02} for a late zone of a slow meteor). Later observations are often possible, but they usually measure mostly wind effects.

We compute apparent diffusion rates and an ionization curve from Fresnel-pattern amplitudes of each observed meteor. Anomalies in the results then indicate additional effects to be investigated.

2.4 Diffusion Heights

We have begun analysis of heights computed from the measured diffusions for 13,672 meteors observed in 1962 to 1965. This analysis first became possible upon completion of corrections to the reductions. McKinley's (1961) expression of Greenhow and Neufeld's (1955) diffusion rates

$$\log_{10} D = 0.067\, h - 1.6 \qquad (2\text{-}6)$$

was used to find heights h, in kilometers, from apparent diffusion rates D, in square centimeters per second. Greenhow and Neufeld's result was chosen because it is in harmony with atmospheric models, not because it seemed a good determination. (We believe that their statistical analysis is faulty because selection effects were ignored.) Greenhow and Hall's (1960) more careful diffusion measures are vitiated by recombination, as we discuss later. We will show the effect of recombination on our diffusions below; it is small for many of the relatively faint meteors that we observe.

We observe apparent diffusion at three to seven different points on each meteor trail and combine these values into a mean value of the diffusion height at the maximum of the ionization curve of each meteor. We also find an internal standard error of that height, the apparent atmospheric scale height, and its standard error. Representative distributions of these errors are shown below in subsection 2.10. In the present statistical analysis, we use the errors primarily to eliminate inconsistent and distorted data.

Figure 2-1 shows the distribution of diffusion height at the maximum of the ionization curve, as a function of the magnitude at the maximum, for 10,163 meteors. Figure 2-2 shows the same heights as a function of velocity at maximum ionization. Meteors whose standard error in height exceeded 4 km or that yielded an unreasonable scale height have been omitted. True height will differ from these diffusion heights by up to about 3 km, depending on height and probably also on time. True heights are not available for these

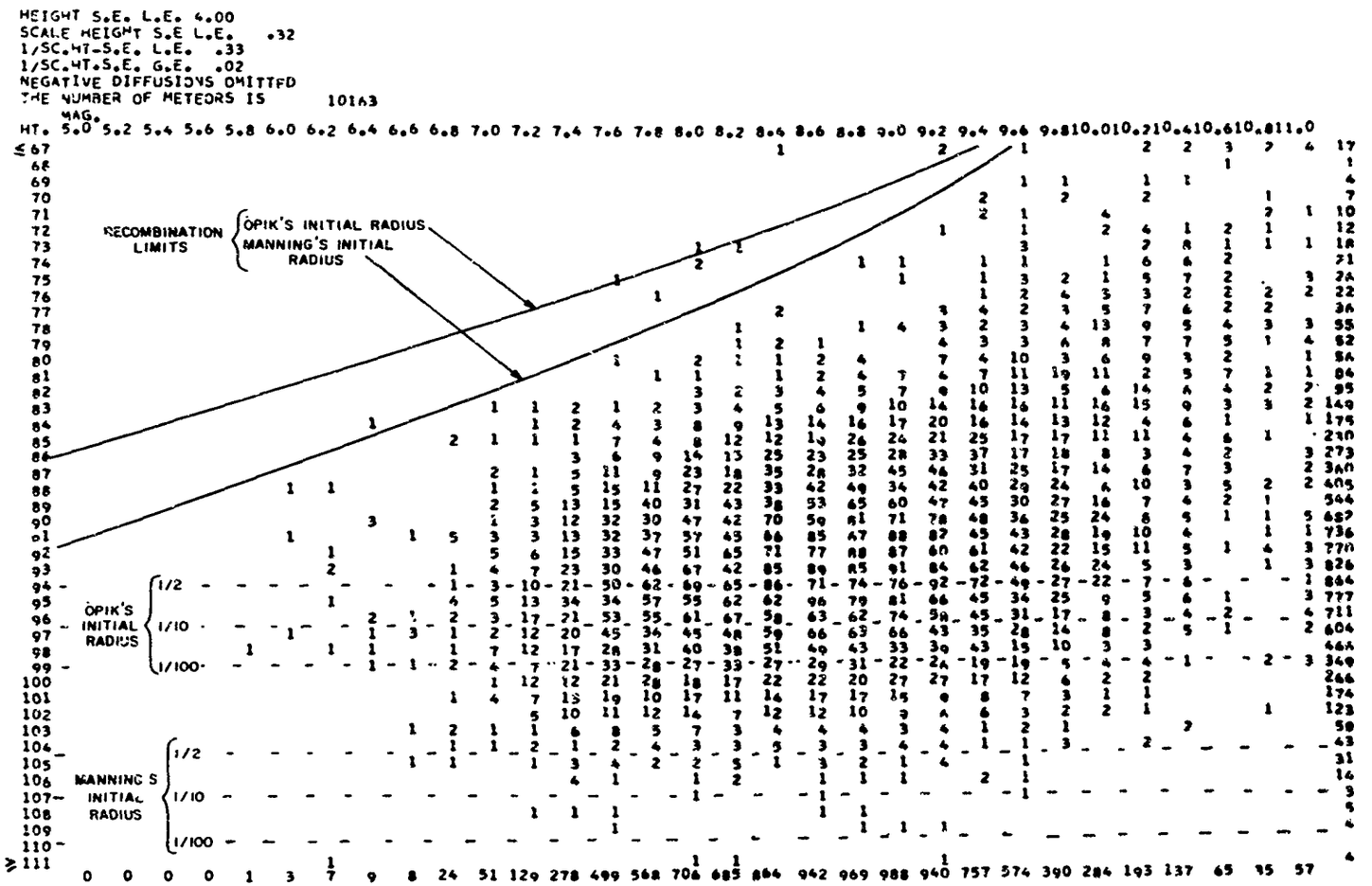

Figure 2-1. Diffusion heights at maximum ionization of 10,163 meteors, as a function of radar magnitude at maximum ionization. The recombination limits are from equation (2-15). The initial radius limit is shown for received voltage attenuations of 1/2, 1/10, and 1/100 (corresponding approximately to 1/2, 1/10, and 1/100 in number of meteors observed). Considering that the standard errors of these heights are 4 km or less, these are good fits to the recombination limit and initial radius limit using Manning's initial radius.

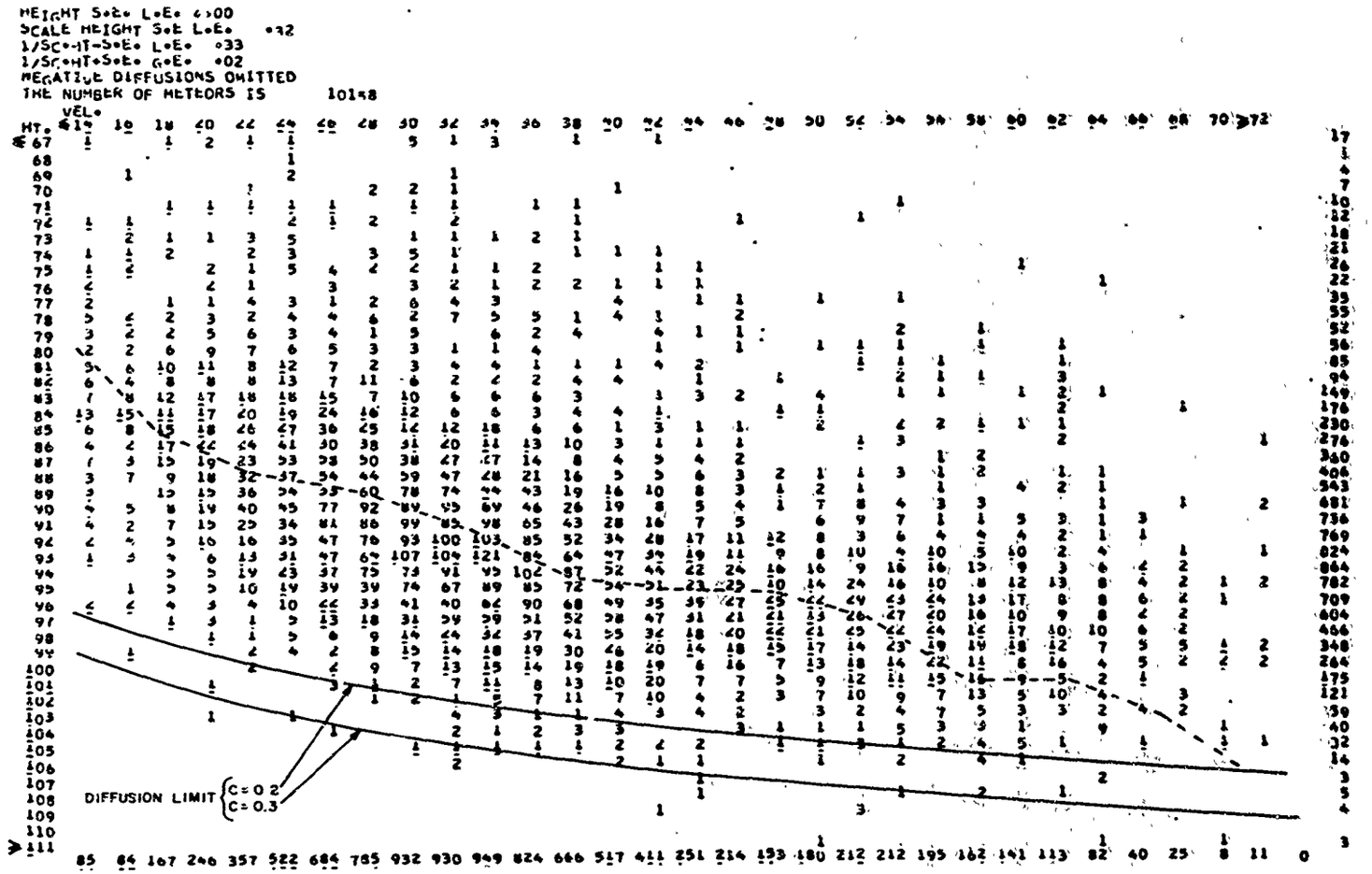

Figure 2-2. Diffusion heights of 10,163 meteors at maximum ionization, as a function of velocity at maximum ionization. The standard error of height is 4 km or less. The diffusion limit is computed by use of equation (2-7). The dashed line shows heights at maximum light of 361 Super-Schmidt meteors (Hawkins and Southworth, 1958).

meteors; but diffusion heights are preferable for the present purposes because we are examining effects that depend directly or inversely on atmospheric density, like diffusion, so that density changes with time do not smear the diagram.

2.5 Diffusion Ceiling

Rapid diffusion eliminates the second and later maxima in the Fresnel pattern, so that the pattern cannot be reduced. (With phase measures, it can be roughly reduced, but phase was not observed on these meteors.) Figure 2-2 includes curves for Loewenthal's (1956) constant

$$C = 8\pi DF_0/\lambda^2 V \quad , \tag{2-7}$$

which is the ratio of the amplitude decay time under diffusion to the time of crossing the principal Fresnel zone. Meteors with $C \leq 0.2$ can usually be reduced, and meteors with $C \geq 0.3$ usually cannot, depending on the ionization curve (Southworth, 1962). There is excellent agreement between the meteors and the predicted ceiling.

A different diffusion ceiling has eliminated a few high, faint meteors from the lower right-hand corner of Figure 2-1. We did not reduce Fresnel patterns with fewer than five extrema. Thus, we omitted meteors whose initial magnitude was above our minimum sensitivity but whose rapid diffusion pushed the magnitude below our sensitivity limit at or before the second minimum (the fourth extremum).

2.6 Initial Radius

The newly formed ion column must expand rapidly for a millisecond or so until it cools to ambient temperature. Manning (1958) and Öpik (1955) have published different estimates for the resulting "initial radius" of the column, both proportional to atmospheric mean free path. The initial radius places an abrupt ceiling on observations, and Figures 2-1 and 2-2 show heights

where echo amplitudes would be attenuated by factors of 0.5, 0.1, and 0.01 on both estimates. It is clear that Öpik's initial radius is too large, at least at our upper limit of height and for our range of magnitude. The observed height ceiling shows that Manning's radius is either correct or too small, since the diffusion ceiling could be the actual upper bound. However, we will find that Manning's radius is about right (at least at lower heights and for our magnitudes) when we consider recombination below.

2.7. Recombination

Recombination of the electrons in the ionized column has often been considered (see, for example, Öpik, 1955), but the uncertainties in the atomic and molecular species present and in the rate constants have made it difficult to predict. Further, recombination has not been recognized in the observations, so that it has been judged to be negligible (McKinley, 1961). More recently, however, a relatively high rate constant has been found for dissociative recombination of certain molecular ions. Mehr and Biondi (1969) have finally obtained reliable laboratory measures for dissociative recombination of the most likely molecules in the meteor environment, N_2^+ and O_2^+. If metallic ions, such as are seen in meteor spectra, are created first, we may plausibly expect fast charge transfer to the atmospheric molecules (Öpik, 1958). Then recombination can be expressed by

$$dn/dt = -\alpha n n_i \quad , \tag{2-8}$$

where n is the electron volume density, n_i is the volume density of ion species that recombine at rate α, and Mehr and Biondi's value of α is 3×10^{-7} cm^3 sec^{-1} for the ambient temperature at meteor heights. If all ions recombine at rate α, we have $n_i = n$. Here we will use

$$dn/dt = -2 \times 10^{-7} n^2 \quad , \tag{2-9}$$

allowing for other ions that do not recombine so fast and for some atmospheric heating that reduces the value of α.

If we neglect the effect of recombination on the radial distribution of electrons in the column, we can compute the effect of recombination on the total line density on the electrons as follows. The density at distance r from the column axis is taken to be exponential with radius ρ:

$$n = (q/\pi\rho^2) \exp(-r^2/\rho^2) \quad , \tag{2-10}$$

where q is the electron line density. Initially, we have $q = q_0$ the original line density, and $\rho = r_0$ the initial radius. The effect of diffusion (neglecting recombination) is

$$\rho^2 = r_0^2 + 4Dt \quad , \tag{2-11}$$

and the effect of recombination is

$$\frac{dq}{dt} = -\alpha \int_0^\infty n^2 \, dr = -\frac{\alpha q^2}{2\pi\rho^2} \quad . \tag{2-12}$$

When we combine equations (2-11) and (2-12),

$$\frac{dq}{q^2} = -\alpha \frac{dt}{2\pi r_0^2 + 8\pi Dt} \quad ; \tag{2-13}$$

then, integrating with respect to time, we find

$$\frac{1}{q} = \frac{1}{q_0} + \frac{1}{q_{lim}} \quad , \tag{2-14}$$

where

$$q_{lim} = \frac{8\pi D}{\alpha \ln[1 + (4Dt/r_0^2)]} \quad . \tag{2-15}$$

Numerical integrations (Southworth, to be published) have confirmed that equations (2-14) and (2-15) are a close approximation to more exact theory.

Measured values of D from radar meteors that are bright enough for recombination to be important will be too large because some of the observed amplitude decay is caused by recombination. For a given magnitude, this error increases with meteor velocity because fast meteors are observed sooner (equations (2-2) and (2-3)).

We have observed recombination in three ways. We first saw it in ionization curves derived as described in subsection 2.3. Figure 2-3 is an example. The digits represent radar magnitudes derived from the principal Fresnel zone (left-most digit) and later zones as observed at stations 2, 3, 4, and 6, all corrected for diffusion in the interval since the zone was formed. Recombination is seen in the upward slope of the first few digits for each station; these show that the electron line density appears greater when measured sooner after formation, even after correction for diffusion. (The later digits for each station show fragmentation, discussed in subsection 2.8.) It is not plausible that the ionization curve should have a bump just after the principal zone for each station, on this and on many other similar meteors. Some process that removes electrons from the column for only a few hundredths of a second is required, and recombination suits.

Our second observation of recombination is in the lower bound to heights in Figure 2-1. Radar magnitudes M are defined in terms of q (per centimeter) by Kaiser's (1955) relation

$$M = 35 - 2.5 \log_{10} q \quad . \tag{2-16}$$

Figure 2-1 shows curves of $M_{lim} = 35 - 2.5 \log_{10} q_{lim}$ using Manning's and Öpik's values of r_0 (exact values from Southworth, 1962) and t = 0.03 (an average time for the center of the measured part of the Fresnel pattern, for different velocities and lengths of Fresnel pattern). The upper bound (2-15) on observable radar magnitudes is well confirmed, as is Manning's initial radius.

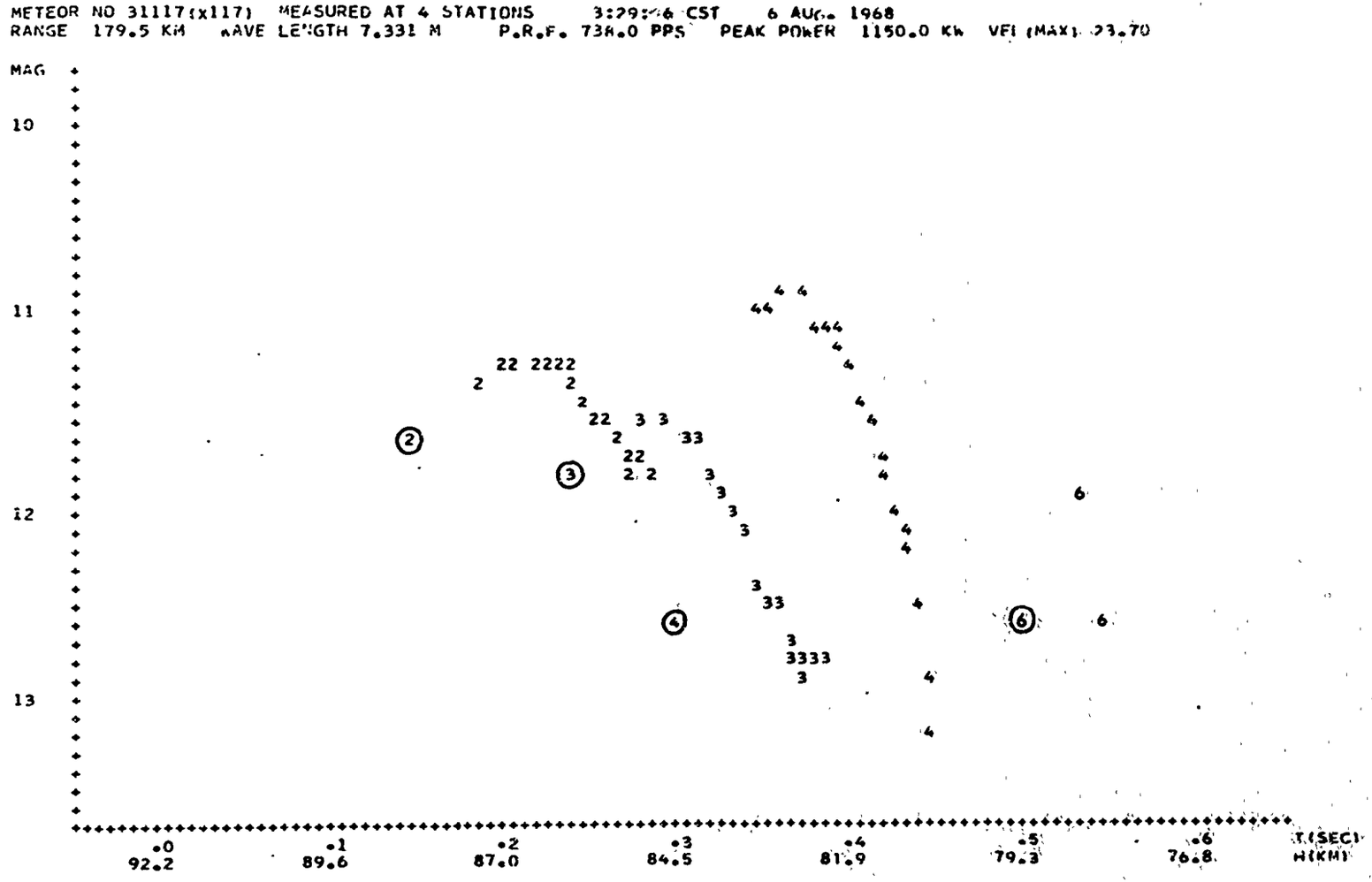

Figure 2-3. An observed ionization curve, showing recombination and fragmentation. The circled digits represent values from the principal Fresnel zones for stations 2, 3, 4, and 6. The following digits represent values from the later zones at each station.

Attachment of electrons to neutral atoms or molecules has been proposed (Davis, Greenhow, and Hall, 1959) to explain an observed lower bound on radar heights of bright photographic meteors. Attachment cannot explain the lower bound to height in Figure 2-1, because attachment to atmospheric atoms or molecules would give a lower bound independent of magnitude, and atmospheric species vastly outnumber meteor atoms or molecules for these meteors. On the other hand, recombination seems to be an adequate explanation for Davis, Greenhow, and Hall's observations. The importance of attachment should be reconsidered with recombination taken into account.

Our third observation of recombination appears in Figure 2-4. This is similar to Figure 2-1, except that more stringent limits have been placed on the scale height and on the standard error of the height of maximum. The relative distribution in Figure 2-4 is essentially similar to that in Figure 2-1, except that a band of meteors just above the recombination limit has been eliminated. This band represents the meteors where recombination is large enough to disturb the consistency between diffusion heights at different stations on the same meteor.

2.8 Fragmentation

If the meteoroid is not a single body but has broken into fragments, the composite Fresnel pattern of the group can be constructed as the sum of individual Fresnel patterns. Differences in fragment size will cause differences in deceleration of the various fragments and will spread them along their common trajectory. In the composite Fresnel pattern of several or more fragments, this corresponds to smoothing out the later oscillations; and in the ionization curves constructed from observations and from single-body theory, this corresponds to progressively fainter magnitudes for the later Fresnel zones. This effect is obvious in Figure 2-3 and in a large proportion of our meteors. It corresponds to fragment spreads of the order of 50 to 200 m along the trajectory; smaller fragment separations are below our resolution.

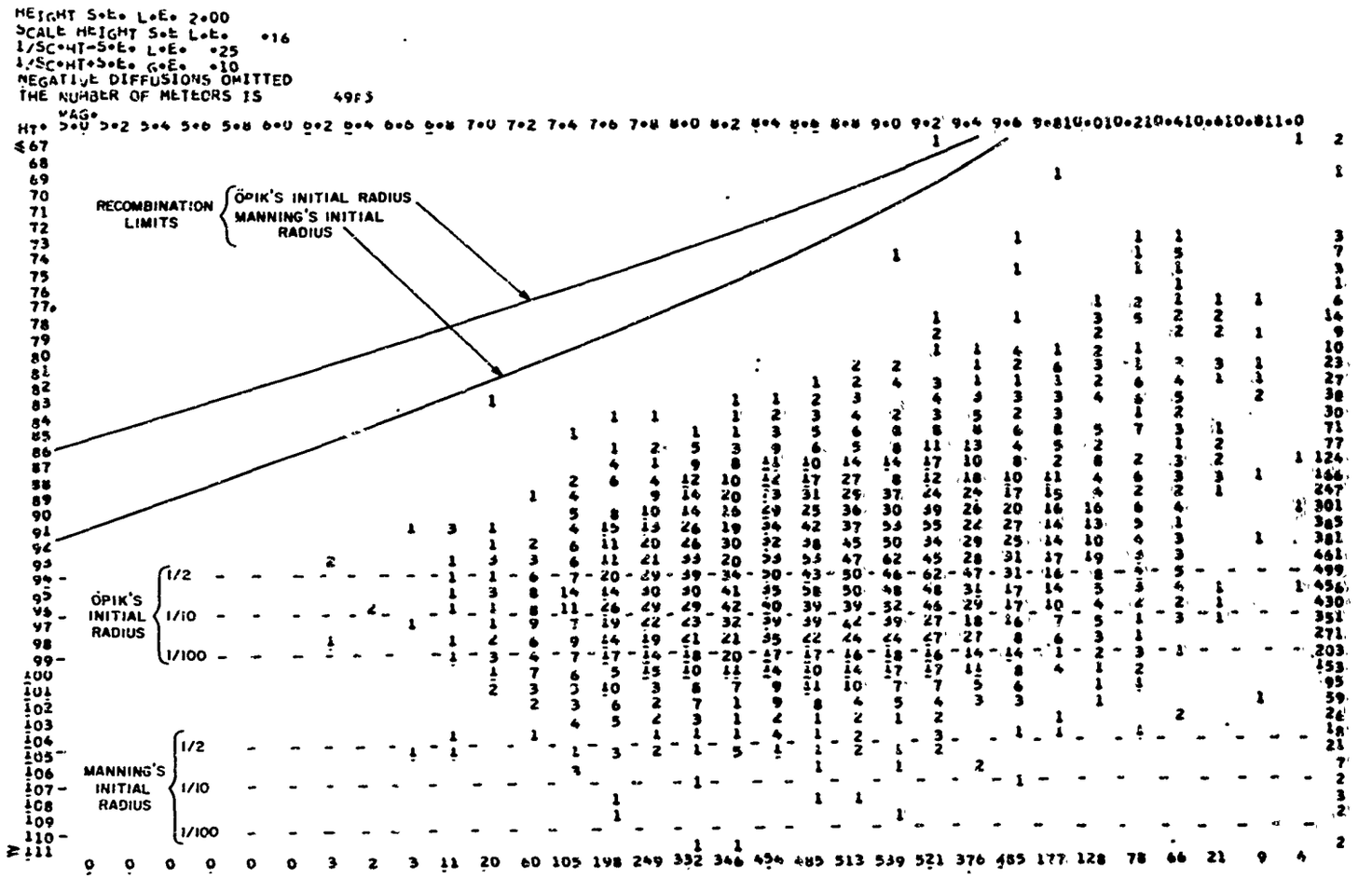

Figure 2-4. Diffusion heights at maximum ionization of 4985 meteors as a function of radar magnitude at maximum ionization. These meteors are a subset of the meteors in Figures 2-1 and 2-2, with standard errors in height of 2 km or less and with more closely restricted scale heights.

Numerous meteors give evidence of a group of fragments spread by 400 m or more, in addition to a tighter group (see Figure 2-5). Here all the Fresnel oscillations are attenuated, and the magnitude from the principal zone alone indicates the presence of the broader groups of fragments.

Fragmentation was directly observed in the Super-Schmidt meteors as elongation of the meteor image and could be inferred in several other ways. The present radar meteors, although much smaller, are similar to the Super-Schmidt meteors in fragmentation and in related effects. Jacchia (1955) and Hawkins and Southworth (1958) showed that Super-Schmidt meteors have shorter light curves than single-body theory predicted; we find similar ionization curves for the radar meteors (shown in subsection 2.11 below). These ionization curves tend to confirm the occurrence of fragmentation.

Much of the mischief that recombination makes in attempted use of diffusion measures for atmospheric density could be avoided if the amount of recombination could be accurately assessed from the Fresnel oscillations. Fragmentation, however, also affects the Fresnel oscillations, and in such a way that neither the amount of recombination nor the spread of particle fragments can be accurately deduced from the observations of many meteors.

2.9 Systematic Errors Caused by Recombination

Greenhow and Hall (1960) have made the most careful attempt, to date, to observe atmospheric density changes from study of meteors. They measured diffusion from radar meteors as functions of height (85 to 118 km) and time. Their rate of observation and lowest observed height show that they were observing magnitudes near the left edge of Figure 2-1. It is not possible to correct their published observations for recombination; indeed, we could not correct more than a few if we had their original data. However, we can recognize the qualitative effects of recombination on their measures.

Three of Greenhow and Hall's principal results are out of harmony with other measures of the atmosphere: 1) The mean scale height was 9 km; 2) the density at their mean height of 96 km varied regularly through the day, with a minimum near 0600 hours and a maximum near 1800; and

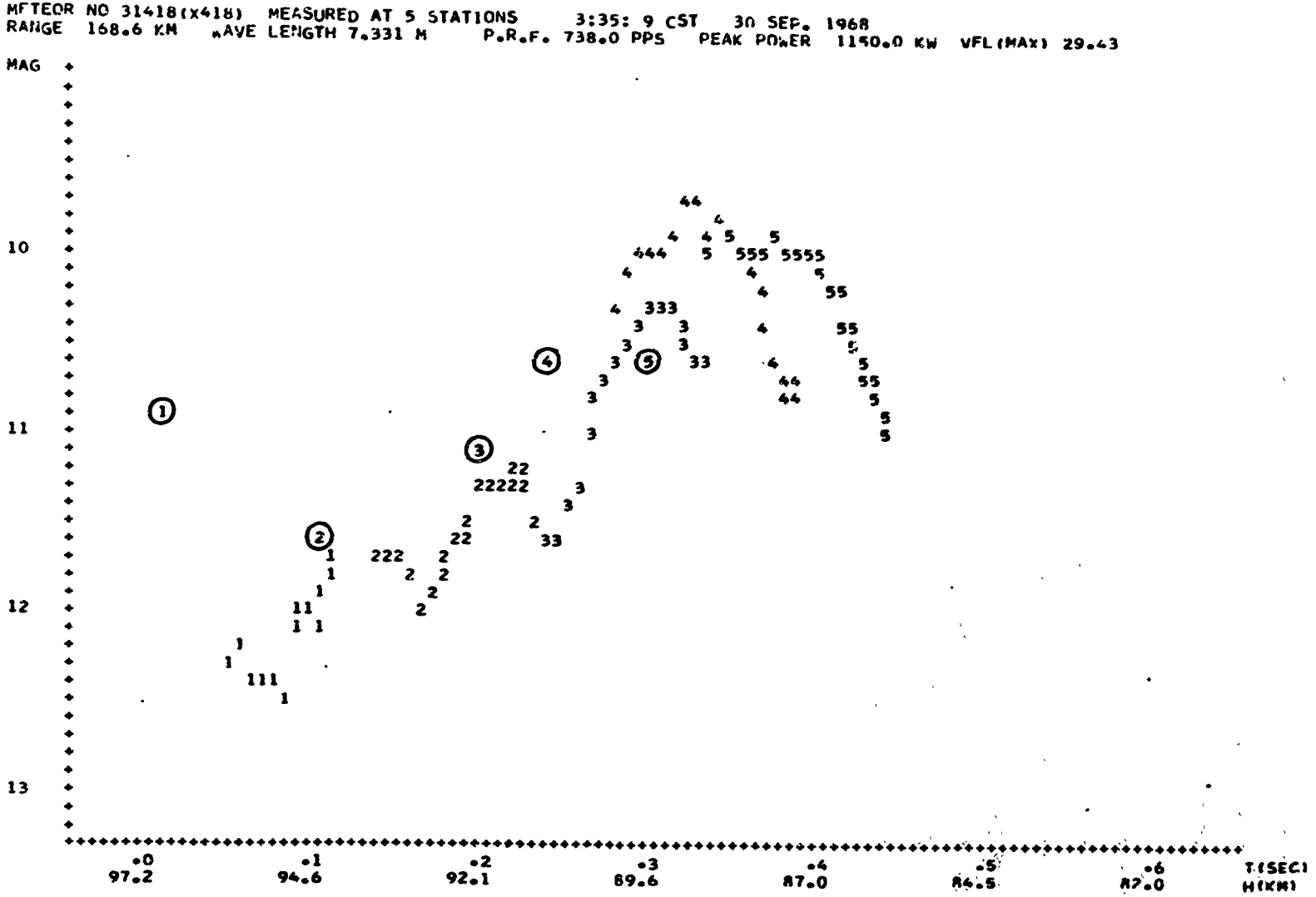

Figure 2-5. An observed ionization curve showing recombination and more than usual fragmentation.

3) the scale height varied regularly through the day, with a minimum near 0600 and a maximum near 1800. A priori, it is suspicious that these variations should be in phase with the diurnal variation of meteor velocities, where high velocities predominate in the morning and low velocities in the evening. In fact, all three effects are readily explained in terms of recombination: 1) their mean scale height is too high because their lower meteors were much affected by recombination and their higher meteors hardly at all; and 2) their density at 96 km varied because the faster meteors observed in the morning were observed sooner after the column was formed, so that the measured diffusion contained more recombination than the slow meteors in the evening at the same height; 3) their scale height varied because the fast meteors in the morning were higher, so that the slope of the overall sample was less perturbed by recombination, while the evening sample consisted mostly of meteors with appreciable recombination. Figure 2-6 gives a schematic representation of these effects.

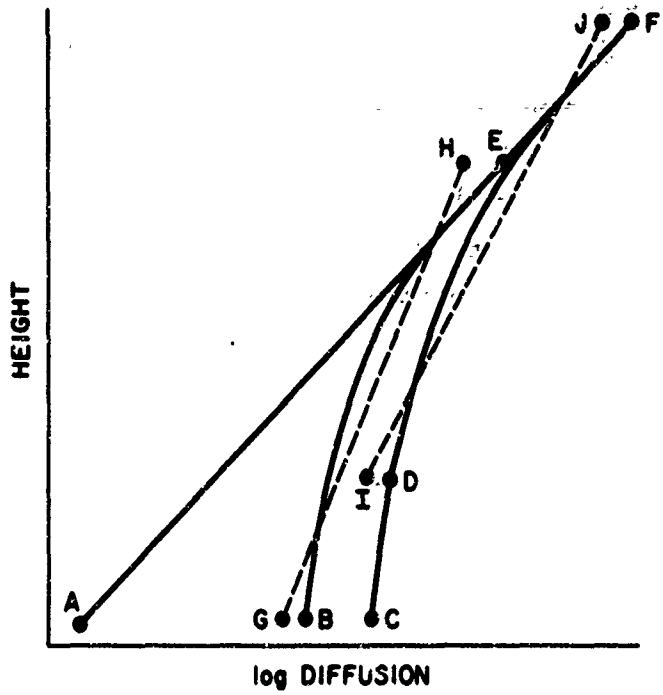

Figure 2-6. Schematic explanation of Greenhow and Hall's results: AF – true diffusion; BF – diffusion plus recombination in the evening; CF – diffusion plus recombination in the morning; GH – linear fit to evening sample BE; IJ – linear fit to morning sample DF.

2.10 Observed Errors in Diffusion Measures

Routine analysis of the Havana meteors includes computation of a "decay" constant from every Fresnel pattern. The oscillations are numerically smoothed out and a straight line is fitted to the logarithms of the smoothed amplitude as a function of time; the slope of the line measures the exponential decay rate. The decay rate is interpreted as diffusion, which would cause the signal S to vary with time t as

$$\frac{1}{S}\left(\frac{dS}{dt}\right)_D = -16\,\pi^2\,\frac{D}{\lambda^2}\,, \qquad (2\text{-}17)$$

where D is the apparent diffusion constant, and λ is the radar wavelength (McKinley, 1961). The routine reduction yields accurate differences in height between the different parts of a meteor trail that are observed at different stations. By comparison of the different values of D found at different heights on the same meteor trail, we can evaluate the errors that occur in practice when measuring D in two different ways. The several measures on each meteor have routinely been combined to give the height derivative of density (the inverse scale height) and the best available estimate from the decay data for the height of the reflection point from station 3. The inverse scale heights can then be compared with the known atmosphere, and the heights with other estimates of the height derived from geometrical circumstances (Hawkins and Southworth, 1963).

Figure 2-7 shows the distribution of internal standard errors of a sample of estimates of diffusion height, found by comparing the decays observed at different points on a single meteor trail. Figure 2-8 shows the distribution of the differences between the estimates of diffusion height and the geometric estimate ("radiant height") for a sample of meteors. The standard error in the radiant heights is determined primarily by the width of the antenna beam and is approximately 6 km. It is obvious from the differences in Figure 2-8 that there is some source of error besides the 6 km in radiant height and the 2 or 3 km in diffusion height that appears in Figure 2-7.

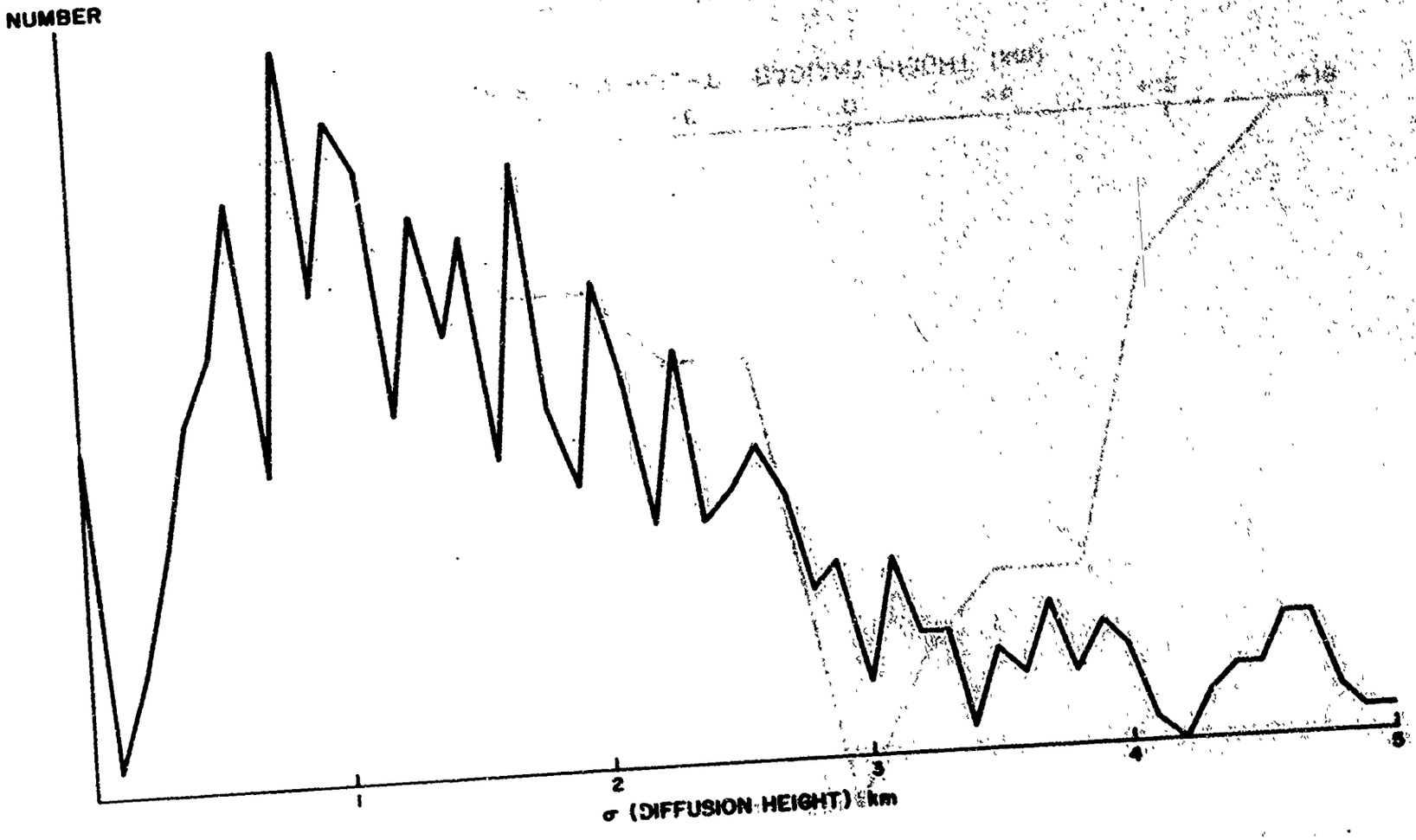

Figure 2-7. Distribution of internal standard errors of estimates of diffusion height.

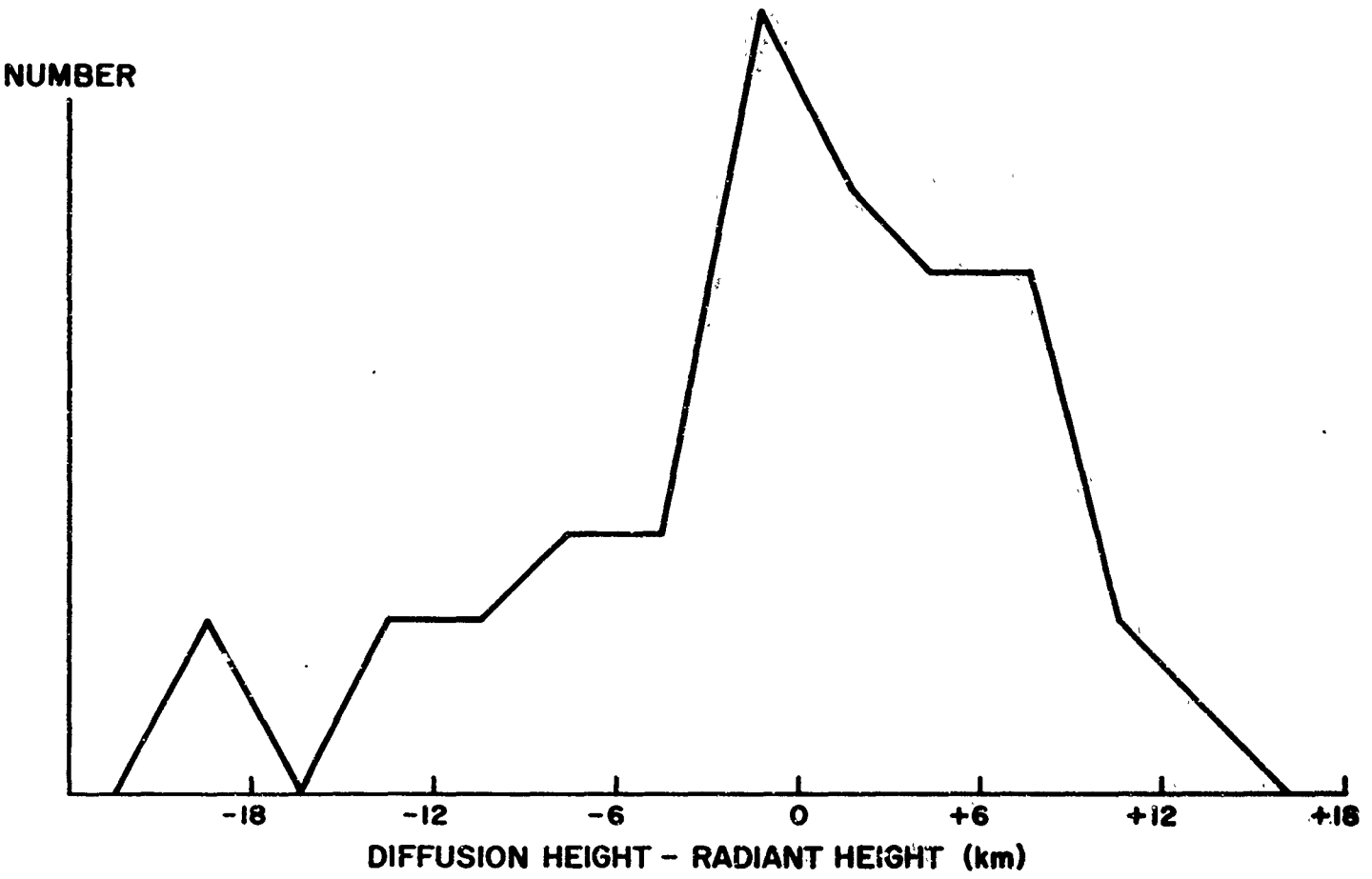

Figure 2-8. Distribution of differences between estimates of heights, by diffusion and by geometry.

We can now identify this source of large errors as the effect of recombination.

Figure 2-9 shows a sample of the inverse scale height computed, with their "internal" standard errors estimated from the agreement of different decay constants on the same meteor. They are plotted as a function of height to permit discovery of any correlation between scale height and height, but no correlation is evident in the figure. The true inverse scale height is ~0.16, agreeing roughly with the mean of the values plotted. Nonetheless, it is clear that there is a source of error not represented in the internal errors. Again, we can identify the large errors with recombination.

2.11 Wind Shears

A further source of error in diffusion measures results from variation in the (generally horizontal) wind velocity with height. Greenhow and Neufeld (1960; see also Bedinger, Kanflich, Manring, and Layzer, 1968) found that the median value of the vertical gradient dV_h/dz of the horizontal wind is 0.011 sec^{-1}, and the rms value approximately 0.025 sec^{-1}. Such a "wind shear" causes the radar specular reflection point to move along the meteor trail with a vertical speed

$$V_{zr} = -\frac{dV_h}{dz} R \cos^2 Z_R \left(1 - 2\frac{dV_h}{dz}\frac{R}{V_m}\cos Z_R\right)^{-1}, \qquad (2\text{-}18)$$

where R is the slant range to the meteor trail, Z_R is the zenith distance of the radiant, and V_m is the meteor's velocity. Representative values of R and V_m are 200 km and 30 km sec^{-1}; and small values of cos Z_R are relatively infrequent.

The distribution of electrons along a meteor trail is necessarily not uniform. We do not yet know whether there are small irregularities, but the overall distribution in height is known to be similar to the distribution of luminosity from faint photographic meteors. Figure 2-10 shows the

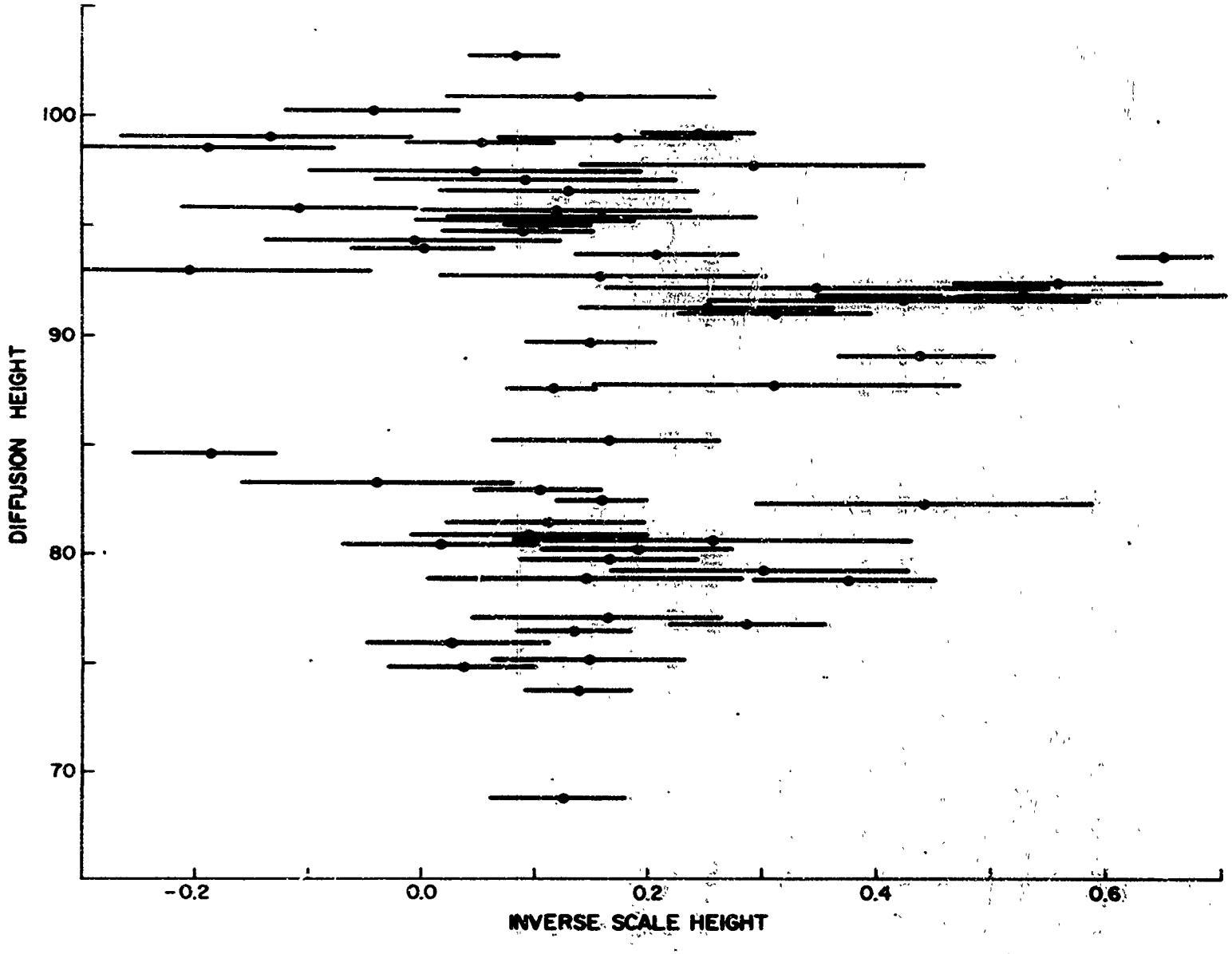

Figure 2-9. Estimates of inverse scale height, as a function of height.

IONIZATION CURVE

MLIM -MMAX	HBEG-HMAX +	10	9	8	7	6	5	4	3	2	1	0	0	1	2	3	4	5	6	7	8	9	10	HMAX-HEND +
0.0,1																								
.2,3				1				1	1							1		1	1					
.4,5				1		2	2	6	7	3					1	9	7	8						
.6,7					2	6	10	17	23	12	1				6	26	23	6	3	1				
.8,9				1	1	3	3	27	37	33	7			3	17	39	37	13	10	4	5	1		
1.0,1					1	6	17	35	48	40	7			4	15	62	61	25	13	1	5		2	
1.2,3			1	2	4	18	26	53	81	67	10			1	36	74	86	49	21	6	4	5	2	
1.4,5				3	4	12	34	73	102	79	21		1	6	32	115	109	59	22	7	8	1	2	2
1.6,7		1		3	7	14	38	76	119	106	23			7	45	124	120	67	40	17	6	4		3
1.8,9			1	4	5	11	40	81	127	126	24			8	46	150	125	64	35	15	10	5	2	2
2.0,1		1	1	1	7	12	44	57	85	142	41			9	42	135	113	75	32	15	8	5	1	3
2.2,3		1		1	4	15	28	59	79	105	34	1		6	29	101	107	54	27	9	3	3	4	3
2.4,5			2	2	2	7	24	58	66	94	41		2	7	33	80	102	46	22	9	1	1	1	
2.6,7			1		2	7	11	39	58	86	39	2	1	5	29	98	53	42	18	5	1		2	2
2.8,9						4	13	33	41	82	52			4	33	66	80	21	9	9	3		1	2
3.0,1		1				2	6	16	30	59	20	1		2	27	42	35	19	7	1	1	1	1	1
+				2		3	16	30	87	202	149	6		11	71	197	119	74	19	9	2		2	1

Figure 2-10. Distributions of the beginnings and ends of the ionization curves fitted to a large sample of observed radar meteors, with respect to the maxima of the ionization curves. The left half of the figure shows differences in height and magnitude of the beginnings from maxima; the right half shows differences of the ends from the maxima.

the distribution of ionization at beginnings and ends, with respect to the point of maximum ionizations, for a sample of observed meteors. The median slope dM/dz of the ionization curve is approximately 0.6 mag per vertical kilometer, both before and after maximum.

The motion of the reflection point along a nonuniform electron column superimposes on the diffusion variation (2-18) an additional signal variation:

$$\frac{1}{S}\left(\frac{dS}{dt}\right)_W = \pm 0.92 \frac{dM}{dz} V_{zr} \quad . \tag{2-19}$$

With values cited above, this variation is comparable in magnitude to diffusion at 80-km height, but of either sign. The consequent errors in heights derived from diffusion are therefore of the order of a scale height near 80 km and of 1 km near 90 km.

In principle, our multistation radar observations are sufficient to determine the ionization curve and the wind shear and therefore to allow us to correct the diffusion for their effects. We have not yet attempted this, but it is clear that we will often not have sufficient data. Recombination and fragmentation, in particular, make it difficult to determine the ionization curve reliably.

2.12 Conclusions

We find that recombination in the electron column is frequently important, contrary to earlier beliefs. It causes large and systematic errors in measurements of diffusion in meteor trails and invalidates all earlier studies of the atmosphere based on diffusion data. Even with the Havana radar system and elaborate analysis, we will not always be able to identify meteors having significant recombination, and we will hardly ever be able to correct observed diffusions for recombination.

We find that wind shears and rapidly varying electron densities along meteor trails cause a random error in diffusion measures that is often much larger than the apparent accuracy of the observations.

We do not yet know whether useful observations of atmospheric-density variations can be made using radar meteors. We attempted a number of analyses of our diffusion data in the past but never understood the apparent results until we recognized the importance of recombination. It is now clear that any useful analysis will be a large task.

For any future attempts at atmospheric-density studies using radar meteors, we make three definite recommendations. First, high transmitter power and high-gain antennas should be used in order to reach faint meteors (at least mag 10), which are comparatively unaffected by recombination. Second, the equipment should measure sufficient parameters (such as details of the Fresnel pattern) to permit recognition of recombination in most instances, and other parameters (such as echoes at other stations) to permit recognition of self-consistent data. Third, the statistical analysis should take very careful account of selection effects on the data and of the diurnal and seasonal variations in the meteor influx.

3. ENGINEERING DESCRIPTION OF THE MULTISTATIC VHF RADAR NETWORK FOR METEOR TRAIL OBSERVATIONS AND DATA RECORDING*

3.1 Introduction

3.1.1 System purpose

The multistatic VHF radar network is a phase-coherent system that processes radio echoes from meteor trails. Information regarding the echoes is recorded on magnetic tape and on punched paper tape. Computer analysis of the tapes yields determinations of meteor velocities, influx rates, decelerations, radiants, ionization curves, measures of ambipolar diffusion, and three-dimensional space locations. Three-dimensional wind components in the upper atmosphere are also obtained.

3.1.2 Geographical layout

The radar network is located near Havana, Illinois, and is comprised of one main (master) station, site 3; five outlying (neighboring) stations — sites 1, 2, 4, 5, and 6; and two remote stations — sites 7 and 8. The network's layout is shown in Figure 3-1. The coordinates of all stations along with their distance from the master station are presented in Table 3-1.

3.1.3 Simplified system description

Figure 3-2 is a simplified block diagram of the radar network. The master-station frequency-generation system produces the 40.92-MHz transmitter frequency, the mixer and reference frequencies for the master-station

*Appendices containing details of instrumentation are available and may be obtained upon request from AFCRL, Bedford, Massachusetts.

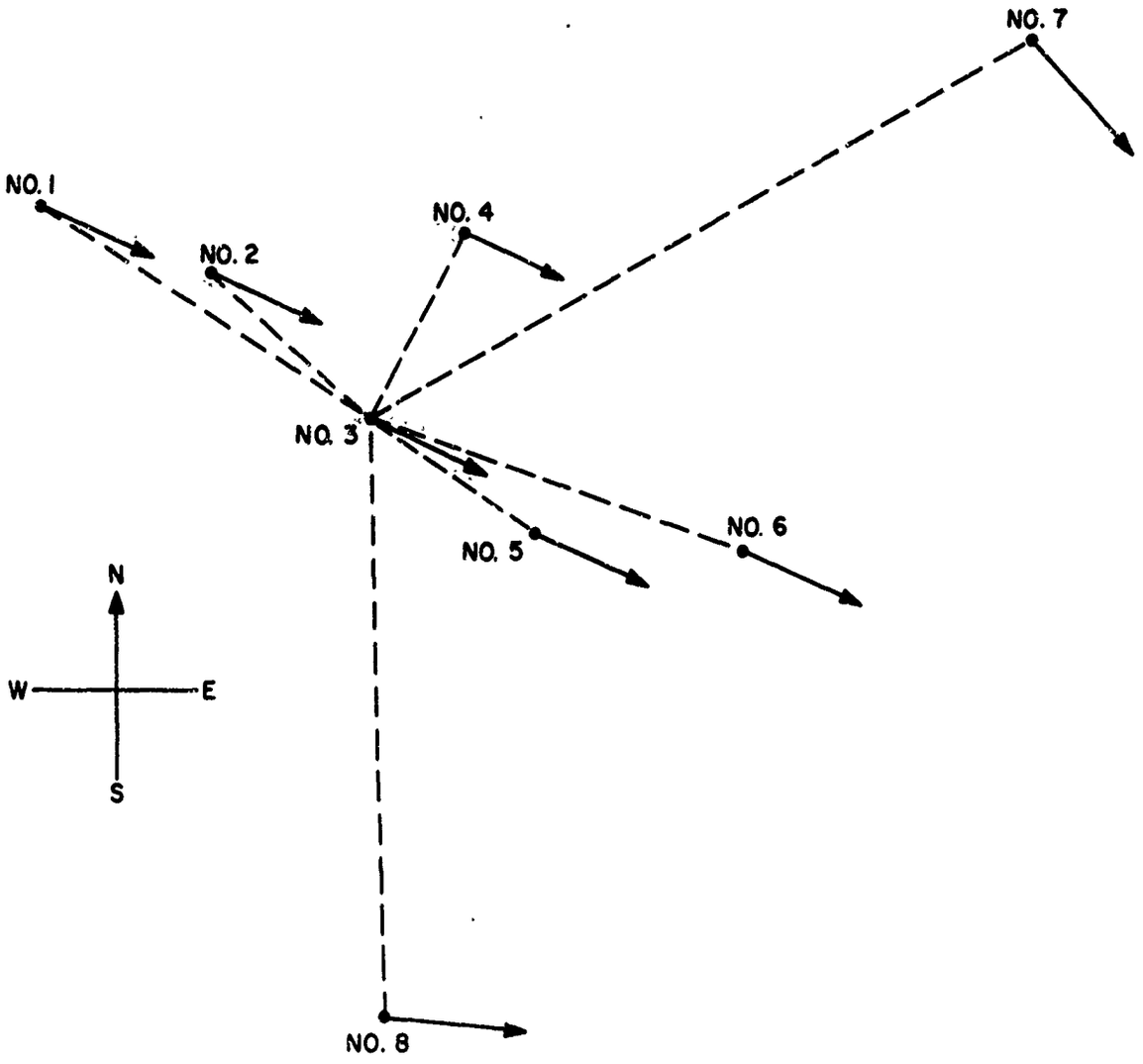

Figure 3-1. Network layout. Dashed lines represent microwave links. Arrows represent antenna axes: azimuth 113° E of N at sites 1 to 6, 139° at site 7, and 94° at site 8.

Table 3-1. Network coordinates

Station No.	Latitude	Longitude	Bearing East of North from site 3	Distance from site 3
1	40°19'34"	90°15'22"	300°44'53"	14.39 miles
2	40°17'36"	90°08'08"	310°08'57"	7.85
3	40°13'11"	90°01'19"	———	———
4	40°18'44"	89°57'46"	26°09'16"	7.09
5	40°09'47"	89°54'32"	123°11'36"	7.17
6	40°09'23"	89°45'45"	107°34'17"	14.41
7	40°25'02"	89°31'44"	62°14'20"	29.39
8	39°54'36"	90°00'51"	178°53'03"	21.39

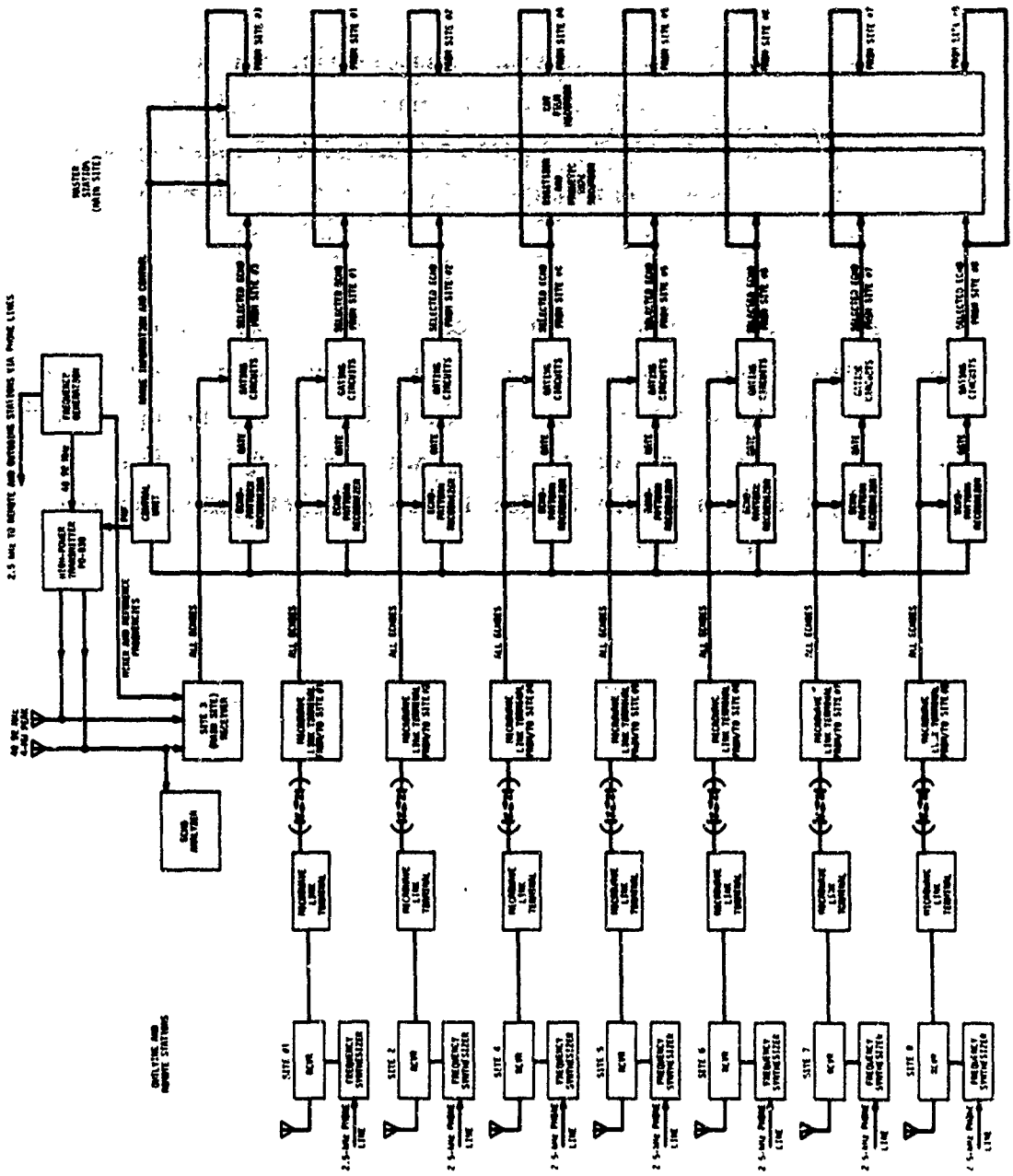

Figure 3-2. Simplified system block diagram of the radar network.

receiver and a 2.5-kHz frequency for the outlying and remote stations. The 2.5-kHz frequency is sent to these stations by telephone line in order to phase-lock their frequency synthesizers to the master synthesizer at the main site.

The transmitted pulse is radiated by the master-station antenna system. Echoes from meteor trails (as well as from aircraft) are received at the master and at the outlying and remote stations. The echoes received at the outlying and remote stations are sent back to the master station by microwave links.

At the master station the echoes from each station are analyzed by echo-pattern recognizers controlled by the central unit. When an echo is selected for recording, the echo recognizer gates that echo through the gating circuits to the digitizer and CRT film recorder. The central unit supplies the pulse repetition frequency (prf) to the transmitter and range information and control to the digitizer and CRT recorder.

The echo analyzer system is connected to one master station antenna. It supplies meteor influx rates on paper tape (see Section 3.15).

3.1.4 Detailed system description

3.1.4.1 Outlying/remote station. Figure 3-3 shows a more detailed block diagram of an outlying/remote site. In the calibration mode the antenna is disconnected from the receiver, and simulated echoes of known amplitude are sent to the receiver from the calibrator.

Control signals for the calibrator are received from the master station via the microwave link in the form of switching tones and of the prf. The tones are received by a tone receiver, which controls the calibrator.

The receiver produces three outputs. The amplitude (A) pulse is proportional to the logarithm of the amplitude A_ℓ of the echo. It is sent to the

master station via the microwave link on a 2.3-MHz subcarrier. The Phase 1 (ϕ_1) and Phase 2 (ϕ_2) pulses are proportional to $A_\ell \cos \phi$ and $A_\ell \sin \phi$, where ϕ is the phase of the echo compared to the transmitted phase. They are multiplexed in time and sent to the master station via the microwave link.

An oscillator at the remote station is phase-locked to the phone-line reference to produce a basic frequency for the synthesizer.

3.1.4.2 Master station (main site). Figure 3-4 is a detailed block diagram of the master station. Only the blocks for one of the seven outlying/remote stations are shown. The outlying/remote station data from the microwave link are sent to the low pass filter and subcarrier receiver. The time-multiplexed ϕ_1 and ϕ_2 pass through the filter and gain-control to the demultiplexer. The subcarrier signal is blocked by the filter.

The subcarrier receiver and inverter amplifier reconstruct the A signal for the buffer delay gate. The buffer delay gate interfaces the echo recognizer and demultiplexer. The trigger for the demultiplexer is derived from the recognizer gate signal and the A signal. When the demultiplexer receives the trigger, it gates out the selected A, ϕ_1, and ϕ_2 signals on separate lines for recording. The ϕ adder allows both ϕ_1 and ϕ_2 to be recorded on the same cathode-ray tube.

The processing of the data collected by the master station (main site) is different because there is no need to multiplex the receiver outputs and because the two antennas are used in conjunction with the transmitter. The TR-ATR networks allow the same antennas to be used for transmission and reception. The master-station receiver outputs A, ϕ_1, and ϕ_2 are the same as the ones of a remote/outlying station and are derived from one of the antenna inputs. The outlying ϕ_3 and ϕ_4 are the phase signals from the second antenna input of the double trough. The adding amplifiers are similar to the demultiplexer and gate the desired signals to the recording equipment. Two triggers are used, one for the amplitude A and one for the phases ϕ. The ϕ signals are time-multiplexed for the CRT recorder so that they may be distinguished on the CRT.

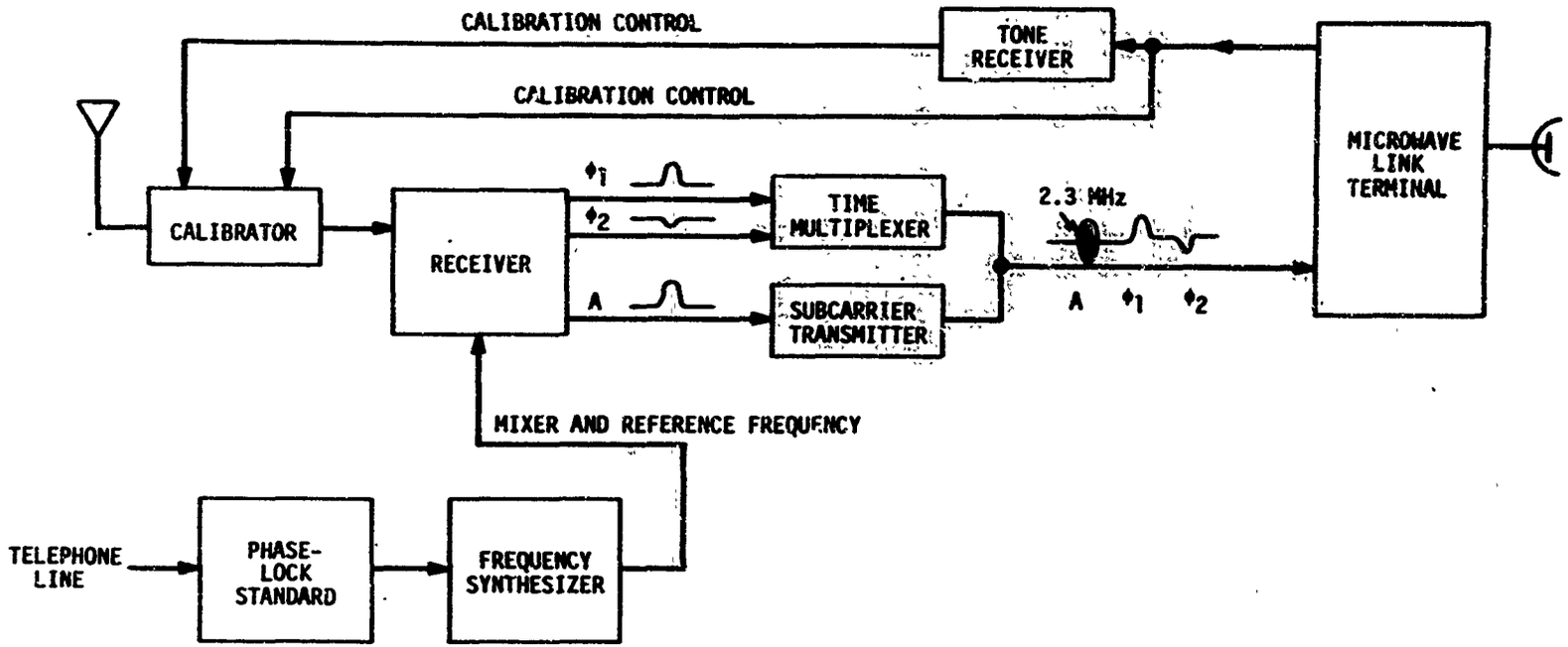

Figure 3-3. Block diagram of the outlying/remote stations.

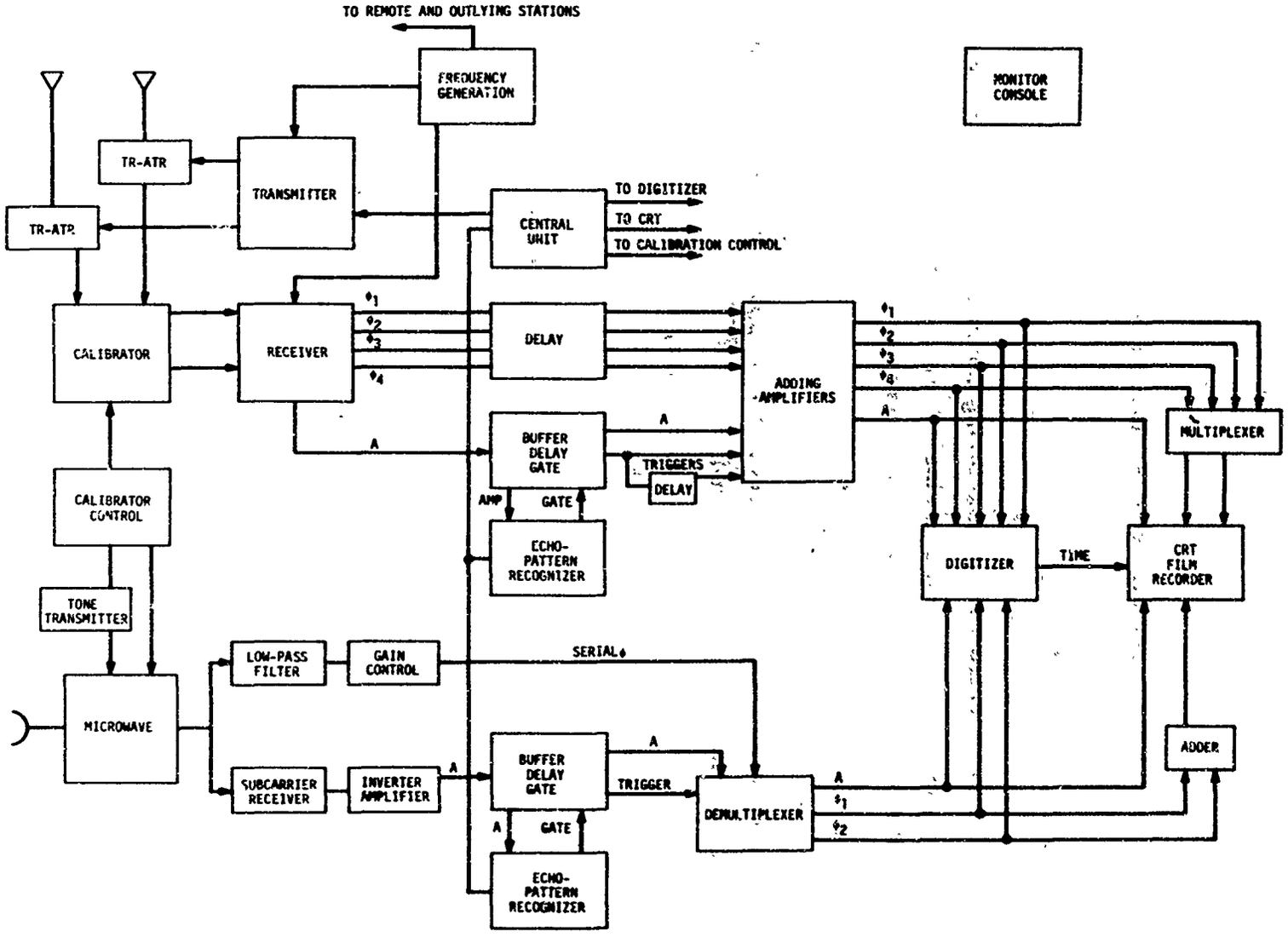

Figure 3-4. Block diagram of the master station (main site).

The calibrator control simultaneously operates the master calibrator directly and the remote/outlying calibrators through the tone transmitter and microwave links.

Individual subsystems are further described in the following sections.

3.2 High-Power Transmitter

The Continental Electronics Manufacturing Company Type PO-830 transmitter was designed for operation at a single frequency in the range of 40 to 42 MHz with the following operating characteristics:

Peak power output	4 Mw
Average power output	20 kw
Pulse waveform	3 μsec at 1330 pps to 100 μsec at 40 pps
Nominal duty factor	0.004
Power supply requirements	230 v, 3 phase, 60 cps
Power source capacity	200 kv-a
Type of emission	Pulsed CW
Output impedance	100 ohms balanced (two 50-ohm unbalanced outputs 180° out of phase)

Although the Continental PO-830 transmitter has a peak power-output capability of 4 Mw, it is normally operated at approximately 2 Mw. The transmitter receives the R.F. carrier input from the frequency synthesizer, while the modulating prf pulse input is generated within the meteor-radar processor and has a period of 1355 μsec. The quasi-gaussian radio frequency pulse has a 6-μsec half-power width. Range ambiguities up to 5 prf periods are resolved by a method of pulse skewing, in the meteor-radar processor, which delays every 5th pulse by 8 μsec. A functional block diagram of the transmitter is shown in Figure 3-5.

3.2.1 Pulse generator

The transmitter amplifier circuits are pulsed CW stages. The intermediate power amplifier, driver amplifier, and power amplifier receive the required

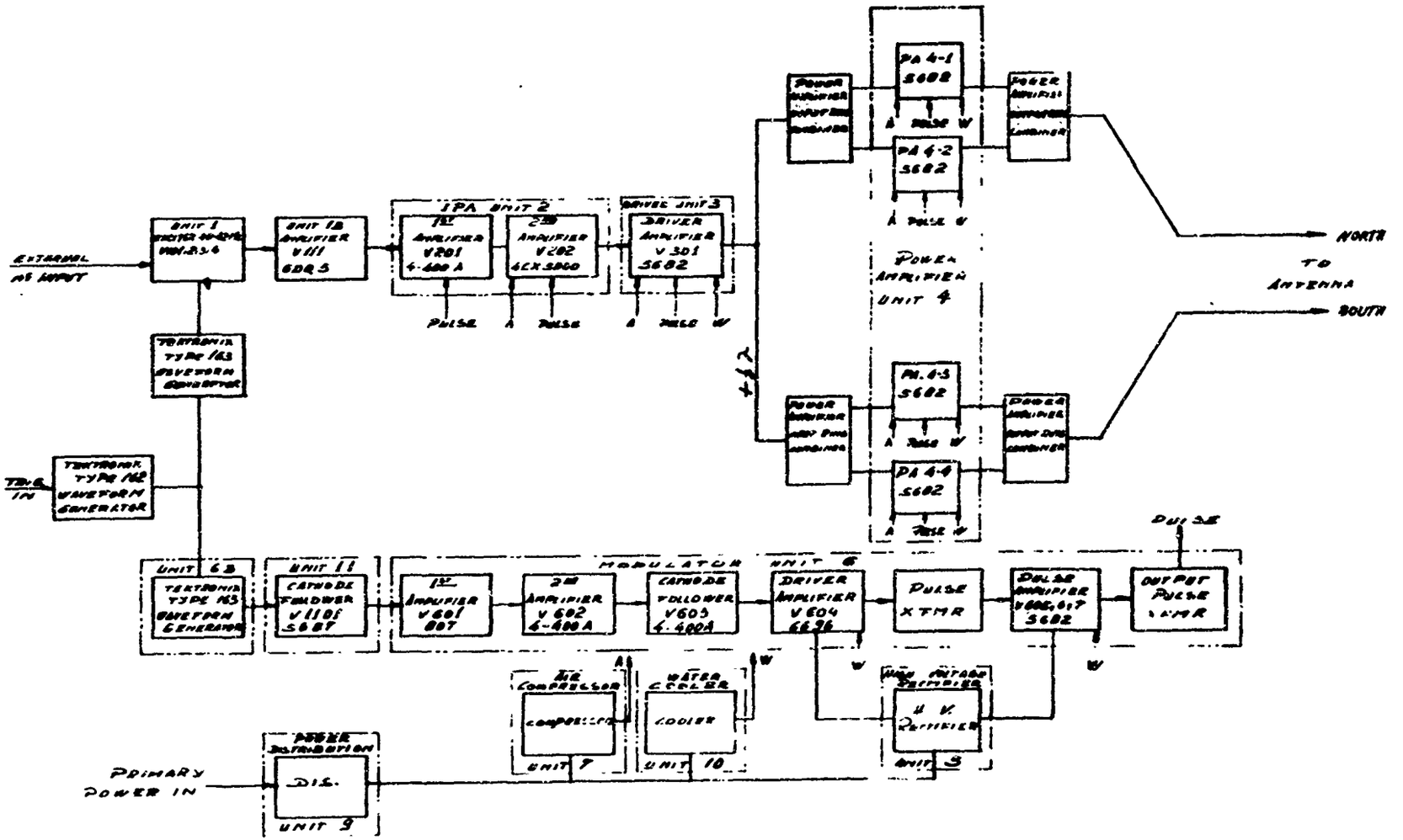

Figure 3-5. Block diagram of the final stages and modulator, PO-830 transmitter.

level of control pulse from the modulator circuits. The low-power-level exciter amplifiers are controlled by pulse amplifiers located within the exciter unit itself. The modulator and exciter units receive their inputs from the same triggering source through Tektronix waveform generators. These generators provide the required impedance matching, pulse delay, and amplitude control.

The basic trigger input signal controls a Tektronix-Type 162 waveform generator whose output drives two Tektronix-Type 163 waveform generators. The first Type 163 generator controls the modulator input stage, V601, through a cathode follower, V1101. The second Type 163 generator directly controls the pulse-amplifier circuits within the exciter unit.

3.2.2 Exciter unit

The exciter unit contains a crystal oscillator, V101A, for internal carrier frequency generation, but is also provided with means for accepting an external frequency source.

The selected R. F. source is coupled through a buffer amplifier, V101B, into a two-stage amplifier, V102 and V103. Each of the amplifiers is normally biased well beyond cutoff and pulsed into the operating range.

The pulser portion of the exciter consists of a direct coupled amplifier, V104A, and a cathode follower, V104B. The pulser receives a signal from the Tektronix generating equipment and amplifies it for proper control of the exciter amplifier-biasing system.

The pulsed R. F. output of V103 is coupled to a class "B" amplifier, a 6DQ5, which drives the first stage of the intermediate power amplifier.

3.2.3 Intermediate power amplifier

The intermediate power amplifier is a two-stage amplifier with pulse voltage applied to the plate of each stage. This pulse voltage is obtained from the output-pulse transformer of the pulse modulator. Resistance-capacitance divider ladders are provided to reduce the applied voltage to the desired value. The approximate plate pulse voltage is as follows:

V201 4-400A	10,000 v
V202 4CX5000	20,000 v .

The screen and bias voltages for both stages are obtained from separate power supplies.

Grid input and plate output tuning controls are present on both amplifier stages. Metering is provided to read V201 cathode current, V202 cathode current, and grid bias voltage.

V202 is mounted in a gas-tight cylindrical housing for operation under compressed air pressure to improve voltage breakdown conditions. Cooling for this stage is provided by means of both air and water circulation.

The intermediate power amplifier delivers pulsed-rf energy to the driver unit V301.

3.2.4 Driver amplifier

The driver amplifier utilizes one Machlett-Type ML-5682 water-cooled triode, V301, in a grounded grid circuit with input and output coaxial tuning cavities. The entire amplifier, including the tube and two cavities, is housed in a gas-tight cylindrical compartment. A filament transformer, tuning motor, and other auxiliary equipment are external to this compartment.

A meter is provided that monitors the R. F. input voltage.

The driver amplifier output line is connected to a dividing circuit that delivers power through coaxial lines into two power amplifier input ring combiners. One of the two coaxial lines is a half-wavelength longer than the other, causing a 180° phase difference between ring combiners. Each ring combiner feeds the inputs of two power amplifier cavities.

2.3.5 Power amplifier

The power amplifier contains four Machlett-Type ML-5682 triodes, V401 through V404. Each tube assembly is identical to the driver amplifier, V301, including cavity tuning provisions. Although each input ring combiner feeds two power amplifier cavities in a parallel fashion, all four cavities can be independently tuned.

Two identical ring combiners transfer the power amplifier outputs to the antenna system. Each of these combiners consists of a rectangle of rigid coaxial transmission line with power amplifier feed points at two corners. A 50-ohm output is provided midway between these feed points. Located at a third corner is a resistive load or "waster."

In normal operation, two power amplifiers deliver signals of equal amplitude and phase to the combiner inputs. The combined power then appears at the output terminals. Should any unbalance occur between the amplifier outputs, the difference in power is absorbed at the waster and neither amplifier senses the unbalance.

3.2.6 Pulse modulator

The pulse modulator amplifies the prf control signal to the 50-kv level used in pulsing the transmitter amplifier stages. This unit consists of five amplifier stages and two pulse transformers.

The modulator control input pulse is from a cathode follower, V1101, which is driven by Tektronix shaper units. The pulse modulator contains a

two-stage R-C amplifier consisting of an 807 and a 4-400A tube, a 4-400A cathode follower, a driver amplifier utilizing a 6696 tube, and a pulse amplifier using three 5682 tubes in parallel. Pulse transformers are used before and after the final pulse amplifier stage.

The first amplifier stage contains its own plate supply and rectifier. Another separate rectifier supplies bias for the final pulse amplifier stage.

All the pulse modulator tubes are operated at cutoff during the interpulse interval with the exception of V602. Metering is provided for the pulse modulator.

3.2.7 Monitor and control console

All transmitter tuning and monitoring equipment is located in a central console unit.

3.2.8 High-voltage rectifier

The high-voltage rectifier assembly consists of a standard three-phase full-wave rectifier circuit using two Type 6895 tubes in series at each rectifier position. This unit also contains a single-phase full-wave rectifier, which supplies bias for the four power amplifier tubes and the driver tube.

The rectifier is provided with a ventilating blower and a cold-weather heating system.

3.2.9 Air compressor

The air compressor is provided to pressurize the final stage of the intermediate power amplifier, the driver, the power amplifiers, and the combiners. Owing to the high-peak voltages involved, compressed air is necessary to improve the breakdown characteristics of these units.

The compressor pressurizes its receiver to a value of 80 psi gauge. A pressure-sensitive switch located on the receiver turns the compressor on at 60 psi gauge and off at 80 psi gauge. Thus the receiver pressure remains between these values. An adjustable pressure-reducing valve is located at the outlet of the receiver to reduce this pressure to that required by the various units. The gauge located at the outlet of this valve monitors the outlet pressure.

Under normal conditions, and after the system is initially pressurized, the compressor will run only periodically to replace the air that leaks from the system.

3.2.10 Water-cooling system

The water-cooling system consists of a water storage tank, a circulating pump, and two water-to-air heat exchangers. Each heat exchanger contains a blower and a flow-and-temperature interlocking system including flow gauges. Thermostats control the cycling of the blowers to maintain the proper water temperature.

3.3 Antenna Subsystem

3.3.1 Master station

The output combiners of the transmitter's power amplifier transfer power through a TR-ATR network into a troughguide antenna. This network automatically switches the antenna from the receivers to the transmitter during pulse transmission.

The TR-ATR system, manufactured by the Radiation Engineering Laboratory of Maynard, Massachusetts, is a standard circuit adapted for coaxial line. The TR and ATR sections, which are spaced an electrical quarter-wavelength apart, each consist of a half-wavelength coaxial cavity with a tuning condenser and TR tube. The networks are fabricated from standard 9-inch-diameter coaxial line. The entire system is pressure tight for reliability.

Two asymmetric troughguide antennas are located side by side as a symmetric, integrated unit. The apertures are in phase for transmitting. During reception, each troughguide is used separately through the dual TR-ATR system. The antenna is horizontally polarized in the main beam and has a gain of 22 db when the apertures are connected in phase (feeds connected 180° out of phase).

The double troughguide antenna measures 60 m in length, 21 m in width, and 10.5 m in height. The main beam is directed at an azimuth 113° East of North and has an elevation angle 35° above the horizon. The observed ionospheric volume measures roughly 20 km × 50 km × 50 km and has a characteristic distance from the transmitter of 150 km. The mean height of the volume above sea level is 90 km.

3.3.2 Outlying and remote stations

The five neighboring (outlying) stations (sites 1, 2, 4, 5, and 6) each have double troughguide antennas connected with coaxial matching transformers to provide an input for a single-channel receiver. All troughguide antennas were manufactured by the Radiation Engineering Laboratory.

The two remote stations (sites 7 and 8) have 13-element Yagi antennas resonant at 40 to 42 MHz with a front-to-back ratio of 30 db. The Yagi antennas were manufactured by the Telrex Laboratories of Asbury Park, New Jersey, and carry model number CY13-40-42.

The outlying- and remote-station antennas are positioned to receive reflections from the same volume as the master station.

3.4 Frequency Generation

The purpose of this subsystem is to generate and distribute high-stability reference signals that cause the eight-station network to become phase-coherent. The frequency-generation subsystem is implemented with the master oscillator, the 2.5-kHz generator, the offset frequency synthesizer, and the telephone-line network, Figure 3-6.

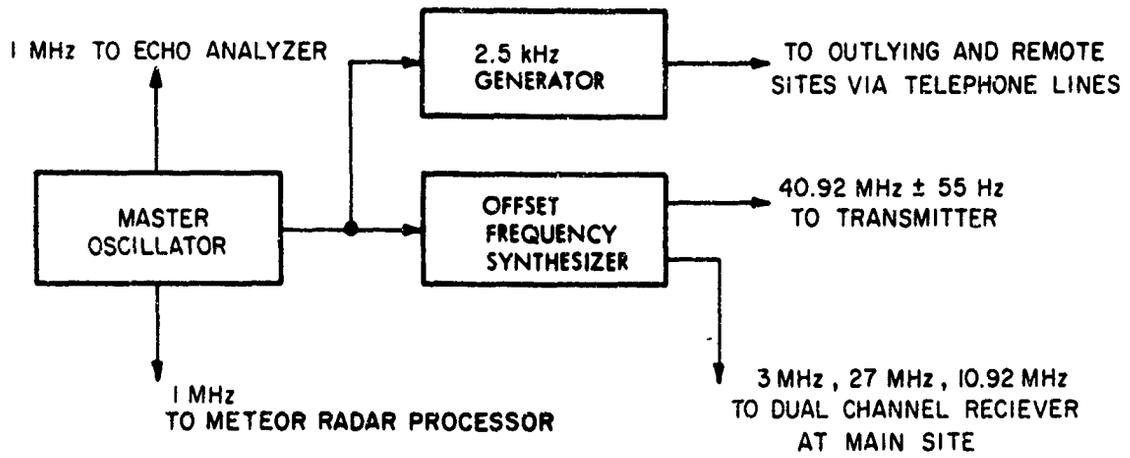

Figure 3-6. Frequency generation at master station.

3.4.1 Master oscillator

The master oscillator produces high-stability outputs of 1 MHz and 100 kHz (Figure 3-7). The 1-MHz output is connected to the meteor-radar processor and echo analyzer as the basis for all timing operations performed therein. The 100-kHz output drives the 2.5-kHz generator and the offset frequency synthesizer.

A Motorola oscillator, type S1054AL, is the basic system frequency standard. The performance details of this oscillator are given in Table 3-2.

The Motorola 1-MHz output drives the meteor-radar processor, echo analyzer, and part of the offset frequency synthesizer. A parallel 1-MHz oscillator output is divided by 10 after passing through a shaper circuit and then enters a driver circuit, which serves as the 100-kHz output of the master oscillator.

3.4.2 Offset frequency synthesizer

The offset frequency synthesizer produces the transmitter carrier frequency and has a switching means that allows the basic 40.92-MHz frequency to be offset by 1-Hz increments up to ± 55 Hz. This offset provision allows the system to simulate known doppler frequencies of 0 to ±55 Hz in single-cycle increments. Nonoffset frequencies of 3 MHz, 10.92 MHz, and 27 MHz are generated by the synthesizer for the dual-channel receiver.

A functional block diagram of the offset frequency synthesizer is shown in Figure 3-8. The 100-kHz input frequency requires that six multipliers and five dividers be used to generate the offset units and tens digits. Two switches are used to select the addition or subtraction operation. All other multipliers and mixers in the synthesizer have frequency ratios of approximately 10:1, and reliably suppress spurious sidebands without retuning. All frequencies to be rejected are at least 10% away from center frequency, and all frequencies to be accepted are at most 0.5% away from center frequency. The divider circuits are fail-safe, producing no output when the input falls below a minimum level.

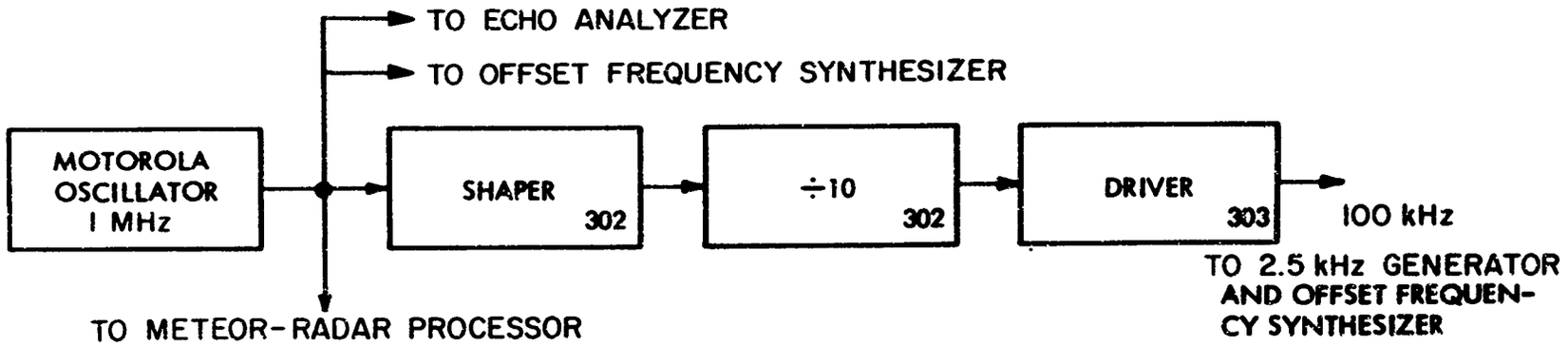

Figure 3-7. Master oscillator.

Table 3-2. Master oscillator performance specifications.

INPUT VOLTAGES	117 v a-c ±10%; 50-60 cps, or 24.5-28.8 v d-c.
POWER CONSUMPTION	less than 15 w
STABILITY $\frac{\Delta F}{F}$ (max.) versus:	
Input voltage change of ±10%	less than $\pm 2 \times 10^{-10}$
Load resistance change of ±10%	less than 1×10^{-10}
Ambient temperature 25°C ±5°C 25°C ±25°C	$\pm 5 \times 10^{-10}$ $\pm 3 \times 10^{-9}$
Humidity 95-100% (50°C)	less than 1×10^{-9}
Short term (1-10 sec interval)	$\pm 1 \times 10^{-10}$
TIME (After 6 hours initial warmup, AL models):	
Plus 1 hour	frequency drift less than 5×10^{-10}
Plus 24 hours	frequency drift less than 2×10^{-9}
Next 24 hours	frequency drift less than 1×10^{-9}
Long term	less than 3×10^{-8} per month
TIME (After 6 hours initial warmup, AH models):	
Plus 1 hour	frequency drift less than 5×10^{-10}
Plus 24 hours	frequency drift less than 2×10^{-9}
Next 24 hours	frequency drift less than 5×10^{-10}
Long term	less than 1.5×10^{-8} per month
WARMUP TIME	at 0° ambient will be within: 3×10^{-7} in 8 min 1×10^{-8} in 12 min
OPERATING TEMP. RANGE	0°C to +50°C
OUTPUT FREQUENCIES	1 MHz and 100 kHz at 1 v rms sine wave into a 50-ohm load
OUTPUT CONNECTORS	standard BNC type
FREQ. ADJUST RANGE	coarse $\pm 2 \times 10^{-6}$ fine 1×10^{-7} indicating parts 10^{10}
CIRCUITRY	proportional control oven, zener regulation, germanium transistors
SIZE AND WEIGHT (less batteries)	
S1054AH and S1054AL	10-1/4" wide × 6-1/2" high × 5" deep, approx. 7 lbs
S1064AH and S1064AL	10-1/4" wide × 6-1/2" high × 10" deep; approx. 11 lbs
S1054ALR and S1054AHR	19-1/4" wide × 7" high × 5" deep, approx 14 lbs
S1064ALR and S1064AHR	19" wide × 7" high × 10-1/2" deep, approx 19 lbs

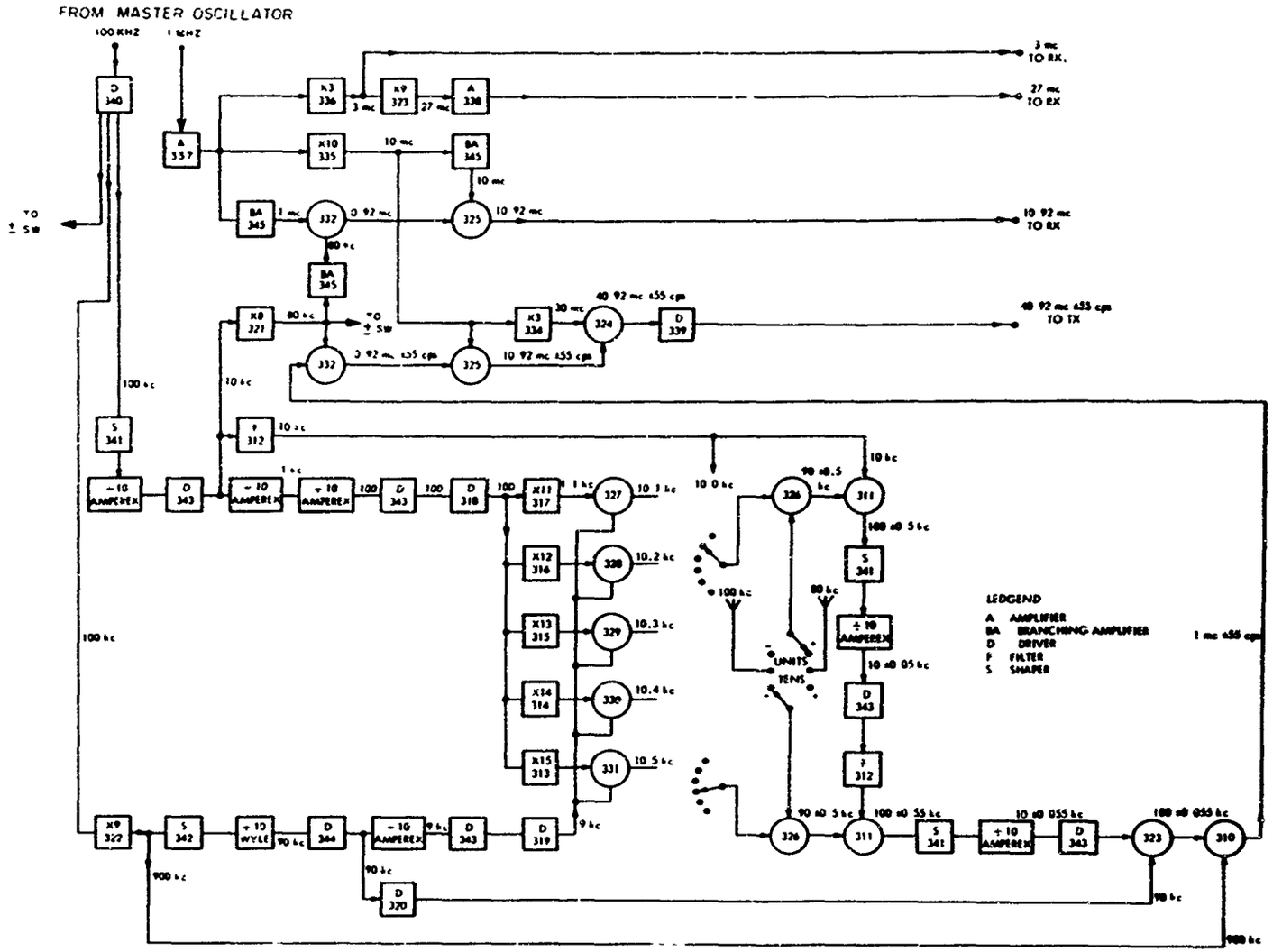

Figure 3-8. Offset frequency synthesizer.

3.4.3 2.5-kHz generator

The 2.5-kHz generator (Figure 3-9) produces the continuous-wave synchronizing signal responsible for remote-site phase coherence. The 100-kHz input signal passes through a divide-by-40 stage consisting of one decade counter and two binary counters. The resulting 2.5-kHz signal is fed through an emitter follower driver stage, an amplifier, and a lightning protector and then applied to a telephone hook point for distribution to the remote sites.

3.4.4 Telephone lines

The telephone lines carry a synchronizing signal from the site-3 2.5-kHz generator to the phase-locked secondary standard at all remote stations. This synchronization allows the entire system to become phase coherent. The high-stability frequency standard at all stations must be made phase coherent in order that the expected doppler frequencies of 0.3 to 300 Hz can be measured. The telephone lines are voice-grade channels with a frequency response of 300 to 3000 Hz and a level of at least -8 dbm into 600 ohms.

A single telephone line carries the synchronizing 2.5-kHz CW tone from the master station to the Havana Central Telephone Exchange. The hook point at the master station is a Triad TY-53X transformer with a 330-ohm resistor shunted across the primary input winding. A distribution amplifier located at the Central Exchange performs a 1-to-7 branch that passes the tone through the lines connected to the remote sites.

The minimum anticipated doppler frequency of 0.25 Hz requires that the maximum allowable frequency error in the synchronizing network be approximately 5×10^{-10}.

3.5 Dual-Channel Receiver

The master station contains a dual-channel (interferometric) receiver with separate channels connected to each section of the troughguide antenna.

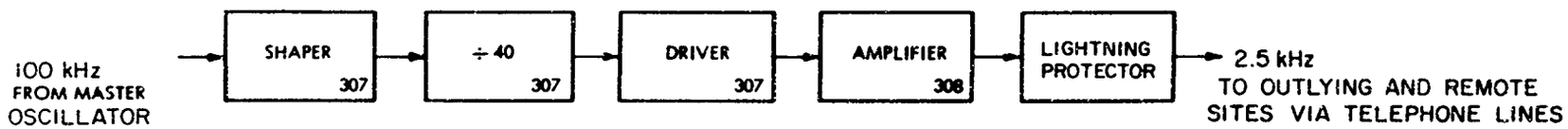

Figure 3-9. 2.5-kHz generator.

The outputs of the phase comparators in each channel are proportional to the sine or cosine of the received wave phase. This phase information provides Doppler sense through the implementation of two outputs in quadrature for each channel. Five types of information (A, ϕ_1, ϕ_2, ϕ_3, ϕ_4) are therefore made available.

The two receiver channels operate in an identical manner except that the received echo is obtained through different sections of the troughguide antenna. The echo angle of arrival can be determined, through data processing, by computing the relative phase difference of the two doppler signals as received through the antenna sections.

The dual-channel receiver block diagram is shown in Figure 3-10. The preamplifier has a noise figure of 2.5 db and sufficient isolation to prevent the local oscillator frequency from being radiated by the antenna. The receiver input is protected by a neon lamp and a varactor diode limiter.

The signal is heterodyned to 30 MHz so that standard linear and logarithmic I.F. amplifiers can be used. The linear I.F. unit is an RHG Model ET3002, and the log I.F. amplifier is an RHG Model LT3002. A 230-kHz filter is used because the RHG units have a 2-MHz passband. The third harmonic of the 10.92-MHz local oscillator is well outside the resulting I.F. passband. The log I.F. is of the successive detection type and is linear to within ±10% (<1 db). Its output is buffered with an emitter follower. The linear I.F. drives a mixer that translates its output to 3 MHz for the phase-measuring system. Linearity and dynamic range are preserved throughout the chain.

Signal attenuation of 0 to 41 db is available through a switching arrangement on the receiver front panel. Proper dynamic range is obtained with a 10-db setting.

The transmitter pulse blanking circuits keep most of the transmitted signal from the I.F. circuits. Without these circuits the transmitted pulse produces distortions that affect the received signals.

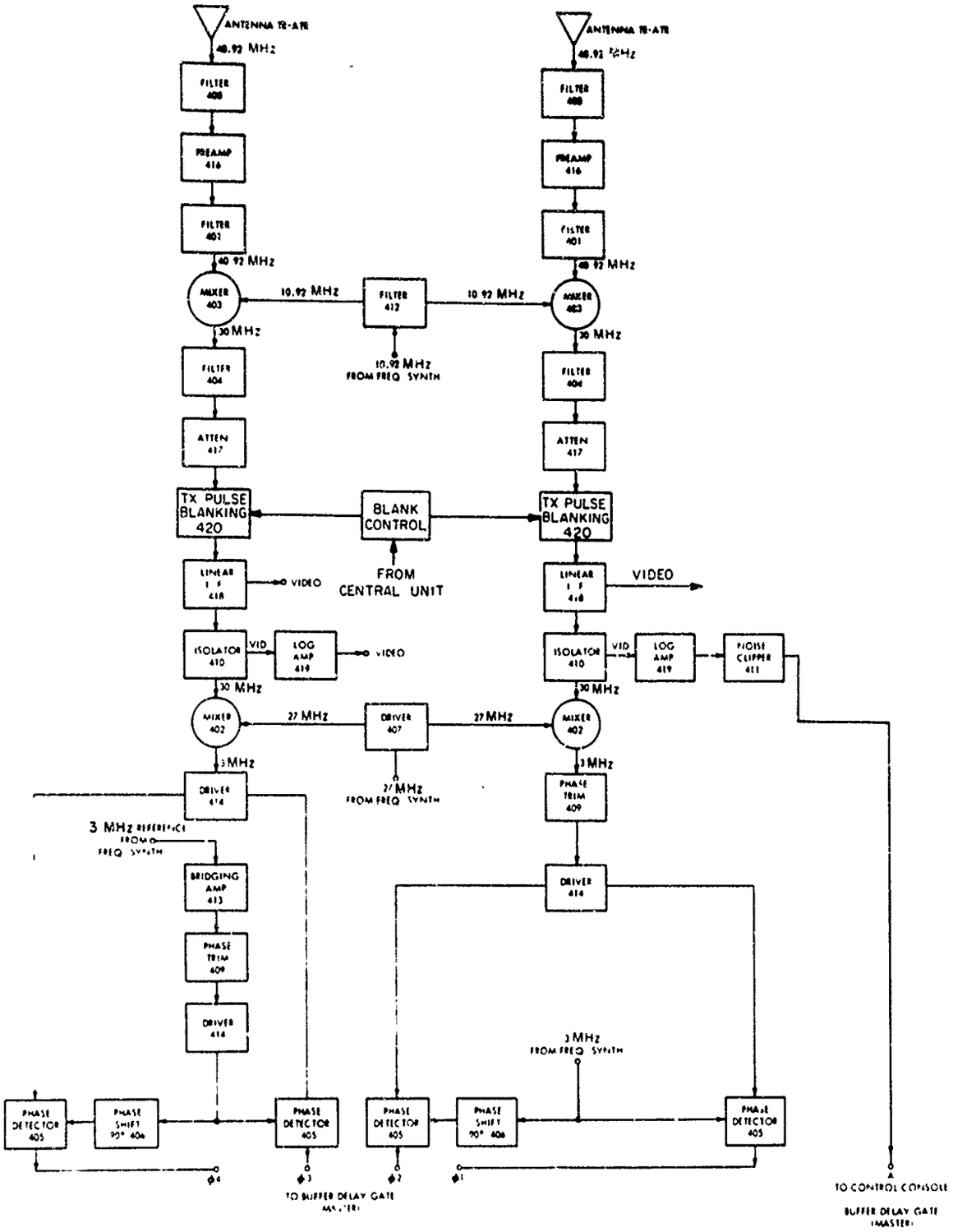

Figure 3-10. Dual-channel receiver.

The mixer and reference input signals of 10.92 MHz, 27 MHz, and 3 MHz are generated for the receiver by the offset frequency synthesizer. All receiver amplitude and phase outputs are connected into the master site data-flow circuits. The amplitude output is also brought to the monitor console.

3.6 Typical Outlying/Remote Station

The receivers used at the remote sites 7 and 8 are the original prototype units developed by the Advanced Development Laboratories (ADL) of Nashua, New Hampshire. The receivers at the outlying sites 1, 2, 4, 5, and 6 were manufactured by Aerospace Research, Incorporated (ARI), of Boston Massachusetts. The Advanced Development Laboratories' equipment is described in this section. The Aerospace Research, Incorporated, equipment is described in Section 3.14.

The Aerospace Research, Incorporated, equipment is a better integrated system (ARI having had the advantage of the ADL prototype to work from), and it should be used as the model for any future duplications of the radar network.

Each outlying/remote station contains an antenna, a single-channel receiver, a phase-locked secondary standard, a frequency synthesizer, a multiplexer, a subcarrier transmitter, a calibrator, a tone receiver, and a microwave link. The block diagram for this equipment is shown in Figure 3-3. The subcarrier units are described in Section 3.8, the calibrator and tone receiver in Section 3.13.

The 2.5-kHz reference signal, brought from the master station to the remote sites by telephone line, is connected to the phase-locked secondary standard. The secondary standard produces phase-coherent 1-MHz and 100-kHz signals, which are operated on by the frequency synthesizer for the generation of the receiver-reference signals. The receiver describes target echoes by producing three parallel outputs: A, ϕ_1, and ϕ_2. The signal A is

sent on the subcarrier, while ϕ_1 and ϕ_2 are time-multiplexed and sent directly on the microwave, as bipolar video signals.

3.6.1 Phase-locked secondary standard

A block diagram of the phase-locked secondary standard is shown in Figure 3-11. The phase-lock loop has a long time constant so that the short-term stability of the oscillator cannot be disturbed.

The 2.5-kHz synchronizing signal enters a lightning protection network that safeguards the input circuits of the secondary standard. The signal passes through a 2.5-kHz amplifier and filter that removes telephone-line noise. It then enters a phase detector, which performs a comparison between the reference signal and the 2.5-kHz driver output. The output of the phase detector is a 2.5-kpps pulse with its width proportional to the phase difference. The pulse feeds the integrator circuit for controlling the frequency of the 1-MHz voltage-controlled crystal oscillator. An isolator-driver stage prevents loading of the oscillator. A decade-counter divider reduces the frequency to 100 kHz. A second decade counter and two binary counters further reduce the frequency to 2.5 kHz for application to the phase detector, thereby closing the loop. The 2.5-kHz driver stage prevents loading of the divider circuits. The 100-kHz filter amplifier extracts the 100-kHz component from the first decade divider providing a clean sine wave output of adjustable amplitude for driving the remote-site frequency synthesizer.

3.6.2 Frequency synthesizer

The frequency synthesizer (Figure 3-12) receives the phase-locked 1-MHz and 100-kHz sine waves from the secondary standard. Three phase-coherent signals are generated for the single-channel receiver. These signals consist of 10.92-MHz and 27-MHz local oscillator frequencies and a 3-MHz reference phase-detector frequency.

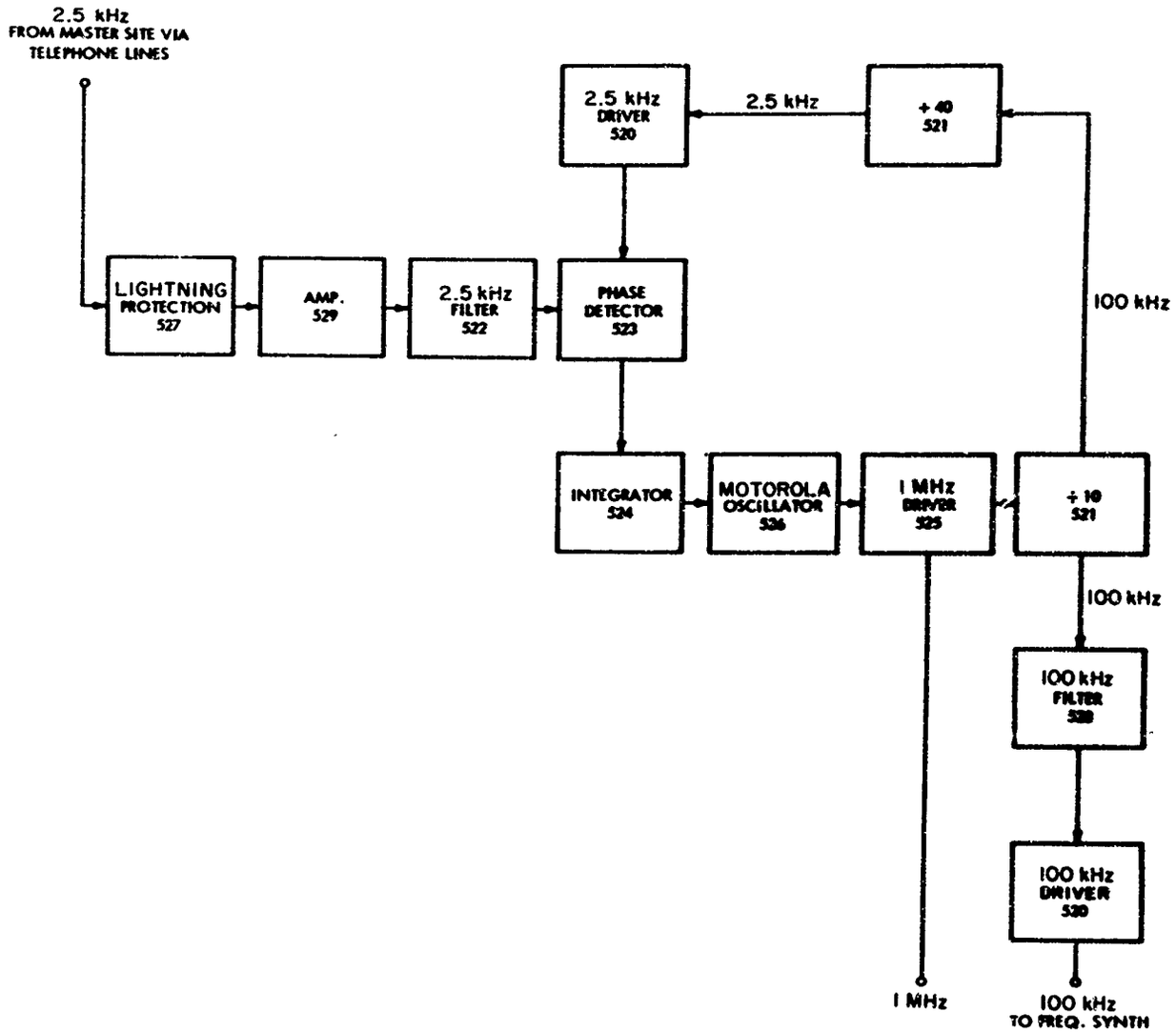

Figure 3-11. Phase-locked secondary standard.

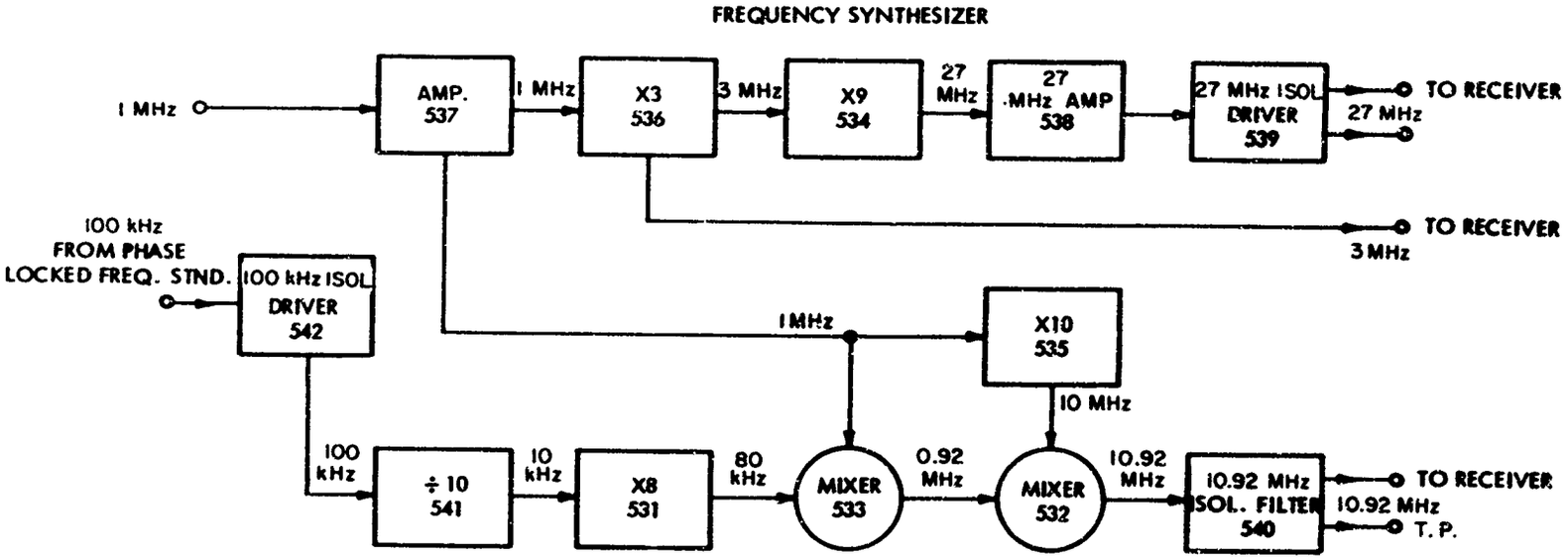

Figure 3-12. Frequency synthesizer.

3.6.3 Single-channel receiver

A block diagram of the single-channel receiver is shown in Figure 3-13. This receiver is a one-channel version of the receiver used at the master station and produces amplitude, phase, and phase-sense information.

The receiver is a double-conversion heterodyne unit followed by two phase detectors operating in quadrature. The 40.92-MHz echo returns are converted to 30 MHz, from which are derived both linear and logarithmic video data. The 30-MHz I.F. is also fed into a second mixer for conversion to 3 MHz, which is brought to the phase detectors. The phase detectors operate in quadrature to eliminate phase ambiguity.

The receiver dynamic range exceeds 60 db, of which 40 are available at any one time. A front panel attenuator provides selection of the desired 40 db. Maximum sensitivity is obtained with a 0-db attenuation. When strong signals are being received, the maximum dynamic range is obtained by using the minimum attenuation that prevents linear I.F. amplifier saturation.

3.6.4 Time multiplexer

The time multiplexer (Figure 3-14) obtains the phase data from the single-channel receiver and serializes the phase 1 and phase 2 information at 25-μsec intervals. The time-multiplexed signals are then brought to the microwave link for transmission.

3.7 Microwave Links

The outlying/remote stations are connected to the main site by wideband microwave links that transmit the broadband amplitude and phase information to site 3 for processing. The microwave equipment transmits at frequencies of approximately 7 GHz. The signal-to-noise ratio is in excess of 50 db. Each of the seven microwave links is comprised of two terminals and contains a service channel for voice communication. All links operate over a single hop path without the need of relay stations.

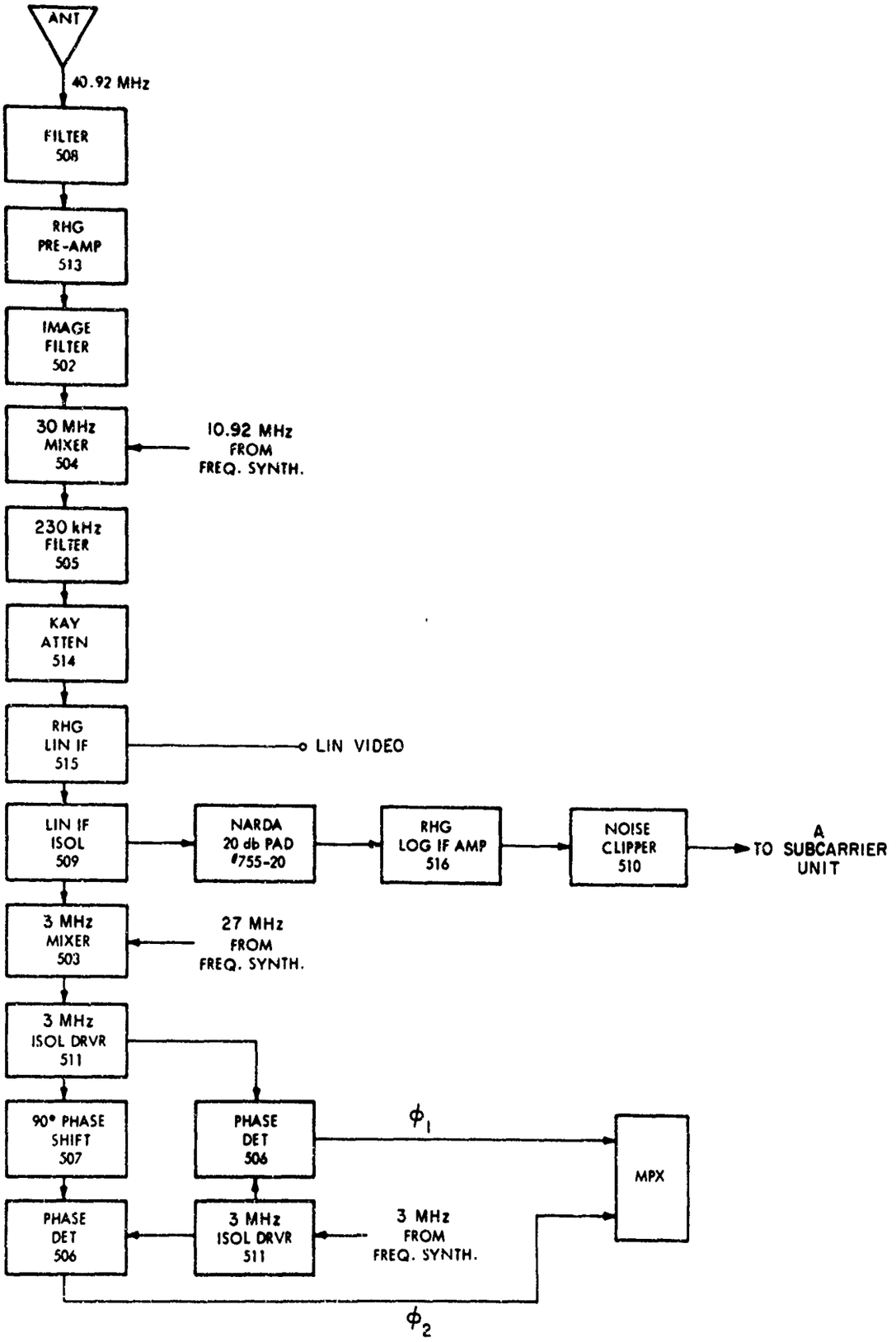

Figure 3-13. Model 1235 receiver.

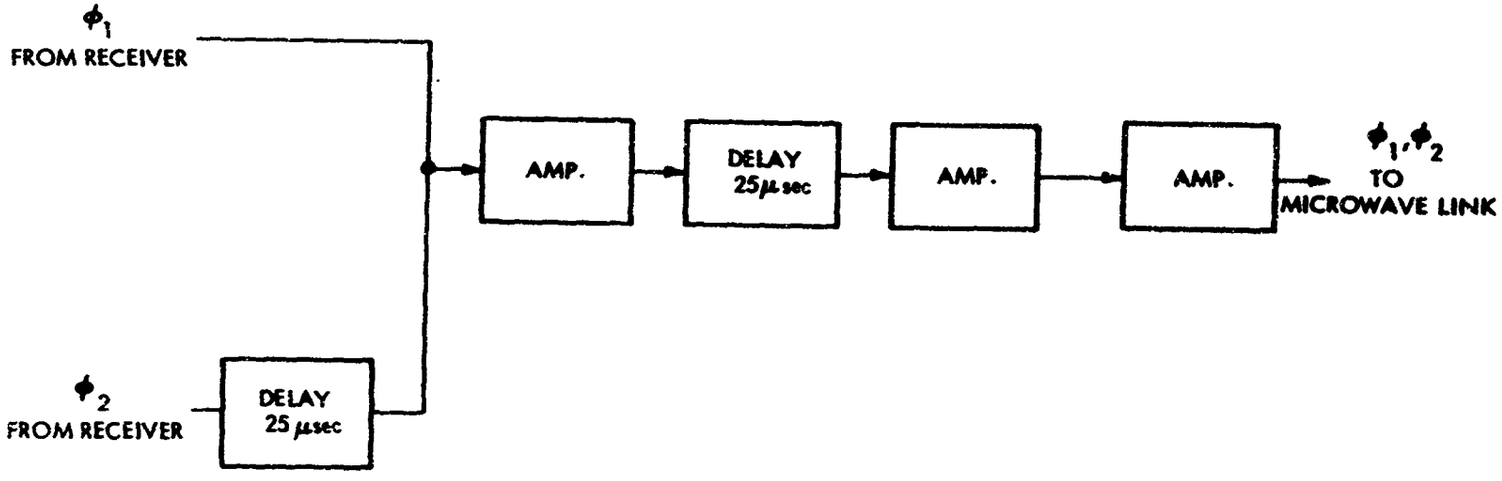

Figure 3-14. Time multiplexer.

The master station is connected to sites 1, 2, 4, 5, and 6 by Raytheon MCR-1000 links, which have a R.F. power output of 1 w and a 3-MHz baseband. Collins MW502A units, with a R.F. output of 100 mw, connect the main site with sites 7 and 8 and have a baseband of approximately 360 kHz.

Table 3-3 lists the dimensions of the microwave towers, dish antennas, and reflectors used at the outlying/remote stations. The master station uses a 130-ft tower and a 200-ft tower. The 130-ft tower links the master station with sites 2, 4, and 5. The 200-ft tower contains reflectors for site 1 and laser antenna for site 6 at a 150-ft height and reflectors for sites 7 and 8 at the 200-ft height. Table 3-4 lists the antennas and reflectors located at the master station and the corresponding remote-station link.

3.8 Signal Flow

The demultiplexers, adding amplifiers, buffer delay gates, and subcarrier units constitute the bulk of the signal handling equipment.

3.8.1 Main site signal flow

Signals A, ϕ_1, ϕ_2, ϕ_3, and ϕ_4 are delayed 10 μsec and sent to the adding circuits (Figure 3-15). This allows time for the pattern recognizer and "And" circuit to function. The pattern recognizer sends a 16-μsec gate to the "And" circuit. The A signal arrives during this gate and enables the "And" circuit. The "And" circuit triggers the variable delay, which, in turn, operates the gate pulse generator and delay gate generator. The variable delay and delay gate generator are adjusted to send signals to the adding amplifiers at the same time the A or ϕ signal arrives there. When both signals arrive at the adding amplifier, an output proportional to the inputs is produced. A pedestal is added to the ϕ signals to convert the bipolar input to a monopolar output.

3.8.2 Outlying/remote station signal flow

The buffer delay gate functions the same as for the master station (Figure 3-16). There is no need to delay the ϕ signals as they are already

Table 3-3. Dimensions of microwave towers, reflectors and antennas at the outlying/remote sites.

Station	Tower height	Antenna size	Reflector size
1	110 ft	4 ft	6 × 8 ft
2	40	4	none
4	110	4	6 × 8
5	70	4	6 × 8
6	150	4	6 × 8
7	290	6	8 × 12
8	220	6	8 × 12

Table 3-4. Dimensions of antennas and reflectors at the main site.

Link	Antenna size	Reflector size
1	4 ft	6 × 8 ft
2	4	6 × 8
4	4	6 × 8
5	4	6 × 8
6	8	none
7	4	8 × 12
8	4	8 × 12

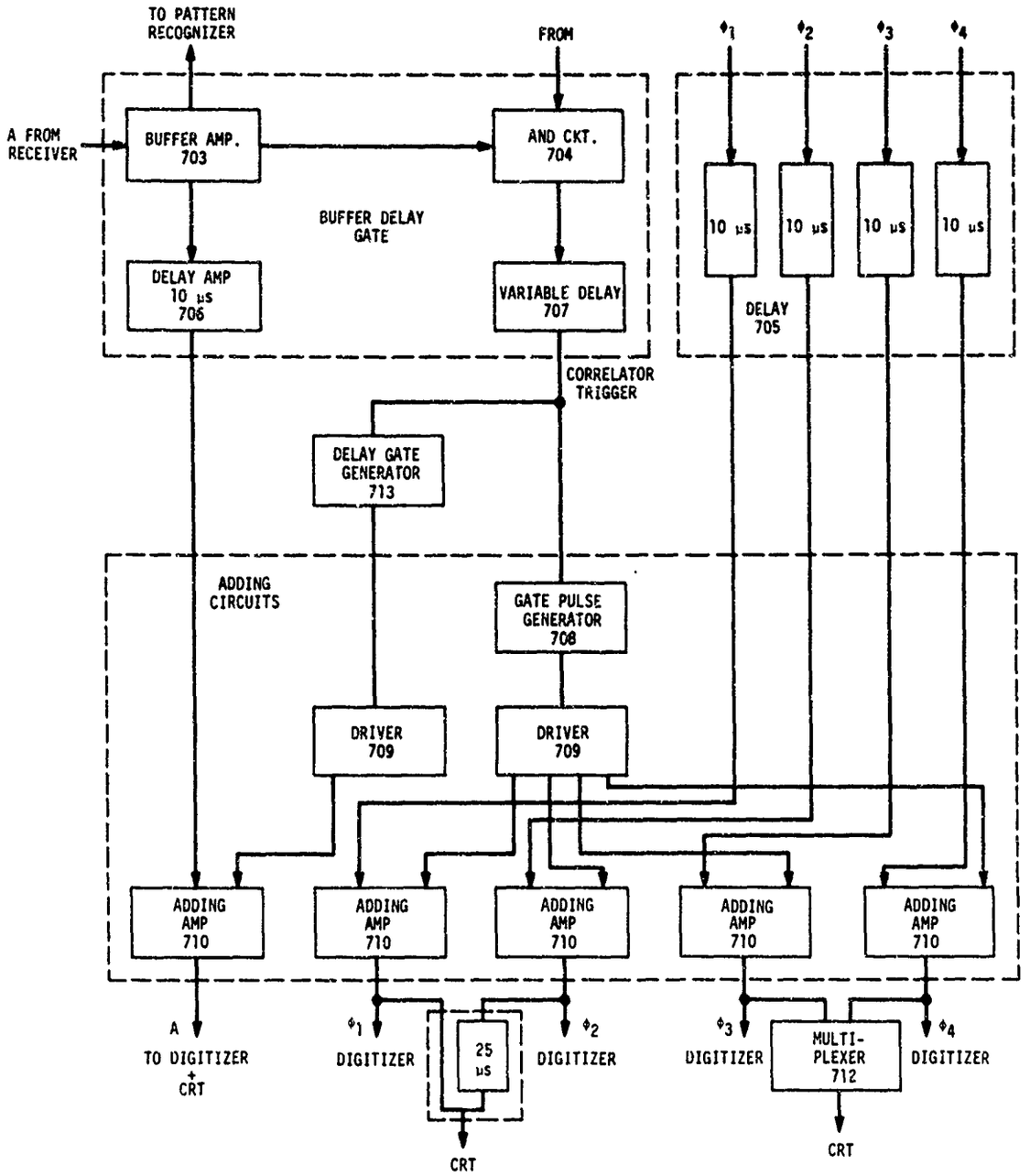

Figure 3-15. Signal flow at the main site.

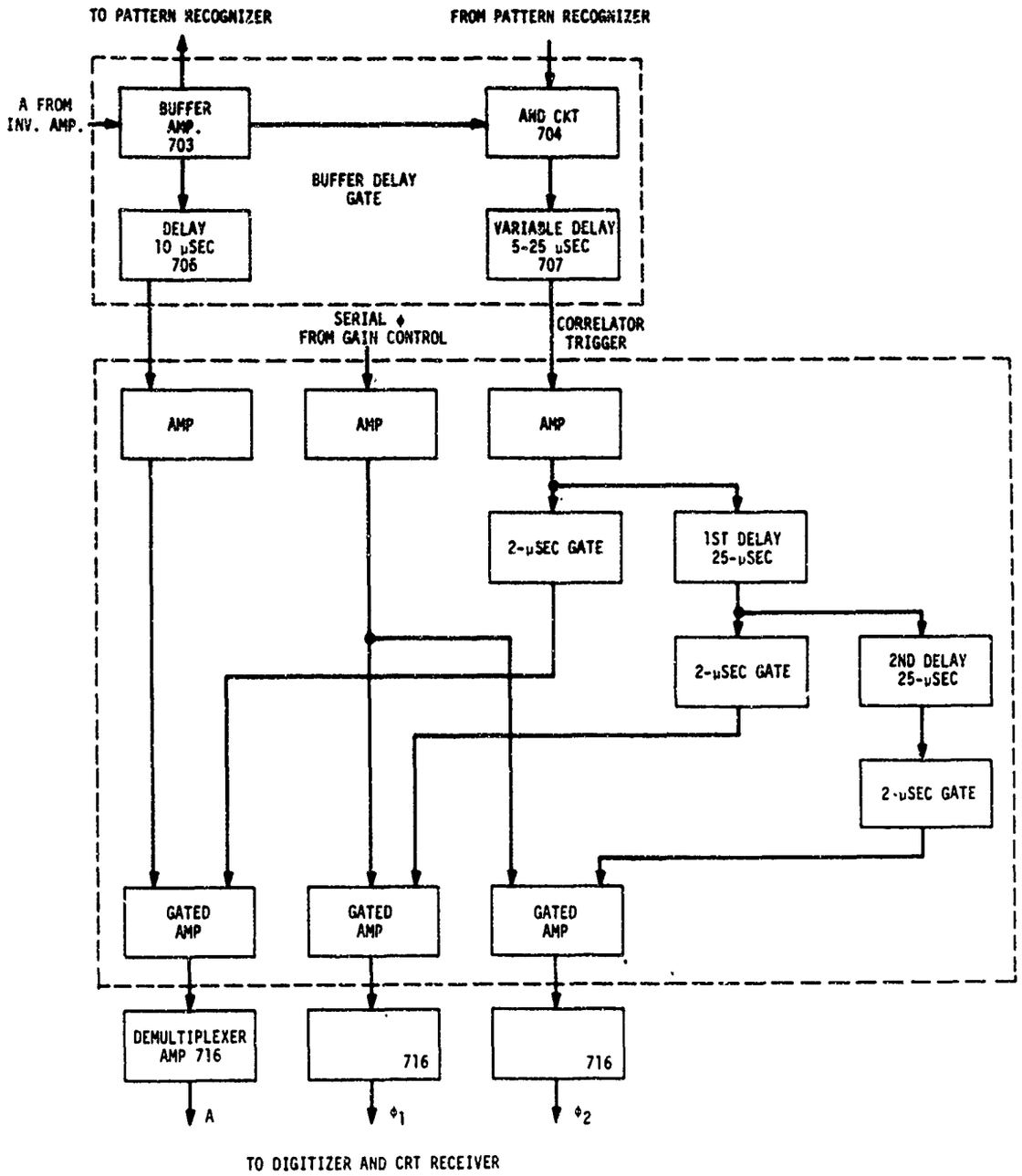

Figure 3-16. Flow of the signals from the outlying/remote stations.

delayed by the time multiplexer. The variable delay and 25-μsec delays of the demultiplexer are adjusted so that the 2-μsec gate arrives at the gated amplifier at the same time as the A or ϕ signal. A pedestal is added to the ϕ, since the digitizer cannot record bipolar signals.

3.8.3 Subcarrier units

In the subcarrier transmitter (Figure 3-17) the amplitude (A) from the radar receiver modulates a 2.3-MHz carrier to produce a pulse-modulated 2.3-MHz signal in the baseband of the microwave link. The receiver accepts this 2.3-MHz pulse while rejecting the time-multiplexed phase signals present in the same baseband of the microwave link. The pulse-modulated 2.3 MHz is detected, filtered, and amplified to produce an inverted A at the output of the receiver.

3.9 Meteor-Radar Processor

3.9.1 Purpose

The purpose of the meteor-radar processor is the following:

A. To recognize, with an adjustable probability of error, target echoes from interference, regardless of the amplitude of interference.

B. To determine which target's echoes and which interference signals are to be recorded.

C. To execute range measurements on the selected echoes.

D. To control automatically the motion of the tape and film in order to have records of the proper length.

E. To track individual targets throughout their lives and to maintain memory of them for a preselected duration after their end, in order to avoid repeated recordings of long-lasting or fading echoes.

F. To generate auxiliary signals for the digitizer and transmitter.

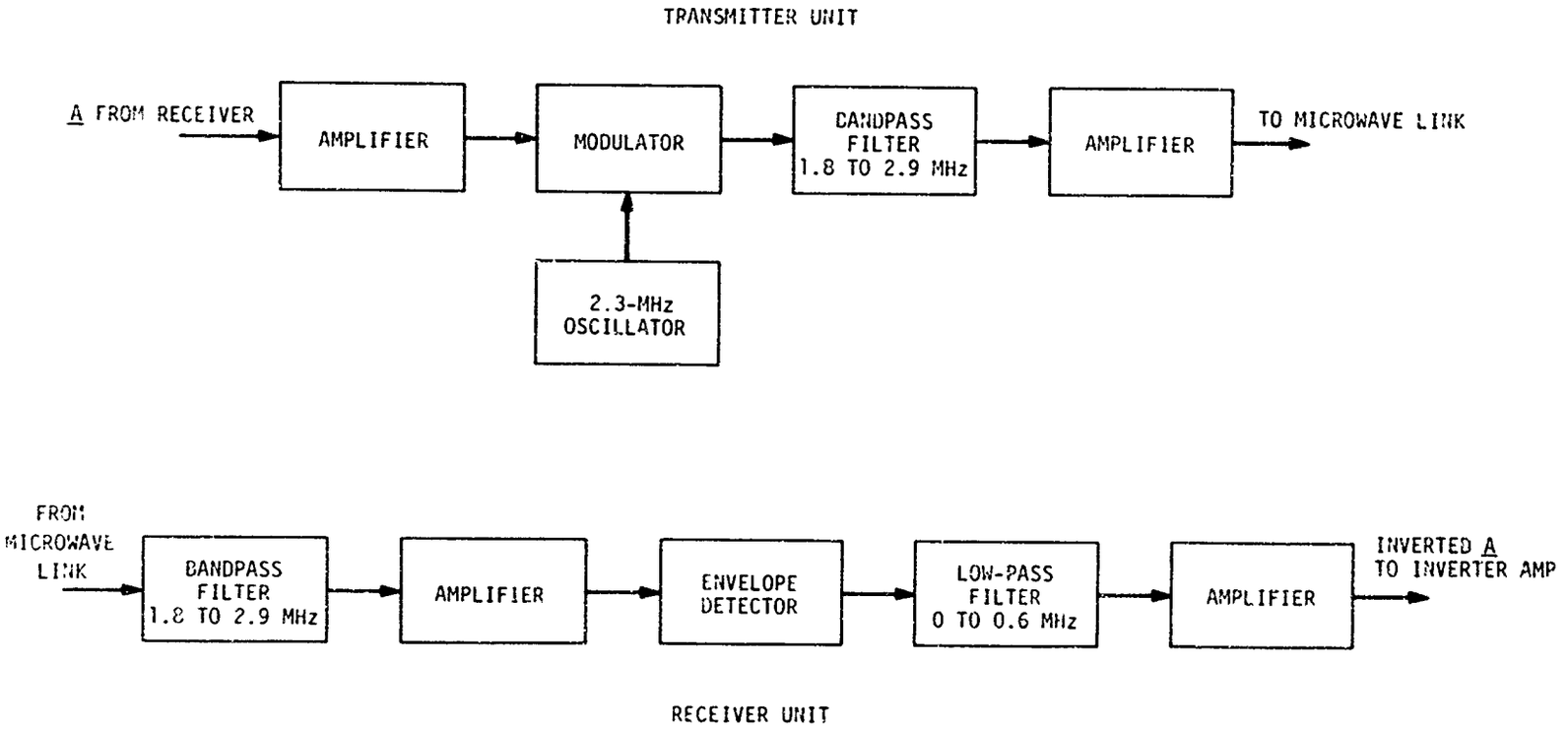

Figure 3-17. Block diagram of subcarrier units.

3.9.2 Equipment

The meteor-radar processor is located at the master station, site 3. The processor is comprised of eight pattern recognizers and one central unit arranged within two standard 19-inch relay racks. Each rack contains its own power supply and circulating-air blower. Solid-state circuit cards, containing silicon semiconductors, are used throughout the units.

The pattern recognizers and central unit are connected within the system as shown in Figure 3-18.

3.9.3 Processing organization

The system has been organized into three distinct levels of processing, i.e., recognition, decision, and control. This organization results in a converging reduction of data.

3.9.4 First-level processing

The purpose of this processing level is to recognize target echoes and to track them throughout their entire lives.

Each site has a corresponding pattern recognizer that has the capacity for simultaneously recognizing 26 targets. The eight pattern recognizers may consequently perform first-level processing on a maximum of 208 contemporary signals. In order to execute this large amount of processing without a prohibitive quantity of hardware, the first-level processing is performed with circulating self-programed digital words.

A delay medium for digital signals is connected in a close loop with an operating digital circuit. Digital bits circulating within the system are grouped in independent words that contain a 3-bit program part and a 13-bit data part. The word capacity of the circulation system is determined by the bit rate and the length of the delay line. When the word enters the operating

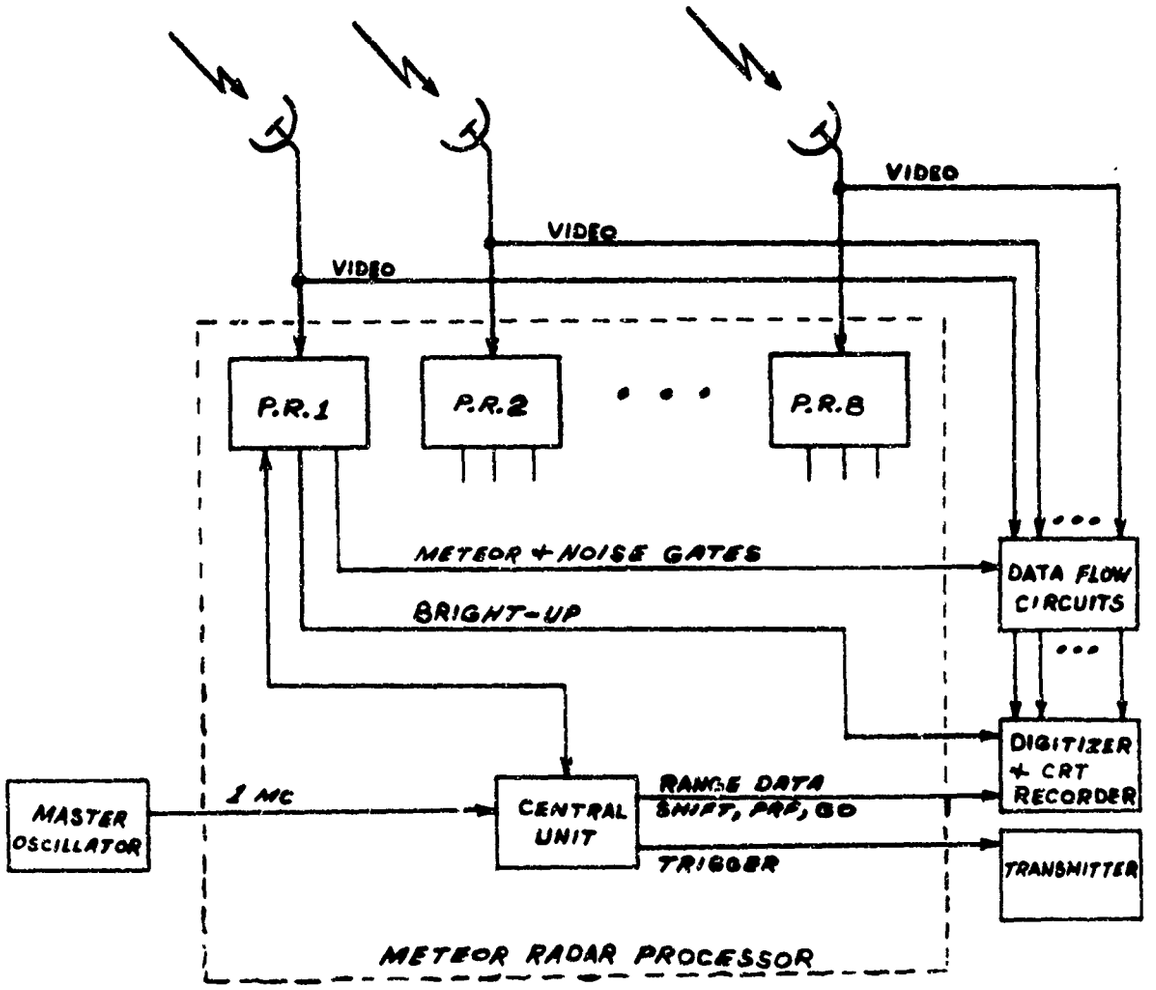

Figure 3-18. Block diagram of meteor-radar processor.

circuit, the program portion of the word organizes the circuit for a particular operation to be performed on the data and program bits. After the operation is executed, the modified word recirculates and once more enters the operating circuit where an additional operation is executed. In this way a long process can be performed on stored or arriving data, step by step, in many circulations. Moreover, many independent processings can be performed by several words circulating simultaneously in the system.

The processing performed upon a word in circulation is controlled by the program bits associated with that word. These bits may have a configuration corresponding to the states indicated in Figure 3-19. Four states and six state transitions are possible.

000 The circuit is awaiting input data.

A A detected signal causes a transition to state 100.

100 A word is placed in circulation. The presence or absence of a signal from the corresponding range is noted in succeeding circulations of the word and the data bits are appropriately changed – a binary 1 is added or subtracted during each circulation.

B The data count within the word reaches a preset value K of 4, 8, 16, or 32. A transition to state 101 occurs. With K equal to 16, the data bits are changed to 1000010010000.

C The data count reaches the preset value but another circulating word is currently in state 101. A transition to state 111 occurs.

D The data count reduces to zero because of the absence of input signals from that range corresponding to this word. A transition to state 000 occurs.

101 A target echo recognition signal is generated. The word remains in circulation to track the target, but counting is restricted from 1000000000000 to 1000010011111.

E A transition to state 111 occurs because the data count falls to 1000000000000 or because of an order from the central unit.

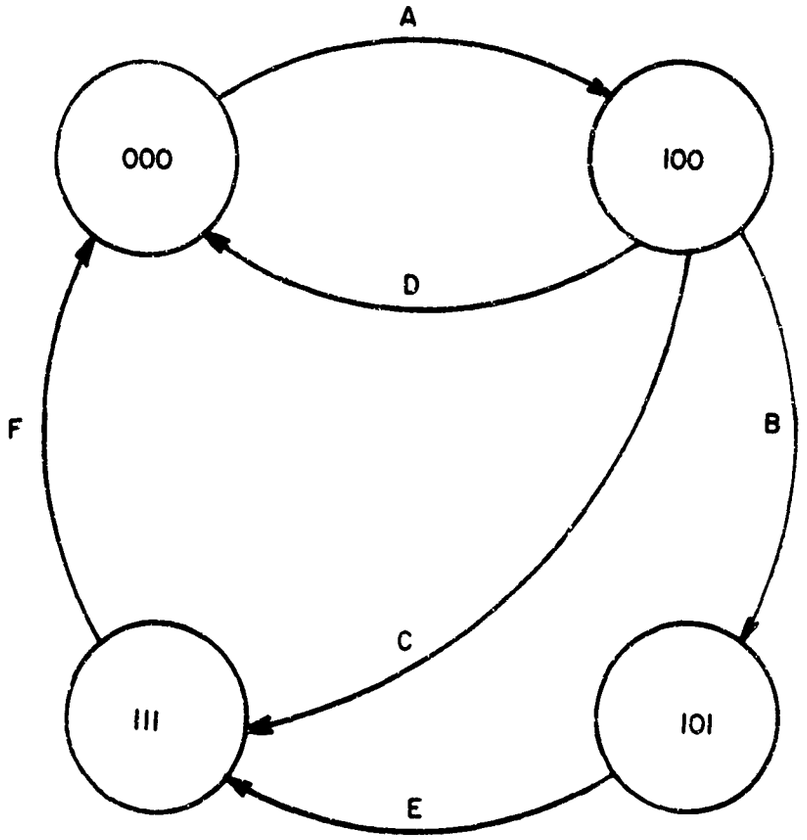

STATES	STATE TRANSITIONS
000	A
100	B
111	C
101	D
	E
	F

Figure 3-19. States and state transitions.

111 The word is kept in circulation with plus and minus counts continuing in order to track the target.

F The data count reaches zero. A transition to state 000 occurs.

The counting operation permits the discrimination of unwanted signals from target echoes by utilizing arithmetical and logical functions.

Many targets are not stationary in space and consequently produce echoes with a time drift between sweeps. In order to track echoes having motion, the circulation word period is allowed to undergo a self-correction in each circulation of ±1 μsec, depending on whether the echo drift is advanced or delayed in time.

3.9.5 Second-level processing

Decisions are made during this processing level that determine the data to be recorded. Each pattern recognizer allows only one of the many targets simultaneously recognized and tracked to be recorded at any single time. Recognized targets being tracked but not recorded may be subsequently recorded, but only if another pattern recognizer activates a record.

An additional function of this processing level is to select sample intervals for interference (terrestrial origin) and noise-signal (cosmic origin) recording.

3.9.6 Third-level processing

Third-level processing is performed by the central unit after receiving signals from the second processing level. The purpose of this level is to control the recording devices for acceptance of data, thereby minimizing the use of magnetic tape and film.

This processing limits the recording of long-duration targets to a predetermined maximum interval of their early life. A target existing longer than this interval may be recorded again but may not itself activate a new

record. The range measurements are executed at this level, and the required auxiliary signals are generated.

3.10 Digitizer and Tape Recorder

The purpose of the Baird-Atomic digitizer is to accept 26 video input channels and one digital input and to record them digitally on half-inch magnetic tape with a format suitable for computer processing. The 27 input channels represent the amplitude outputs of all eight receivers, the ϕ_1 and ϕ_2 outputs of the seven remote receivers, the ϕ_1, ϕ_2, ϕ_3, and ϕ_4 outputs of the master receiver, and a target-range channel from the meteor-radar processor. The digitizer recording is started and stopped by the central unit.

The digitizer (Figure 3-20) consists of a 27-to-18 multiplexer, an 8-bit analog-to-digital converter, logic circuits that provide both transverse and longitudinal parity, a time-of-day clock, and a magnetic-tape transport. The transport is a seven-track Potter MT 36 that incorporates vacuum buffering, 2-1/2-minute rewind, 15-sec tape threading, and 3-msec start time. This unit records at 36 inches/sec with a packing density of 556 bits/inch.

A playback feature provides an analog output of one of the 18 digital channels. The channel is selected by a panel switch on the digitizer.

3.11 CRT Film Recorder

The CRT film recorder contains 18 Tektronix-Type 360 oscilloscopes so arranged that the 70-mm camera film moving in front of them is able to record 18 noninterfering traces (Figure 3-21). The cathode-ray tubes are unblanked and the film started when an echo from any station is to be recorded. The tubes are blanked and the film is stopped when the echo ends, or after a predetermined time interval if the echo persists. An individual amplitude display appears as a series of vertical lines proportional in length to the amplitude of the oscilloscope input signal. The phase display appears as a series of double vertical lines. The ϕ_2 line is blanked every fifth pulse to distinguish between ϕ_1 and ϕ_2 on the film.

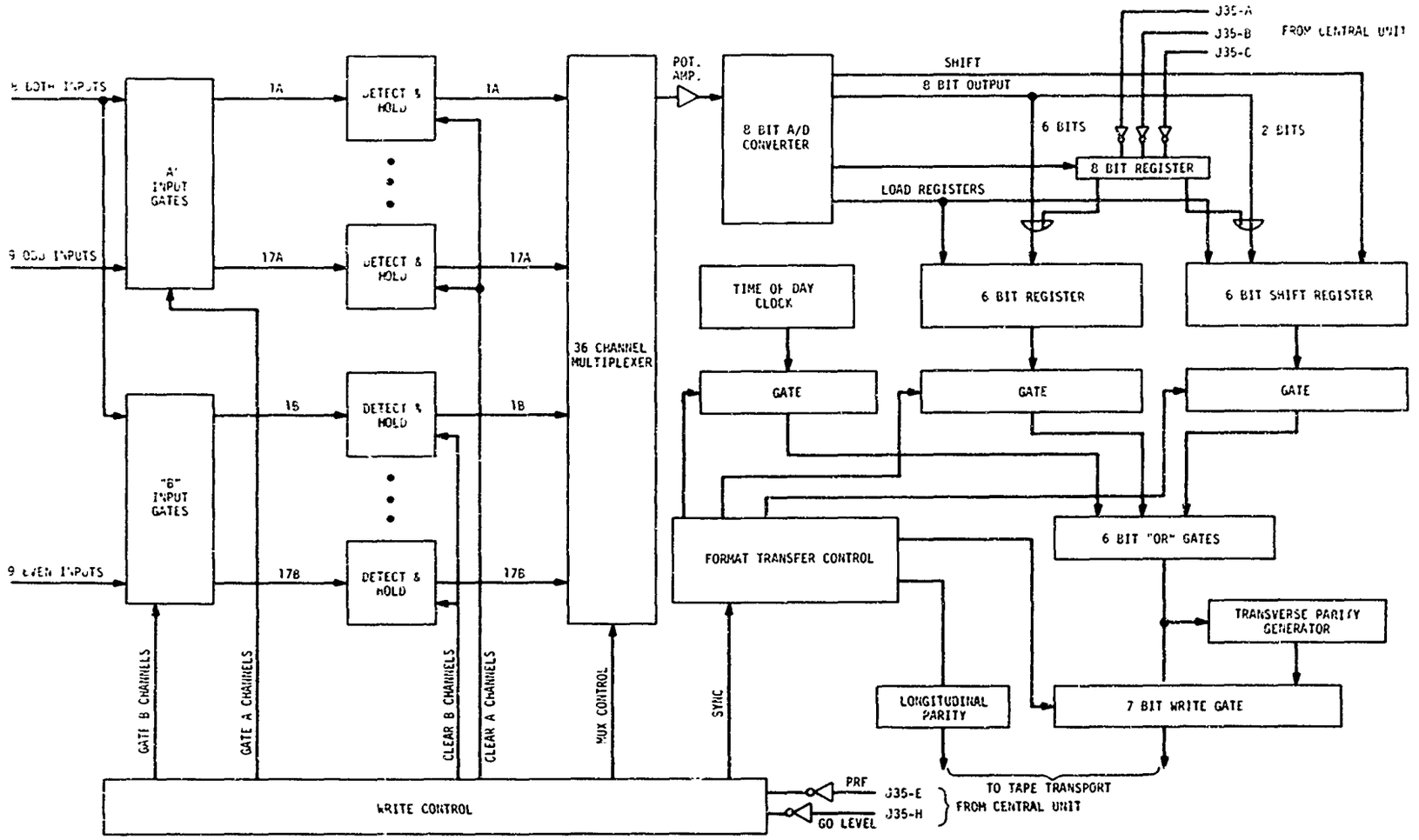

Figure 3-20. Block diagram of digitizer circuits ("write-in" logics).

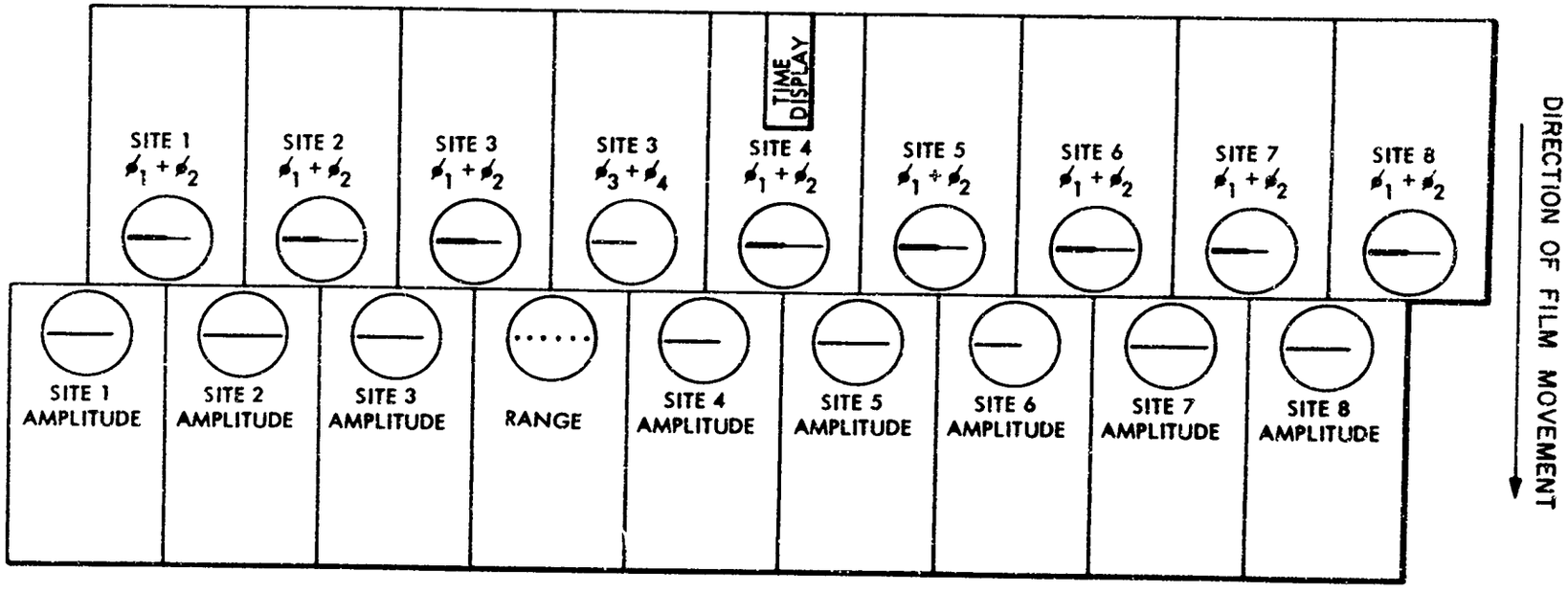

Figure 3-21. Oscilloscope display.

The range display produces a series of 10 equally spaced range marks, over a sweep equivalent to 200 km, once every 5 prf periods. One of these marks is blanked out when a range measurement is being recorded. A coding system within the meteor-radar processor correlates the blanking with a specific station. The appearance of a dot on one of the following four sweeps indicates the target range of that station.

The 27 data-input channels to the CRT film recorder (Figure 3-22) represent the amplitude outputs of all eight receivers, the ϕ_1 and ϕ_2 outputs of the seven remote receivers, the multiplexed ϕ_1 ϕ_2 and ϕ_3 ϕ_4 outputs of the master receiver, and a target-range channel from the meteor-radar processor. The ϕ_1 and ϕ_2 data of each remote station are multiplexed in a phase-adder circuit within the film recorder and appear on a single oscilloscope.

A slave digital time display unit, controlled by the digitizer, is photographed through a mirror arrangement and presented on each CRT film recording at the end of the record.

3.12 Monitor Console

The monitor console contains eight Tektronix 3-inch oscilloscopes to allow the operator to monitor the eight receiver outputs. They are currently connected to monitor the multiplexed phase signals from the remote stations and the amplitude from the master station.

The console also contains controls for the CRT recorder.

3.13 Calibrators

3.13.1 Control unit

The calibrator's control unit supplies a modulating signal and control signals to the master and outlying/remote calibrators. In the "operate" mode the antennas are hooked to the receiver. In the "calibrate" mode the antenna

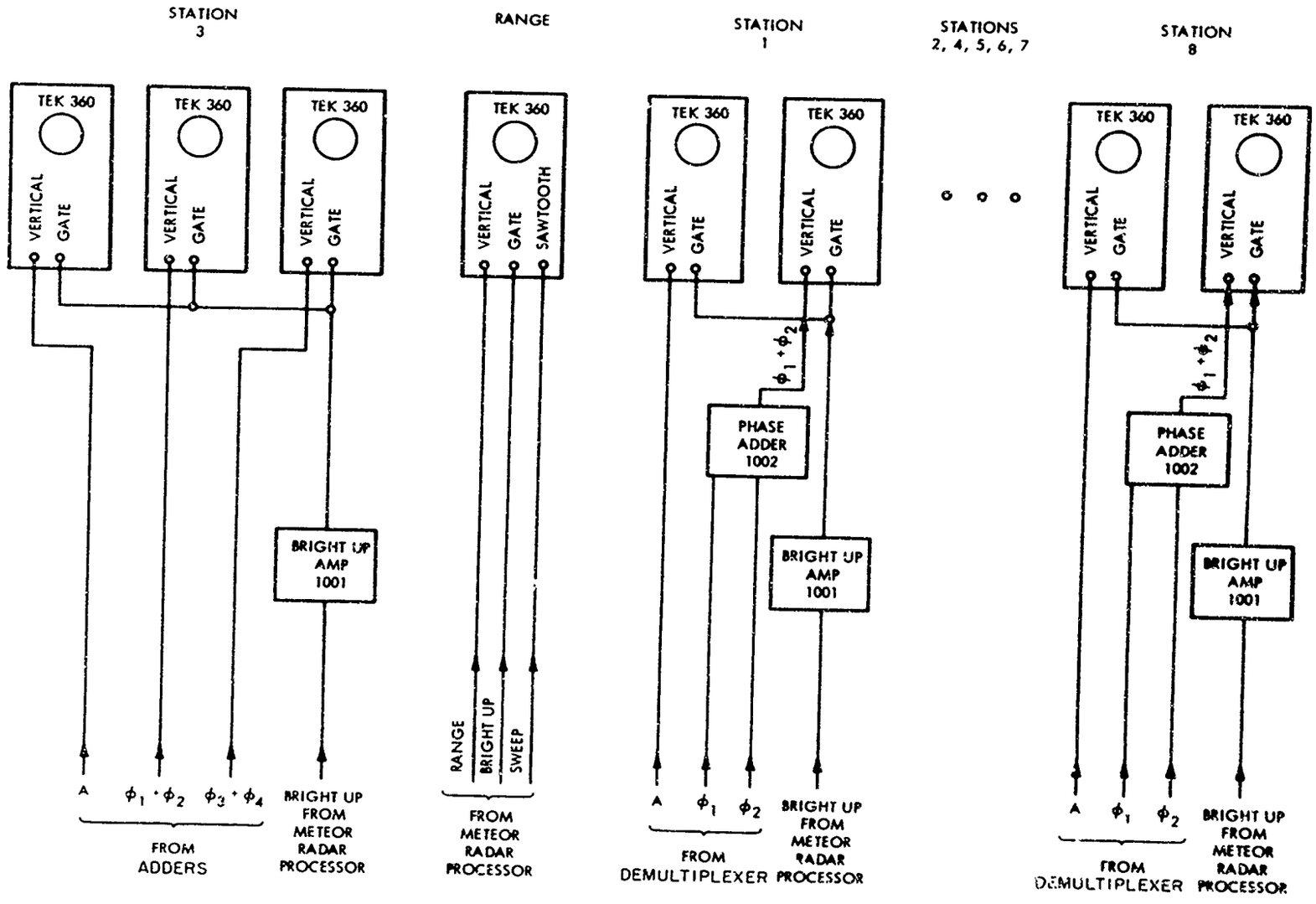

Figure 3-22. CRT inputs.

is disconnected and a pulse, which simulates the received pulse, is sent to the receiver. The level of this pulse is known. The pulse can be attenuated by 0 to 65 db in 5-db steps. Attenuation can also be inserted between the antenna and the receiver to reduce the system sensitivity.

3.13.2 Calibrators at the outlying/remote sites (Figure 3-23)

The oscillator produces a continuous 40.92 MHz, which is modulated by the modulator to produce the simulated pulse. The relay and attenuator are controlled by the logic to switch from the antenna and attenuate the pulse.

3.13.3 Main-site calibrator (Figure 3-24)

The oscillator and modulator produce the calibrating 40.92-MHz pulse, which is attenuated by the remote control attenuator. The power divider provides a pulse of equal amplitude and phase for each input of the receiver. This also calibrates the interferometer feature of the receiver.

In order to reduce the sensitivity of the receivers at the main site, an attenuation pad can be inserted between antenna and receivers.

3.14 ARI Receivers

ARI constructed five phase-coherent receivers and a demultiplexer, using as a prototype the receivers previously developed by Advanced Development Laboratories. The ARI receivers are installed at the five outlying sites. The input and output characteristics are the same as in the ADL equipment, although the method of obtaining the output signals is different. The block diagram for the basic receiver is shown in Figure 3-25 and the frequency synthesizer, phase detectors, and multiplexer in Figure 3-26. The demultiplexer block diagram is the same as the one illustrated in Figure 3-16. Demultiplexer amplifiers are not necessary for the ARI demultiplexer.

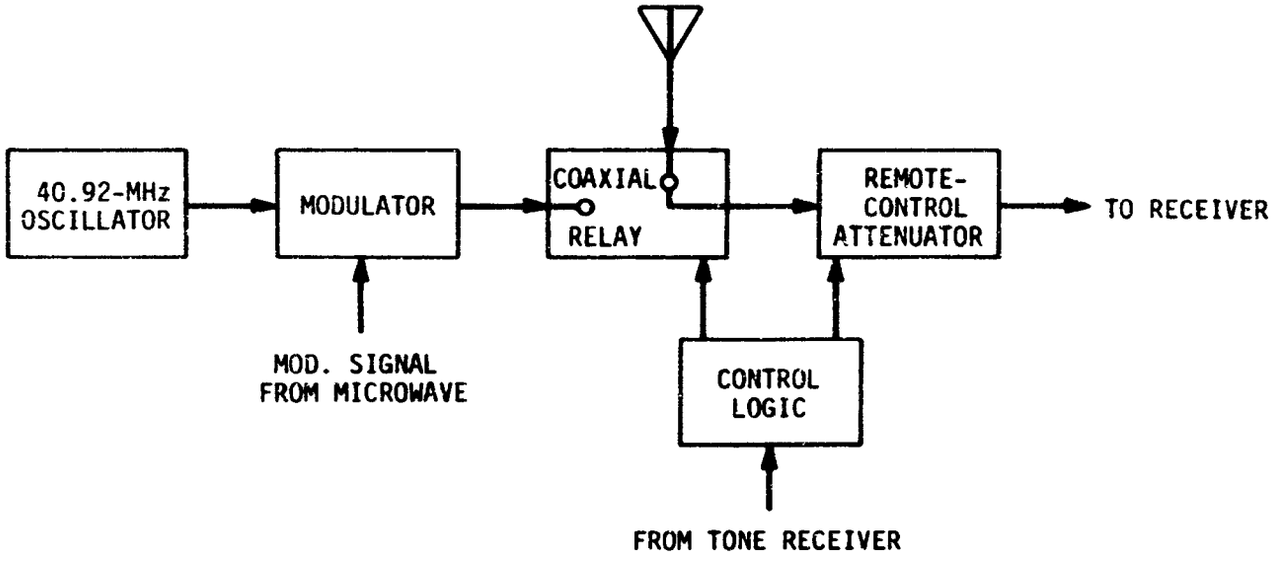

Figure 3-23. Calibrator of the outlying/remote sites.

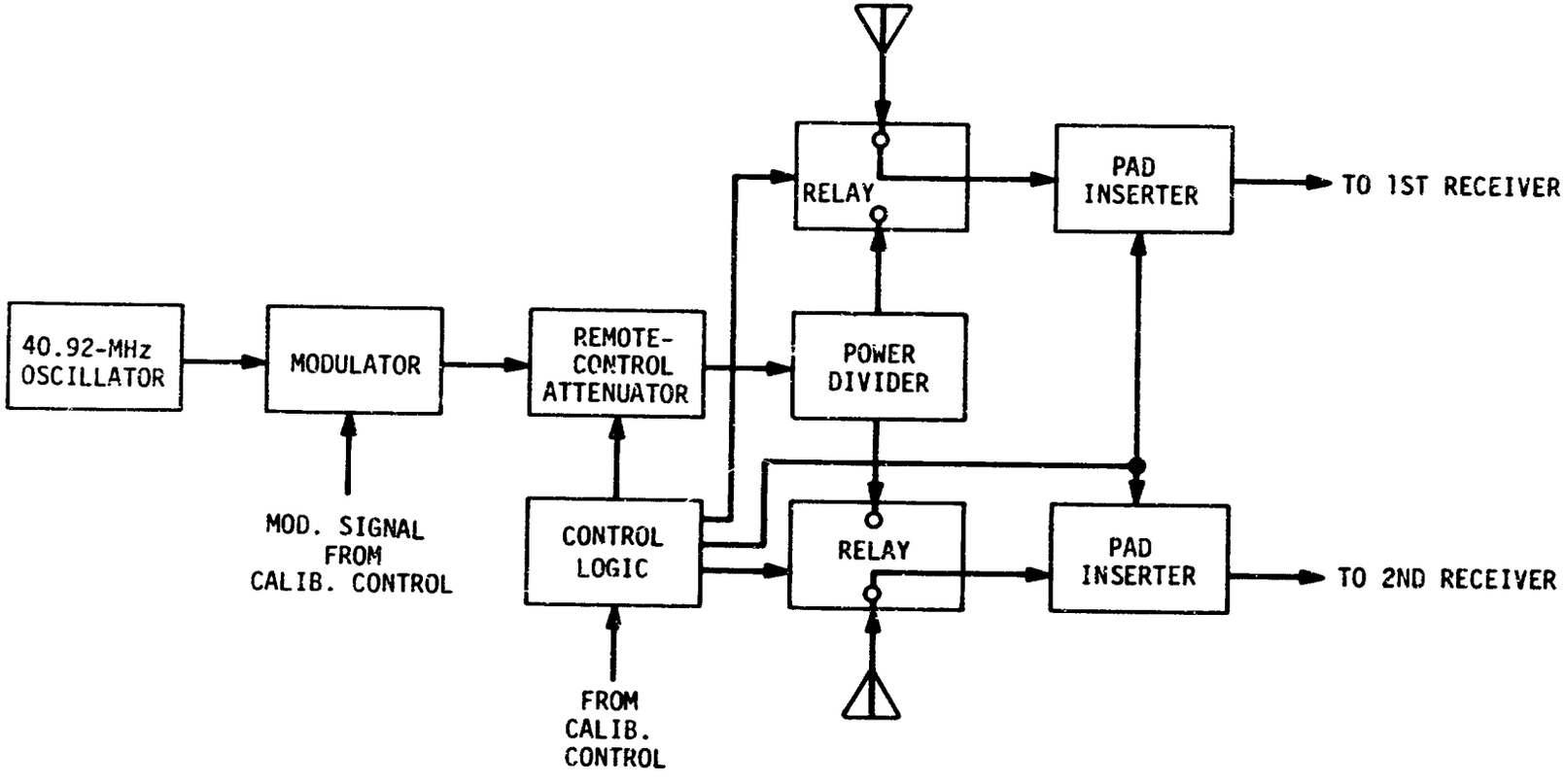

Figure 3-24. Main site calibrator.

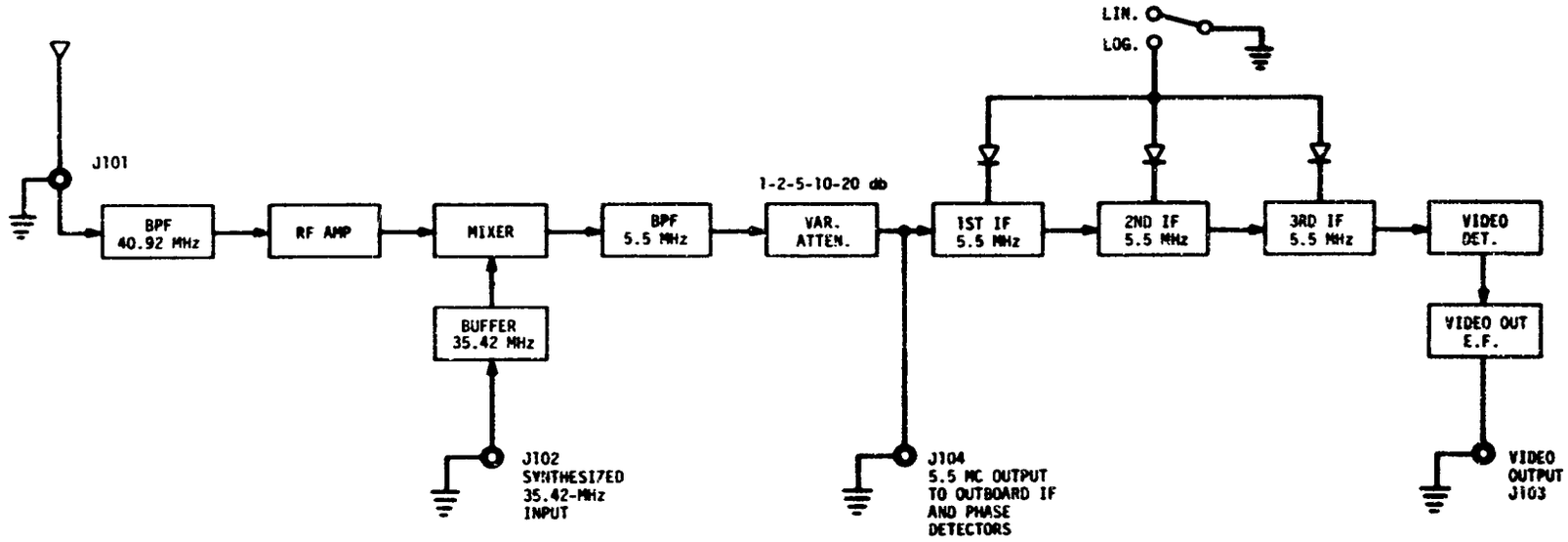

Figure 3-25. Block diagram of the ARI receiver, Model PR-40A.

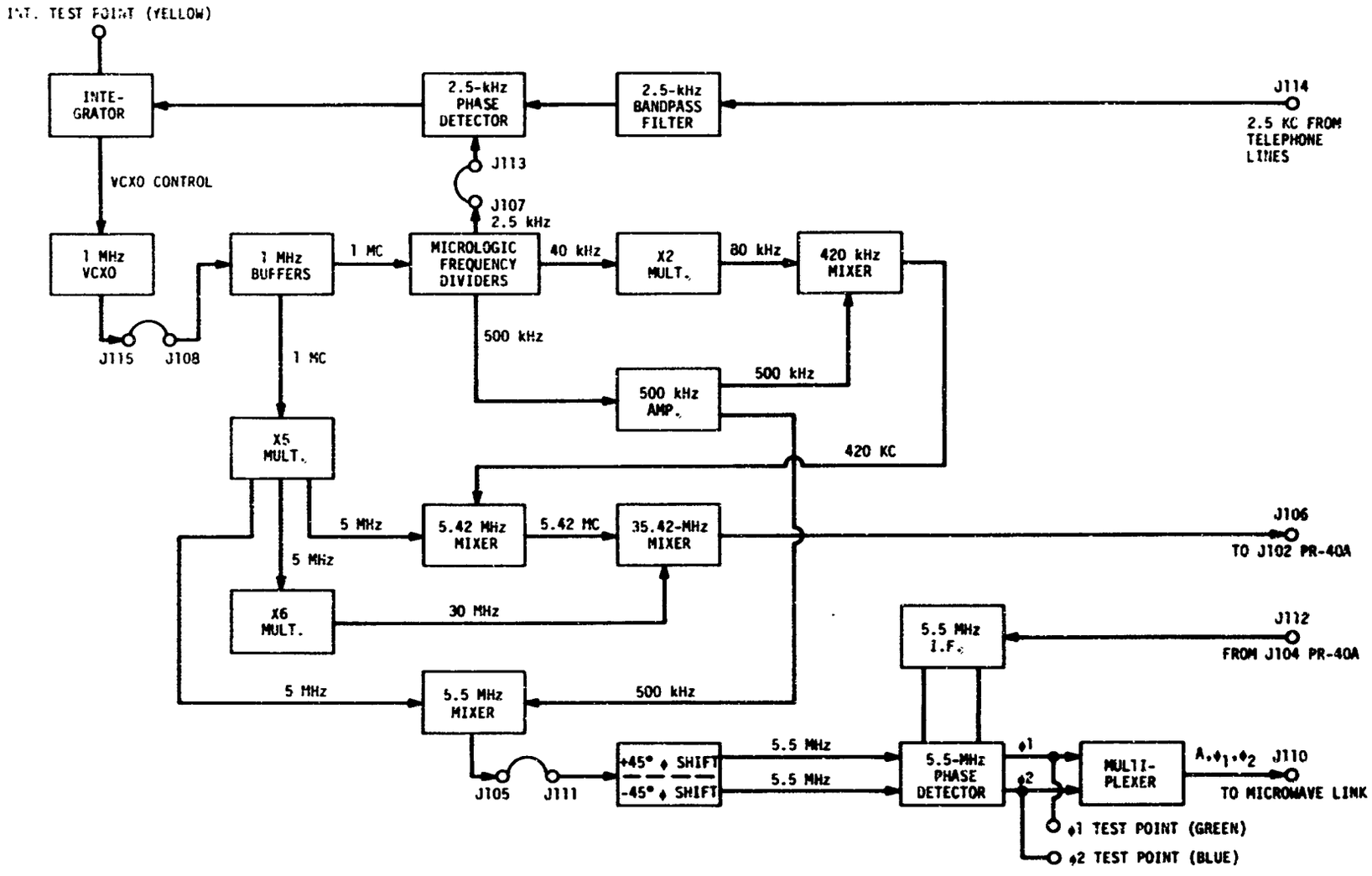

Figure 3-26. Block diagram of the ARI frequency synthesizer and secondary frequency standard.

3.15 Echo Analyzer

The echo analyzer counts echoes that exceed a preset amplitude threshold and stores the results on punched paper tape. Figure 3-27 shows the block diagram of this unit, which is connected through its own receiver to one of the main station's antennas along with the dual-channel receiver. The receiver output is analyzed by the analyzer's logics in order to discriminate between meteors, interference backscatter, and airplanes. The analyzer utilizes the circulating page system (similar to the one of the meteor radar processor described in Section 3.9) and performs the calculations necessary for the recognition of meteors in real time. Four different thresholds are used in a time sequence that repeats itself every half hour. The calibrator injects known amplitudes into the receiver in order to adjust or check the threshold settings. The clock controls the time sequence and supplies time marks for the tape. The keyboard allows an operator to add additional information to the tape.

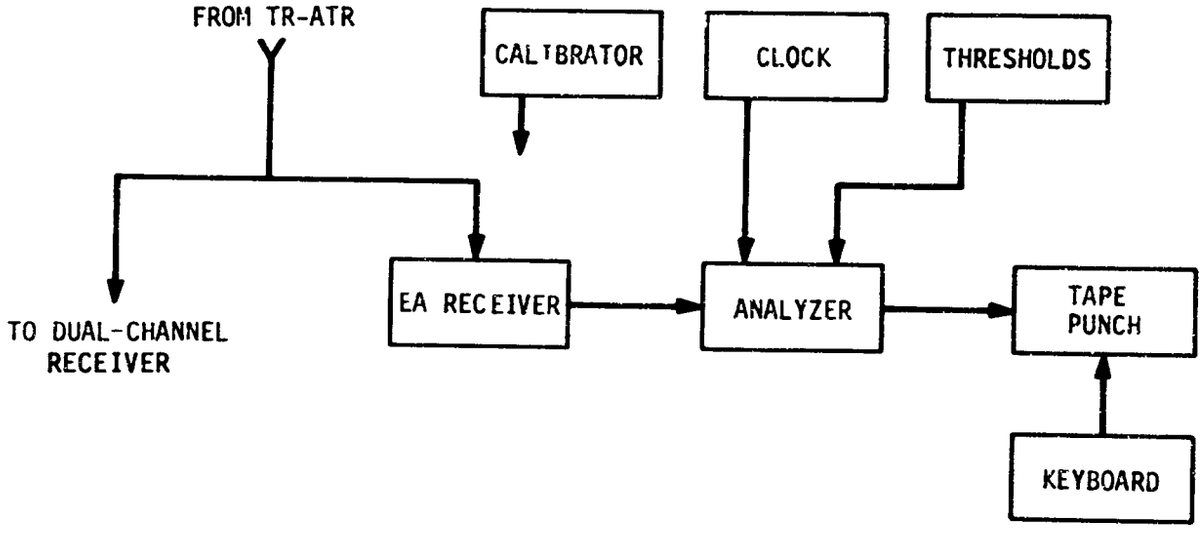

Figure 3-27. Block diagram of the echo analyzer.

4. DATA-REDUCTION PROGRAMS

4.1 Introduction

The Radio Meteor Project radar network records meteor echoes on film in analog form and on magnetic tape in digital form that is suitable for further processing by a digital computer.

A computer program (called MANAGE) to reduce meteor echoes has been written, debugged, and tested. This program can read the data and complete the final reduction without intervention. Often, however, it is more convenient and reliable to divide the reduction into several partial steps that can be separately supervised in the event of inaccurate recorded data.

The reduction process can be divided into four steps: (a) a visual search of the films for the meteor echoes that are likely to give results (although the program rejects unsuitable echoes, this preliminary search saves considerable computer time); (b) reading and analyzing the calibration data; (c) reduction of Fresnel (diffraction) patterns and phase data; and (d) final reduction of the meteor.

4.2 Calibration Data

Each receiving station has its own calibrator, and calibrations are usually recorded every hour. Precisely controlled signal generators insert pulsed signals, at the system pulse repetition rate, through precision attenuators into the receivers. One digitizer and film record is made at each of 11 attenuator steps (5 db/step) when a central control unit advances the attenuators and starts the signal generators at all sites. Both phase and amplitude data are recorded simultaneously so that both are calibrated over their full dynamic ranges, about 60 db for amplitude and 35 db for phase. These calibrations are recorded on both the film and the magnetic tape.

The reduction of calibration data is divided into two parts; the first deals with amplitudes, the second with phase data. Phases are reduced only if amplitudes are successful. From all the recorded amplitudes, a table of input voltages against digital output is produced, stored, and punched for each individual station. Depending on the setting of the equipment, there are usually 10 or 11 calibrating values, so that it is possible to use linear interpolation among them. When this table has been successfully produced, another table of input voltages against phase outputs is stored and punched for further use.

4.3 Reduction of Diffraction Patterns and Phase Data

This segment of the program takes most of the computer time necessary to reduce a meteor from a magnetic tape. The partial output produced, which is the input for the final part of the reduction, is the same kind of output as was generated in the past by people reading film, but is much more accurate and reliable.

At each station, the amplitude data are treated first. The signal at each pulse is converted to microvolts at the antenna, using the results of calibration; saturated signals are rejected. The maxima and minima of the Fresnel patterns are sought by a special pattern-finding procedure. The first maximum is first recognized as the first group of high amplitudes in the record at that station, the first minimum as a following group of lower amplitude pulses, and so forth. Then the first two maxima and the first minimum are more definitely recognized by virtue of good least-squares fits to empirical expressions of the proper shapes. Finally, all maxima and minima that can be reliably detected are measured in order from the first maximum, by similar least-squares fits.

If five or more points are measured in the amplitudes the phase data are converted to volts and analyzed. The received phase is computed at every suitable pulse and corrected for the phase shifts caused by the Fresnel diffractions. They are finally fitted by a set of phase coefficients used to find atmospheric winds and wind shear.

This kind of analysis is performed for each receiving station and also for an extra set of phase data collected at the main station, where the pulsed-radar transmitter is located. Here there are two separate receivers connected to two antennas. The additional set of phase data recorded at this station gives an interferometric measure of the angle of arrival, which is necessary to determine the height of the meteor. The additional amplitudes are not digitized, but they are used for other studies.

When three or more of these stations successfully give amplitude data, punched and printed output is produced, which can be examined and/or used for further reduction. Range measurements (not yet analyzed) are included in this output.

4.4 Final Reduction

When enough data are generated in the partial reduction described earlier, they are used to derive all the information about the meteor and the atmosphere.

The amplitude diffraction data and the range furnish the velocity of the meteor. A measure of the velocity is given at each specular reflection point, as well as the time at which the point was reached. These velocities and times give the direction cosines of the radiant, which are necessary to compute the orbit and the meteor height. When the direction cosines are computed and there is a good measure of the angle of arrival of the echo from the interferometric data recorded at the main station, the height of the meteor is computed. The phase data are used at this stage of the reduction to correct the direction cosines and height of the meteor. After this correction is applied, the phase data are used to produce a wind profile along the meteor path in one dimension. Printed output and punched cards are generated for further use. The antenna patterns and the received and transmitted power are used to compute the magnitude of the meteor at different times. An ionization curve is fitted through these magnitudes, and a graph of it is printed. Then the density and the mass of the meteoroid are computed, as well as atmospheric density and scale height.

A summary of all geometric and physical quantities is printed during the reduction so that all the information about each meteor and the adjacent atmosphere is easily found. Most of these results are punched on cards, which can be used in different studies on the atmosphere and on the meteors themselves.

Figure 4-1 is a flow chart of this final reduction program. Earlier stages of the processing are shown in the flow charts given in the User's Manual (Figures 1-1a and 1-1b of Section 1, Volume II).

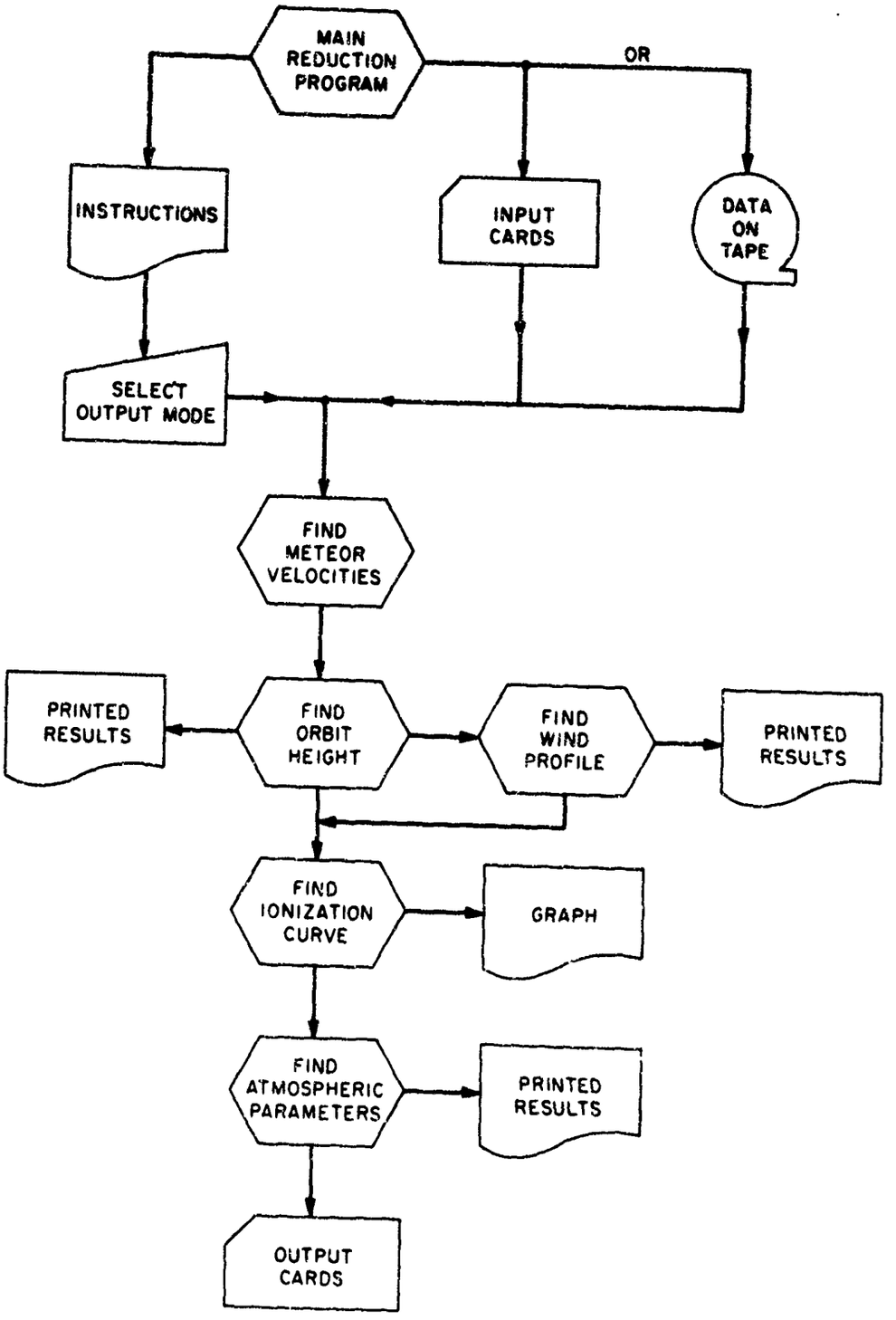

Figure 4-1. Flow chart of final reduction program.

5. CONCLUSIONS AND RECOMMENDATIONS FOR FUTURE ACTIVITY

The main question that this research project had to answer for the U. S. Air Force was whether it was feasible with a system of the Havana type to collect hourly enough meteor echoes to describe adequately the wind pattern in the height range 80 to 100 km.

The answer is positive. The eight-station network that operates in Havana, Illinois, has proved that when data collection is complemented with digital recording and with computer processing in a high-speed machine, sufficient samples are obtained of the wind pattern. The meteor-radar approach appears therefore a feasible and practical avenue for high-altitude wind determinations.

As a matter of fact, if the high-altitude winds must be measured with continuity in a specific volume of the upper atmosphere, the method investigated by the Smithsonian Astrophysical Observatory with Air Force sponsorship is the only approach now known. The nearest method capable of providing similar data is photographic monitoring of rocket-launched chemical releases, but because of the short duration (about 1 hr at most) of the artificial trail produced in this way, repetitive launches are necessary to ensure the continuity of data gathering. Its practicality is therefore questionable for observations extending beyond a few hours.

The program has provided a partial answer concerning the feasibility of measuring density, pressure, temperature, and scale height in the 80 to 100 km altitude range from information extracted from the amplitude decay vs. time of the meteor echoes. The findings of the project are rather pessimistic in this respect: earlier measurements are worthless, and useful new measurements are problematic.

Finally, an answer has been given to the question whether a number of stations smaller than eight (the present Havana configuration) or, more generally, a simpler system would be sufficient to gather range-doppler data in adequate quantity and quality to furnish the description of the wind pattern. The answer to this question is negative. Even with the present eight-station system, the data collected routinely are barely sufficient for the task. A smaller system would tend to omit measurements of changes in the wind comparable in importance to those it observes.

If accurate measurements of the vertical components of the wind vectors are of particular relevance, the two remote sites should be located even farther apart from the main site than they are at present, which would further complicate the system in terms of intermediate relay stations in the radio links and in other respects.

The Observatory therefore offers the conclusion that the Air Force should consider the duplication of the Havana eight-station scheme essentially as it is for cases where continuous and localized monitoring of winds at meteor heights is a requirement.

It is certainly true that the experience gained with the operation of the system has pointed out numerous ways by which improvements can be introduced into the instrumentation to make it more reliable and less costly.

Before system deployment, some additional short-duration developmental effort would be in order in a few areas. For instance, recent developments in high-stability clocks (rubidium vapor, cesium beams, etc.) and recent extensions of the Loran C network make feasible the establishment of a simpler open-loop phase-coherent network, with a consequent possibility of avoiding the use of telephone lines for reference-tone distribution. Among the other units that would also be designed differently today in order to incorporate recent technological developments are the digital recording system, the doppler measurement circuits, and the signal handling unit.

Basically, however, the instrumentation as it now is in Havana constitutes an adequate operational system.

In the area of data reduction, more efficient computer programs could be written and would bring forth considerable savings in machine time. Here too, however, the basic tenet of the SAO approach (wind determination through the computation of the orbital parameters of the meteoroid) still maintains its full validity as a data-reduction principle.

In summary, if the AFCRL needs to satify urgent operational requirements for high-altitude wind determinations, the recommendation of the Observatory is to implement replicas of the Havana system without additional investment in funds and time. The Observatory would be most interested in participating in this activity with both its scientific and engineering resources.

If some time could still be spared, the recommendation of the Observatory would be to devote a 6 to 12 month effort to the refinement of the method proved feasible by the research performed in Contract AF 19(628)-3248, both in instrumentation and in data processing. This additional effort would maximize the practicality of the system as a fully operational tool for the real-time determination of meteor wind patterns.

6. REFERENCES

BEDINGER, J. F., KNAFLICH, H., MANRING, E., and LAYZER, D.

1968. Upper atmosphere winds and their interpretations – I. Planet. Space Sci., vol. 16, pp. 159-193.

DAVIS, J., GREENHOW, J. S., and HALL, J. E.

1959. The effect of attachment on radio echo observations of meteors. Proc. Roy. Soc., ser. A, vol. 253, pp. 130-139.

GREENHOW, J. S., and HALL, J. E.

1960. Diurnal variations of density and scale height in the upper atmosphere. Journ. Atmos. Terr. Phys., vol. 18, pp. 203-214.

GREENHOW, J. S., and NEUFELD, E. L.

1955. The diffusion of ionized meteor trails in the upper atmosphere. Journ. Atmos. Terr. Phys., vol. 6, pp. 133-140.

1959. Measurements of turbulence in the upper atmosphere. Proc. Phys. Soc., vol. 74, pp. 1-9.

GROSSI, M. D.

1963. High altitude wind measurements by collecting and processing meteor radar echoes. Conference on Direct Aeronomic Measurements in the Lower Ionosphere, Conference Record, pp. 82-88, December, U. of Illinois, Urbana, Ill.

HAWKINS, G. S.

1963. The Harvard Radio Meteor Project. Proceedings of the Symposium on the Astronomy and Physics of Meteors, Smithsonian Contr. Astrophys., vol. 7, Washington, D.C.

HAWKINS, G. S., and SOUTHWORTH, R. B.

1958. The statistics of meteors in the earth's atmosphere. Smithsonian Contr. Astrophys., vol. 2, pp. 349-364.

1963. The physical characteristics of meteors. Harvard Radio Meteor Project, NASA Research Report No. 10, 44 pp.

JACCHIA, L. G.

1955. The physical theory of meteors. VIII. Fragmentation as a cause of the faint-meteor anomaly. Astrophys. Journ., vol. 121, pp. 521-527.

KAISER, T. R.

1955. The interpretation of radio echoes from meteor trails. In Meteors, ed. by T. R. Kaiser, Pergamon Press, New York, pp. 55-64.

LAYZER, D., and BEDINGER, J. F.

1969. Upper-atmosphere winds and their interpretation -- II. Planet. Space Sci., vol. 17, pp. 1891-1911.

LOEWENTHAL, M.

1956. On meteor echoes for underdense trails at very high frequencies. Lincoln Lab. Tech. Rep. No. 132, M.I.T., December.

MANNING, L. A.

1958. The initial radius of meteoritic ionization trails. Journ. Geophys. Res., vol. 63, pp. 181-196.

McKINLEY, D. W. R.

1961. Meteor Science and Engineering. McGraw-Hill Book Co., New York, 309 pp.

MEHR, T. J., and BIONDI, M. A.

1969. Electron temperature dependence of recombination of O_2^+ and N_2^+ ions with electrons. Phys. Rev., vol. 181, pp. 264-271.

ÖPIK, E. J.

1955. Meteors and the upper atmosphere. Irish Astron. Journ., vol. 3, pp. 165-181.

1958. Physics of Meteor Flight in the Atmosphere. Interscience Publ., New York, 174 pp.

SOUTHWORTH, R. B.

1962. Theoretical Fresnel patterns of radio meteors. Harvard-Smithsonian Radio Meteor Project Res. Rep. No. 14, 60 pp.

WHIPPLE, F. L., and JACCHIA, L. G.

1957. Reduction methods for photographic meteor trails. Smithsonian Contr. Astrophys., vol. 1, pp. 183-206, Washington, D.C.

Unclassified
Security Classification

DOCUMENT CONTROL DATA - R & D

(Security classification of title, body of abstract and indexing annotation must be entered when the overall report is classified)

1. ORIGINATING ACTIVITY (Corporate author)	2a. REPORT SECURITY CLASSIFICATION
Smithsonian Astrophysical Observatory 60 Garden Street Cambridge, Massachusetts 02138	Unclassified 2b. GROUP

3. REPORT TITLE

STUDY OF METEOR WIND MEASUREMENT TECHNIQUES

4. DESCRIPTIVE NOTES (Type of report and inclusive dates)

Scientific Final 1 June 1963 to 31 May 1966 Approved 30 April 1970

5. AUTHOR(S) (First name, middle initial, last name)

Norman F. Deegan, Giuseppe Forti, Mario R. Schaffner, Robert J. Fitzpatrick, Mario D. Grossi, Richard B. Southworth

6. REPORT DATE	7a. TOTAL NO. OF PAGES	7b. NO. OF REFS
February 1970	139	20

8a. CONTRACT OR GRANT NO	9a. ORIGINATOR'S REPORT NUMBER(S)
AF 19(628)-3248 b. Project, Task, Work Unit Nos. 6682-07-n/a c. DoD Element: 65701F d. DoD Subelement: 676682	Final Report (Vol. I) 9b. OTHER REPORT NO(S) (Any other numbers that may be assigned this report) AFCRL-70-0168(I)

10. DISTRIBUTION STATEMENT

This document has been approved for public release and sale; its distribution is unlimited.

11. SUPPLEMENTARY NOTES	12. SPONSORING MILITARY ACTIVITY
TECH, OTHER	Air Force Cambridge Research Laboratories (CRE) L. G. Hanscom Field Bedford, Massachusetts 01730

13. ABSTRACT

Wind data in the height range 80 to 100 km can be obtained with a multistatic VHF phase-coherent pulse-doppler meteor radar capable of monitoring a volume in space measuring approximately 50 km × 50 km horizontally, and 20 km vertically.

An eight-station phase-coherent system has been established for this purpose near Havana, Illinois, by reworking an existing six-station, incoherent, pulse meteor radar operating at 40.92 MHz.

A 4-Mw transmitter and eight receiving sites dispersed up to 50 km away from the transmitter site have been locked together in phase within a few parts in 10^{10} by distributing a 2.5 kHz reference tone via commercial telephone lines.

The system operates satisfactorily and is capable of collecting enough range-doppler samples from meteor trails for an adequate description of the wind pattern at meteor heights.

Wind profiles have been obtained by processing in Cambridge with a CDC-6400 computer the multichannel digital tapes recorded in Havana.

The method can, potentially, be used for real-time wind measurements. It competes favorably with alternative approaches when wind measurements at meteor height must be performed with continuity and without resorting to horizon-to-horizon spatial averaging.

DD FORM 1 NOV 65 1473

Unclassified
Security Classification

14. KEY WORDS	LINK A		LINK B		LINK C	
	ROLE	WT	ROLE	WT	ROLE	WT
meteor trail winds						
high-altitude winds						
VHF (very high frequency) radar						
phase-coherent pulse-doppler radar						
multistatic radar						
meteor trail						
wind at meteor heights						
doppler radar						
three-dimensional wind patterns						
scattering from meteor trails						
meteor echo processing						
wind profiles						
atmospheric density measurements						
atmospheric pressure measurements						
atmospheric temperature measurements						
atmospheric scale height measurements						
Fresnel patterns						
diffusion heights						
diffusion ceiling						
recombination						
initial radius of meteor trail						
fragmentation of meteor						
errors in density measurements due to recombination						
wind shear						
gravity waves						
multistation radar						
line targets						
frequency synthesizer						
reference frequency distribution via telephone lines						
interferometric measurements on meteor echoes						
angle-of-arrival measurements on meteor echoes						
phase-locked secondary standards						
meteor range measurements						
echo-pattern recognition logics						
meteor radar processor						
digitizer						
CRT film recorder						
meteor radar calibrator						
meteor echoes' data reduction						
diffraction pattern						
echo phase measurements						